Modification of Electron Transfer Proteins in the *Chlamydomonas reinhardtii* Chloroplast for Alternative Fuel Development

by

Kiera Reifschneider

A Dissertation Presented in Partial Fulfillment
of the Requirements for the Degree
Doctor of Philosophy

Approved October 2013 by the
Graduate Supervisory Committee:

Kevin Redding, Chair
Petra Fromme
Anne Jones

ARIZONA STATE UNIVERSITY

December 2013

ABSTRACT

There is a critical need for the development of clean and efficient energy sources. Hydrogen is being explored as a viable alternative to fuels in current use, many of which have limited availability and detrimental byproducts. Biological photo-production of H_2 could provide a potential energy source directly manufactured from water and sunlight. As a part of the photosynthetic electron transport chain (PETC) of the green algae *Chlamydomonas reinhardtii*, water is split via Photosystem II (PSII) and the electrons flow through a series of electron transfer cofactors in cytochrome b_6f, plastocyanin and Photosystem I (PSI). The terminal electron acceptor of PSI is ferredoxin, from which electrons may be used to reduce $NADP^+$ for metabolic purposes. Concomitant production of a H^+ gradient allows production of energy for the cell. Under certain conditions and using the endogenous hydrogenase, excess protons and electrons from ferredoxin may be converted to molecular hydrogen. In this work it is demonstrated both that certain mutations near the quinone electron transfer cofactor in PSI can speed up electron transfer through the PETC, and also that a native [FeFe]-hydrogenase can be expressed in the *C. reinhardtii* chloroplast. Taken together, these research findings form the foundation for the design of a PSI-hydrogenase fusion for the direct and continuous photo-production of hydrogen *in vivo*.

ACKNOWLEDGEMENTS

I owe a great deal to a great many people who have made this accomplishment possible.

I am indebted to my family, both close and extended, for fostering in me a curiosity about the natural world. I am also extremely grateful for the unfailing encouragement of my parents as I traveled the path to completing this research. Thank you both.

I also owe gratitude to my husband for his imperturbable patience, grace, and humor in managing my long hours, occasional hot temper, and obsessive quest for answers. His uncanny technical skills were also a lifesaver. Thank you for being both my grounding point and my adventure partner.

Thank you also to my lifetime friends and friends of the road. You were always ready with a kind word, a shoulder to lean on, or a kick-start when needed.

I am thankful for all of my scientific and academic colleagues who have helped along the way. The Redding research group at the University of Alabama was a great place to start out my journey as a scientist. Thanks to Galina Gulis, Jianying Zhang, Brad Bullock and Rajiv Luthra for teaching me the ropes and for being patient with my unending questions. I have fond memories of my time with you all. Thanks also to all past and current members of the Redding lab at ASU, especially to Trish Baker for our lunchtime ‘wild idea' discussions and to Andrey Kanygin for working with me on this project for two years. I am also grateful to Matthew Posewitz and his team at the Colorado School of Mines for their immeasurable knowledge of hydrogenases and

helpful project suggestions. Thanks also to my committee members, Anne Jones and Petra Fromme, for valuable guidance.

Finally, I owe thanks to my advisor Kevin Redding for affording me an extremely unique graduate school experience. When I started out as an intern, I had no way of knowing that my future would involve packing up an entire research lab in liquor store boxes, moving the lab 1,500 miles across the country, starting up and managing the new lab, mentoring scores of undergraduates, completing a hard-won research project, and finding a rewarding but unexpected career path before I had even graduated. You allowed me to pursue projects I was passionate about, even if the chances of success initially appeared dubious. Thank you for allowing me to chase opportunities as they appeared.

TABLE OF CONTENTS

LIST OF TABLES

LIST OF FIGURES

Chapter 1

Introduction

Motivation

Presently, there is a concerted research effort to develop renewable, non-polluting and domestically sourced fuels. While biofuels derived from corn, switchgrass, and sugar beets have garnered substantial public and technical notice and many efforts have reached the pilot or commercial scale, significant interest also lies in using rapidly growing green algae to produce alternative fuels. In addition to swift and low-waste production of biomass and oil, algae are also capable of producing hydrogen, another potential fuel. The research in this dissertation addresses three different yet related subject areas concerning electron flow in photosynthesis and hydrogen production in the green algae *Chlamydomonas reinhardtii.* Presented first is a fundamental analysis of electron transfer in the Photosystem I (PSI) protein that yielded the discovery of mutations that increase electron transfer rates through that protein. Not only is this fundamentally interesting, but it is also applicable to downstream engineering and optimization of fuel production. This work can be found in the second chapter. For the second research effort, presented in the third chapter, the focus is downstream in the electron transport chain with the nuclear-encoded native hydrogenase, which was successfully expressed in the chloroplast of the same green algae. This was proof-of-concept research required for the third topic, presented in the second Appendix, where the two research areas are brought together in the preliminary design of a PSI-hydrogenase fusion protein for the goal of continuous photo-production of biohydrogen.

Human energy consumption

A 2013 report from the U.S. Energy Information Administration (EIA)[1] projects a 56% growth in worldwide energy consumption between 2010 and 2040. The majority of that growth is attributed to countries outside of the Organization for Economic Cooperation and Development (OECD)[a]: non-OECD countries show a 90% increase in energy use as compared to the 17% increase in OECD countries (Figure 1-1A). Renewable energy, along with nuclear power, is the fastest growing energy sector and is increasing at 2.5% per year. Despite this, fossil fuels are projected to provide greater than 80% of the world's energy use through 2040.

The consequences of heavy fossil fuel use are subject to contentious debate. While the 2009 United Nations Climate Change conference in Copenhagen recognized the scientific merit of restraining temperature rises above 2 °C, no binding commitments were obtained concerning the reduction of CO_2 emissions in either the developing or developed world. In addition, although the use of natural gas is increasing and domestic extraction presents a low cost fuel at present, the cost of crude oil, a dominant energy form, continues to rise (Figure 1-1B).

If the possible environmental impacts of increased fossil fuel use have generated only slow policy responses, economic factors tend to produce a more rapid reaction[2]. The economic case for algal biofuels appears promising, and a robust research and

[a] OECD countries include: United States, Canada, Mexico, Austria, Belgium, Chile, Czech Republic, Denmark, Estonia, Finland, France, Germany, Greece, Hungary, Iceland, Ireland, Israel, Italy, Luxembourg, the Netherlands, Norway, Poland, Portugal, Slovakia, Slovenia, Spain, Sweden, Switzerland, Turkey, the United Kingdom, Japan, South Korea, Australia, and New Zealand. For statistical reporting purposes, Israel is included in OECD Europe.

development (R&D) industry has arisen. Recent analyses suggest a reasonable internal rate of return on the technology, provided that co-production of high-value products is pursued inline with biofuel production[3].

Fortunately, the approach to tackling both environmental and economic concerns is similar: a transition away from dependence on solely fossil-fuel energy sources. If economic viability concerns continue to be addressed, it can be argued that a diversity of potential energy sources will ease environmental burdens, as well as strengthen and stabilize domestic energy security.

A large focus within the algal biofuels R&D enterprise has been on liquid hydrocarbon biofuels, for seamless drop-in integration with the existing fuel infrastructure. While algae have demonstrated success in accumulating lipids that can be converted to fuel hydrocarbons[4] they are also capable of producing hydrogen[5]. Interest in hydrogen as an alternative fuel stems from its clean-burning combustion, high efficiency in fuel cell applications[6] and potential for domestic production. An additional application of biologically derived hydrogen is in the generation of industrially valuable compounds. One example is the production of ammonia via the Haber process, usable as an agricultural fertilizer. Unfortunately, the current method of generating hydrogen for use either as a fuel, or as an industrial reagent, is steam reformation of natural gas. This method requires heavy use of fossil fuels for the input of both source material and energy[7].

This provides a motivation for research into hydrogen-production using green algae. Many microorganisms have the capability to produce molecular hydrogen[8]. When undertaken by oxygenic photosynthetic organisms, this involves the use of sunlight

as energy source and water as electron source, both of which are abundant. In such phototrophs, electrons obtained either from the splitting of water at Photosystem II (PSII) or from fermentative catabolism are transferred through a series of electron transfer cofactors to Photosystem I (PSI), which passes the electrons on to ferredoxin (Fd). When growth conditions suppress CO_2 fixation, alternative electron sinks like hydrogen production are activated. Under these conditions, the organism can shunt the flow of electrons from Fd to the enzyme hydrogenase, which evolves H_2 via proton reduction. Solar-driven production of hydrogen from water theoretically provides the most direct route to fuel production. That is, by directing incident energy straight to the production of a fuel (H_2), it avoids the downstream energy losses incurred by synthesizing carbohydrates and lipids (biomass and oil) that could function as a feedstock for methane, ethanol, or oil-based fuels[9]. In photo-production of hydrogen, the fuel production is coupled tightly to photosynthetic electron transfer.

It is generally agreed that for economic viability, coordinated bioengineering to increase the conversion efficiency of photon to H_2 is a necessity. This is being pursued in various ways by a large number of research groups. Strains have been produced that have less antennae[10], leading to less shading and more efficient utilization of photons in large scale cultivation. Strains containing hydrogen-producing enzymes less damaged by O_2 sensitivity are being developed[11], and strains containing blockages in competing electron-use pathways in order to obtain the greatest fuel yield have been presented[12]. In addition to these improvements, H_2 production for commercialization must be a continuous process[13], a departure from the common method of nutrient cycling used at present[14].

Eukaryotic algae

In this research, the eukaryotic green algae *Chlamydomonas reinhardtii* (*C. reinhardtii*) is extensively used. Morphologically, the organism is a unicellular photosynthetic green algae approximately 10 μm in length with two anterior flagella, a single cup-shaped chloroplast, and a distinct cell wall. Initial genetic experiments in the first part of the 20th century suggested the suitability of the organism as a model system, but the idea was not fully pursued until the work of Lewin and Sager in the 1940s and 1950s[15]. Since then, *C. reinhardtii* has been developed into a heavily-used, superior model system to study flagellar structure, cell-cell recognition, cell-cycle control, chloroplast biogenesis, light sensing, and photosynthesis[16].

The chloroplast and tools for engineering

The single, large chloroplast in *C. reinhardtii* takes up nearly two-thirds of the cell volume and is the site of the thylakoid (TK) membranes containing the essential proteins involved in photosynthesis (Figure 1-2). *Chlamydomonas* is a choice model organism for photosynthesis research due to its metabolic flexibility. It is able to grow in the dark or sustain mutations in photosynthesis so long as the organism is supplemented with acetate as a carbon source[15]. An extensive collection of both wild type (WT) and mutant strains is curated and accessible to researchers. Additionally, plasmid constructs for transformation studies and ready transformation protocols for both nuclear[17] and chloroplast[18] genetic manipulations are available. A sequenced genome is accessible for both the nuclear[19] and plastid[20] genomes, and has provided substantial enhancement to research in the organism.

The photosynthetic electron transport chain

While the overall picture of electron sources and sinks in *Chlamydomonas reinhardtii* is complex, those that pertain to photosynthesis and the generation of hydrogen are of specific interest here. Figure 1-2 depicts the relevant movement of electrons (solid lines) in the chloroplast. Electron sources for hydrogen photo-production are the splitting of water by the oxygen-evolving complex (OEC) in conjunction with Photosystem II (PSII), and electrons derived from Glycolysis and the Citric Acid Cycle that feed into the electron transport chain (ETC) at the level of the plastoquinone pool. Electrons donated to ferredoxin may be transferred to a number of acceptors, with $NADP^+$, which in the form of NADPH may go on to participate in carbon-fixation and other anabolic pathways, and H_2 gas production, as two predominant electron sinks[21]. The production of biohydrogen has been hypothesized to function as a bleed-valve, disposing of excess reducing equivalents, and allowing a sufficient proton motive force (pmf) to build up across the thylakoid membrane.

Photosystem I

As roughly outlined by the schematic in Figure 1-2, the core of Photosystem I (PSI) is structured as a heterodimer. No crystal structure yet exists for the algal protein, but a high resolution structure was obtained for both cyanobacteria [22] and plants[23]. The majority of the electron transport cofactors are contained in the protein framework of the two branches: PsaA and PsaB. The mobile carrier, plastocyanin (PC), transfers electrons from cytochrome b_6f to the primary PSI donor, the P700 cofactor. P700 is a reaction centre chlorophyll *a* molecule and is the primary electron donor for Photosystem

I. From P700, the electron transfer path branches and substantial research has elucidated the directionality of transfer in the branches[24].

Cofactors A_0 and A_1 are early electron transfer cofactors. The modified chlorophyll of A_0 transfers electrons to the A_1 phylloquinone (PhQ). After A_1, electrons are transferred to F_X, a four-iron, four-sulfur complex. Transfer to this secondary acceptor from the phylloquinone is the focus of Chapter 2. Basic discoveries here could lead to reengineering both electron transfer direction and rates for optimum fuel production.

After F_X, electrons move to two other iron-sulfur complexes, F_A and F_B, which are bound by the PsaC protein. This protein is revisited in Appendix 2 as the link to the photosystem in the design of a PSI-hydrogenase fusion protein.

The terminal electron acceptor in PSI is the diffusible iron-sulfur protein, ferredoxin (Fd). As mentioned above, electrons are largely routed from ferredoxin to ferredoxin-NADP+ reductase (FNR), resulting in the production of NADPH. If metabolic flux does not require NADPH for carbon fixation or other reactions, the electrons may also be used to produce H_2. This is accomplished in *C. reinhardtii* by an [FeFe]-hydrogenase.

Hydrogenase

The [FeFe]-hydrogenase enzyme of *C. reinhardtii* is bidirectional and catalyzes the reaction $2\ H^+ + 2\ e^-$ D H_2. Directionality of the reaction is biased by redox tuning of the protein, and the *C. reinhardtii* enzyme readily produces molecular hydrogen from protons and electrons obtained from either water splitting at PSII or from catabolic reactions. To date, two chloroplast hydrogenase proteins, HydA1 and HydA2, have been

identified in *C. reinhardtii*[25]. Both belong to the [FeFe]-hydrogenase, or iron-only class. The other major hydrogenase classification is the nickel-iron [NiFe] type. These enzymes are often multimeric and catalyze the same reversible reaction shown above. Despite being evolutionarily unrelated, the hydrogenases share similar non-protein ligands on their active site metals[26]. The work in Chapter 3 will focus on the [FeFe]-hydrogenase found in green algae.

Hydrogenases in the [FeFe] class have been shown to be monomeric in structure and have highly conserved amino acid regions containing four cysteines involved in the coordination of the active centre[12]. This catalytic H-cluster consists of a binuclear iron centre with three CO ligands, two CN ligands, and a bridging azadithiolate[27,28]. The di-iron centre is linked to a [4Fe-4S] cluster by a single bridging cysteine. Recently, HydA1 from *C. reinhardtii*, heterologously expressed in *E. coli*, yielded a crystal structure at 1.97 Å resolution[29]. However, as this structure was prepared in the absence of the required maturation factors HydEF and G[30], it lacked the di-iron subcluster of the H-cluster. Despite this, the overall structure of the active site domain is similar to the resolved structures for the [FeFe]-hydrogenases from *Clostridium pasteurianum*[31] and *Desulfovibrio desulfuricans*[32]. Prior to the *C. reinhardtii* structure determination, the structural information from these latter two resources was used as a reference for the algal system[33]. A predicted structural model of the *C. reinhardtii* HydA2 is also available[34].

The native *C. reinhardtii* hydrogenase is a nuclear-encoded, chloroplast expressed protein[35]. Despite an apparently simple structure, the *C. reinhardtii* hydrogenases have a high specific activity[36]. This makes the organism especially well suited for the photo-

production of biohydrogen. However, with the methods currently in use[33], the reported *in vivo* hydrogen yields from this organism are relatively low. Several groups have had good success in linking hydrogenases *in vitro* to various photosynthetic components and increasing H_2 production by rerouting or controlling electron flow[37-39], but this requires intensive work in the isolation and attachment, as well as the addition of artificial electron donors. When considering a long-term production platform, an engineered *in vivo* system containing an electron-routing fusion may be a strong contender.

In order to pursue the construction of a hydrogenase-photosystem fusion for the direct and continuous photo-production of hydrogen *in vivo*, evidence that a hydrogenase could be successfully expressed in the chloroplast was required. Expression of a fusion protein requires that the components be functionally expressed in the location of choice. In *Chlamydomonas*, the *HYDA1* gene is nuclear and the gene product appears to be imported into the chloroplast following synthesis in the cytosol[35]. It is assumed that the required maturation proteins are imported as well. HydA, as well as the maturation proteins HydEF and HydG, all possess predicted chloroplast transport peptides[40,41]. The homologous recombination that occurs in the chloroplast of *C. reinhardtii* allows precise genomic engineering that is simply unavailable in the nucleus.

This purportedly simple proof-of-concept study became a substantial investigation. In the native system, it is hypothesized that the polypeptide is imported from the cytosol into the chloroplast where it is assembled with its catalytic centre to an active form. In this work, it was found that a native hydrogenase can be expressed and function *in situ* in the chloroplast, but that there is a considerable selective pressure

against it. Experimental conditions were developed under which the chloroplast hydrogenase could be expressed, and its function demonstrated. The origin and mitigation of negative selective pressures were hypothesized and tested, and an application of these findings to future bioengineering goals is discussed.

The overview and goals of this dissertation

The major experimental aspects of this story come in two sections, described in Chapters 2 and 3. In Chapter 2, the movement of electrons through the Photosystem I complex, specifically from PhQ to F_X, was investigated. This was a fundamental study, and it was discovered that mutation of a leucine residue in the protein framework near the PhQ cofactor in PSI disturbed hydrogen bonding to the cofactor, resulting in an increase in electron transfer rates.

In Chapter 3, focus was shifted downstream to the hydrogenase and the expression of that protein in the chloroplast. Considering the fuel and feedstock applications of H_2, work here developed with an eye to future engineering. The difficulty in obtaining a chloroplast-expressed hydrogenase was a stark reminder that engineering living systems can be fraught with challenges not immediately apparent at the start. The hydrogenase is an important electron mediator, and living systems are a complex web of energetic inputs and outputs. Introducing a chloroplast-expressed hydrogenase to the natural system while removing the inherent tight regulation present in the native enzyme resulted in a significant disruption in metabolism. The resulting algae were initially extremely effective in removing the foreign gene. Relative success in engineering was obtained by using a switchable system that attenuated gene expression in the presence of

certain B-vitamins. By this method, a strain of *Chlamydomonas* that contained a chloroplast-expressed hydrogenase was created, and the effects of this change examined. This strain produced twice the amount of hydrogen of the parent strain, and, as a proof-of-concept, now supports the construction of the designed PSI-hydrogenase fusion with the goal of direct and continuous photo-production of biohydrogen.

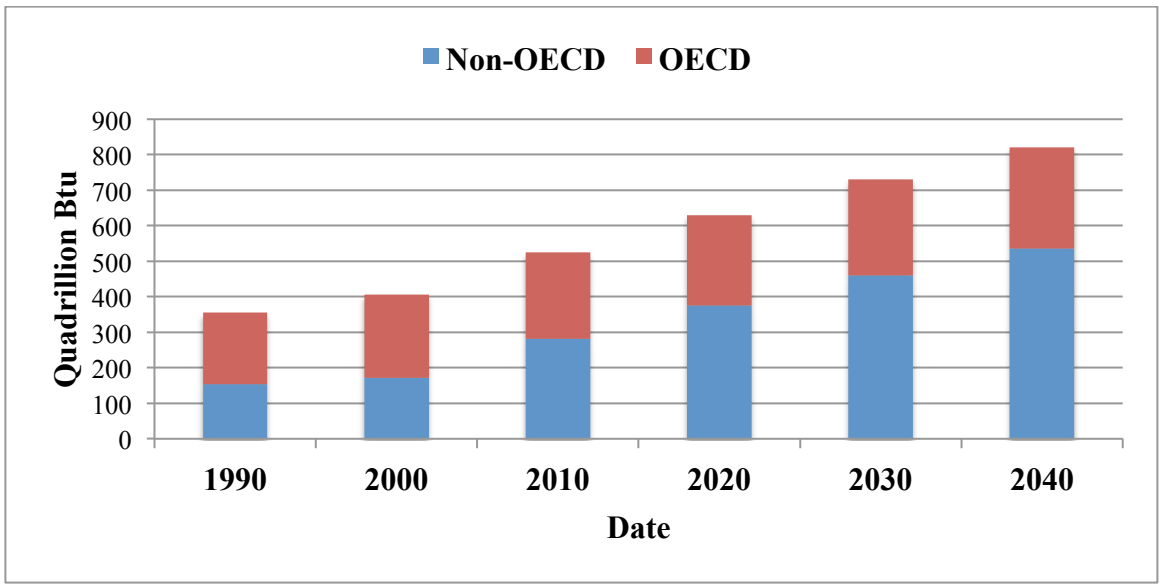

A

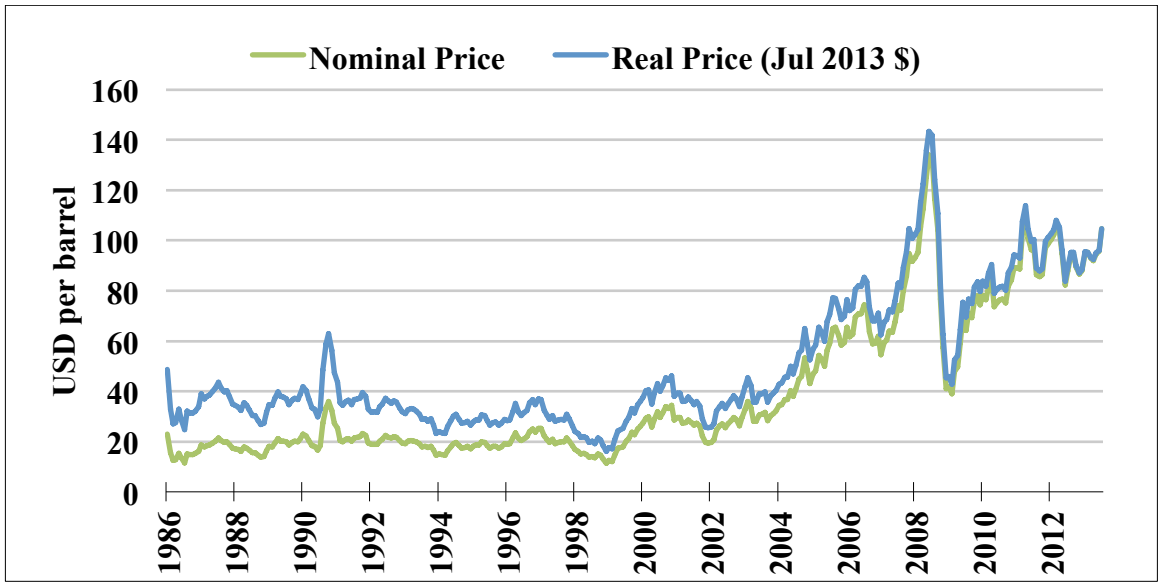

B

Figure 1-1: **World energy consumption and oil price per barrel.** A: World energy consumption, 1990-2040. Data from the U.S. Energy Information Administration (EIA) International Energy Outlook Report for 2013. Values 1990-2010 are historical, 2020-2040 are projected. B: Price per barrel for West Texas Intermediate (WTI), a benchmark for oil prices. Data obtained from the U.S. EIA.

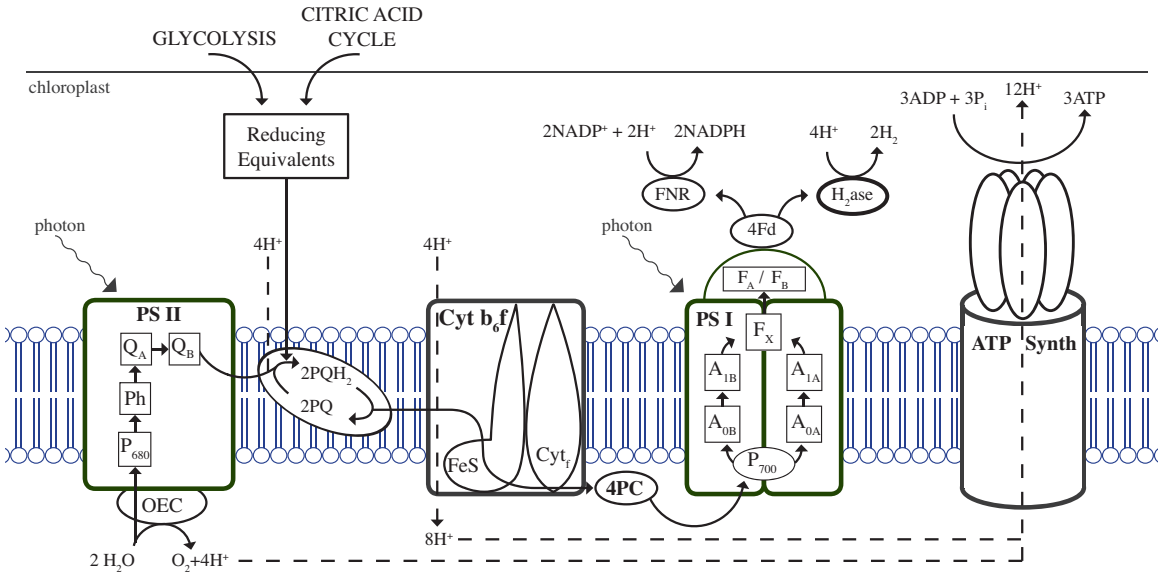

Figure 1-2: Electron transport through the photosystems and associated complexes. Two sources of electrons for the hydrogenase are the PSII-dependent oxidation of water at the oxygen evolving complex (OEC) and the catabolism of storage molecules and subsequent reactions of Glycolysis and the Citric Acid Cycle. The hydrogenase competes for electrons from ferredoxin (Fd) with the Ferredoxin-NADP+ reductase (FNR) and its donation to NADPH and its use in subsequent anabolic reactions.

References

[1] US Energy Information Administration. International Energy Outlook 2013. DOE/EIA-0484(2013) 2013:1–312. Retrieved from http://www.eia.gov/forecasts/ieo/

[2] Murray J, King D. Climate policy: Oil's tipping point has passed. Nature 2012;481(7382):433–435.

[3] Stephens E, Ross IL, King Z, Mussgnug JH, Kruse O, Posten C, Borowitzka MA, Hankamer B. An economic and technical evaluation of microalgal biofuels. Nat Biotechnol 2010;28(2):126–128.

[4] Jones CS, Mayfield SP. Algae biofuels: versatility for the future of bioenergy. Curr Opin Biotechnol 2012;23(3):346–351.

[5] Ghirardi ML, Zhang L, Lee JW, Flynn T, Seibert M, Greenbaum E, Melis A. Microalgae: a green source of renewable H_2. Trends Biotechnol 2000;18(12):506–511.

[6] U.S. Department of Energy. Comparison of Fuel Cell Technologies. Energy Efficiency & Renewable Energy. February 2011. Retrieved from http://www1.eere.energy.gov/hydrogenandfuelcells/fuelcells/pdfs/fc_comparison_chart.pdf

[7] Rostrup-Nielsen J, Sehested J, Nørskov J. Hydrogen and synthesis gas by steam- and CO_2 reforming. In: Advances in Catalysis Volume 47, vol. 47. Elsevier, 2002. p. 65–139.

[8] Vignais PM, Billoud B. Occurrence, Classification, and Biological Function of Hydrogenases: An Overview. Chem. Rev. 2007;107(10):4206–4272.

[9] Oey M, Ross IL, Stephens E, Steinbeck J, Wolf J, Radzun KA, Kügler J, Ringsmuth AK, Kruse O, Hankamer B. RNAi Knock-Down of LHCBM1, 2 and 3 Increases Photosynthetic H_2 Production Efficiency of the Green Alga *Chlamydomonas reinhardtii*. PLoS ONE 2013;8(4):e61375.

[10] Beckmann J, Lehr F, Finazzi G, Hankamer B, Posten C, Wobbe L, Kruse O. Improvement of light to biomass conversion by de-regulation of light-harvesting protein translation in *Chlamydomonas reinhardtii*. J Biotechnol 2009;142(1):70–77.

[11] Ghirardi ML, Togasaki RK, Seibert M. Oxygen sensitivity of algal H_2-production. Appl Biochem Biotechnol 1997;63-65:141–151.

[12] Kruse O, Rupprecht J, Bader K-P, Thomas-Hall S, Schenk PM, Finazzi G, Hankamer B. Improved photobiological H_2 production in engineered green algal cells. J Biol Chem 2005;280(40):34170–34177.

[13] Kruse O, Ben Hankamer. Microalgal hydrogen production. Curr Opin Biotechnol 2010;21(3):238–243.

[14] Zhang L, Happe T, Melis A. Biochemical and morphological characterization of sulfur-deprived and H_2-producing *Chlamydomonas reinhardtii* (green alga). Planta 2002;214(4):552–561.

[15] Harris EH, Stern DB, Witman G. The *Chlamydomonas* Sourcebook. San Diego: Academic Press, 1989.

[16] Harris EH. *Chlamydomonas* as a model organism. Annu Rev Plant Physiol Plant Mol Biol 2001;52(1):363–406.

[17] Shimogawara K, Fujiwara S, Grossman A, Usuda H. High-efficiency transformation of *Chlamydomonas reinhardtii* by electroporation. Genetics 1998;148(4):1821–1828.

[18] Boynton JE, Gillham NW, Harris EH, Hosler JP, Johnson AM, Jones AR, Randolph-Anderson BL, Robertson D, Klein TM, Shark KB. Chloroplast transformation in *Chlamydomonas* with high velocity microprojectiles. Science 1988;240(4858):1534–1538.

[19] Merchant SS, Prochnik SE, Vallon O, Harris EH, Karpowicz SJ, Witman GB, Terry A, Salamov A, Fritz-Laylin LK, Marechal-Drouard L, Marshall WF, Qu LH, Nelson DR, Sanderfoot AA, Spalding MH, Kapitonov VV, Ren Q, Ferris P, Lindquist E, Shapiro H, Lucas SM, Grimwood J, Schmutz J, Cardol P, Cerutti H, Chanfreau G, Chen CL, Cognat V, Croft MT, Dent R, Dutcher S, Fernandez E, Fukuzawa H, Gonzalez-Ballester D, Gonzalez-Halphen D, Hallmann A, Hanikenne M, Hippler M, Inwood W, Jabbari K, Kalanon M, Kuras R, Lefebvre PA, Lemaire SD, Lobanov AV, Lohr M, Manuell A, Meier I, Mets L, Mittag M, Mittelmeier T, Moroney JV, Moseley J, Napoli C, Nedelcu AM, Niyogi K, Novoselov SV, Paulsen IT, Pazour G, Purton S, Ral JP, Riano-Pachon DM, Riekhof W, Rymarquis L, Schroda M, Stern D, Umen J, Willows R, Wilson N, Zimmer SL, Allmer J, Balk J, Bisova K, Chen CJ, Elias M, Gendler K, Hauser C, Lamb MR, Ledford H, Long JC, Minagawa J, Page MD, Pan J, Pootakham W, Roje S, Rose A, Stahlberg E, Terauchi AM, Yang P, Ball S, Bowler C, Dieckmann CL, Gladyshev VN, Green P, Jorgensen R, Mayfield S, Mueller-Roeber B, Rajamani S, Sayre RT, Brokstein P, Dubchak I, Goodstein D, Hornick L, Huang YW, Jhaveri J, Luo Y, Martinez D, Ngau WCA, Otillar B, Poliakov A, Porter A, Szajkowski L, Werner G, Zhou K, Grigoriev IV, Rokhsar DS, Grossman AR. The *Chlamydomonas* Genome Reveals the Evolution of Key Animal and Plant Functions. Science 2007;318(5848):245–250.

[20] Maul JE. The *Chlamydomonas reinhardtii* Plastid Chromosome: Islands of Genes in a Sea of Repeats. Plant Cell 2002;14(11):2659–2679.

[21] Peden EA, Boehm M, Mulder DW, Davis R, Old WM, King PW, Ghirardi ML, Dubini A. Identification of global ferredoxin interaction networks in *Chlamydomonas reinhardtii*. J Biol Chem 2013.

[22] Jordan P, Fromme P, Witt HT, Klukas O, Saenger W, Krauss N. Three-dimensional structure of cyanobacterial Photosystem I at 2.5 angstrom resolution. Nature 2001;411(6840):909–917.

[23] Ben-Shem A, Frolow F, Nelson N. Crystal structure of plant Photosystem I. Nature 2003;426(6967):630–635.

[24] Brettel K, Leibl W. Electron transfer in Photosystem I. Biochim Biophys Acta 2001;1507(1-3):100–114.

[25] Forestier M, King P, Zhang L, Posewitz M, Schwarzer S, Happe T, Ghirardi ML, Seibert M. Expression of two [Fe]-hydrogenases in *Chlamydomonas reinhardtii* under anaerobic conditions. Eur J Biochem 2003;270(13):2750–2758.

[26] Mulder DW, Shepard EM, Meuser JE, Joshi N, King PW, Posewitz MC, Broderick JB, Peters JW. Insights into [FeFe]-Hydrogenase Structure, Mechanism, and Maturation. Structure 2011;19(8):1038–1052.

[27] Nicolet Y, De Lacey AL, Vernède X, Fernández VM, Hatchikian EC, Fontecilla-Camps JC. Crystallographic and FTIR Spectroscopic Evidence of Changes in Fe Coordination Upon Reduction of the Active Site of the Fe-Only Hydrogenase from *Desulfovibrio desulfuricans*. J Am Chem Soc 2001;123(8):1596–1601.

[28] Berggren G, Adamska A, Lambertz C, Simmons TR, Esselborn J, Atta M, Gambarelli S, Mouesca JM, Reijerse E, Lubitz W, Happe T, Artero V, Fontecave M. Biomimetic assembly and activation of [FeFe]-hydrogenases. Nature 2013:1–5.

[29] Mulder DW, Boyd ES, Sarma R, Lange RK, Endrizzi JA, Broderick JB, Peters JW. Stepwise [FeFe]-hydrogenase H-cluster assembly revealed in the structure of $HydA^{\Delta EFG}$. Nature 2010;465(7295):248–251.

[30] Mulder DW, Ortillo DO, Gardenghi DJ, Naumov AV, Ruebush SS, Szilagyi RK, Huynh B, Broderick JB, Peters JW. Activation of $HydA^{\Delta EFG}$ Requires a Preformed [4Fe-4S] Cluster. Biochemistry 2009;48(26):6240–6248.

[31] Peters JW. X-ray Crystal Structure of the Fe-Only Hydrogenase (CpI) from *Clostridium pasteurianum* to 1.8 Angstrom Resolution. Science 1998;282(5395):1853–1858.

[32] Nicolet Y, Piras C, Legrand P, Hatchikian CE, Fontecilla-Camps JC. *Desulfovibrio desulfuricans* iron hydrogenase: the structure shows unusual coordination to an active site Fe binuclear center. Structure 1999;7(1):13–23.

[33] Melis A, Happe T. Hydrogen Production. Green Algae as a Source of Energy. Plant Physiol 2001;127(3):740–748.

[34] Chang CH, King PW, Ghirardi ML, Kim K. Atomic Resolution Modeling of the Ferredoxin:[FeFe] Hydrogenase Complex from *Chlamydomonas reinhardtii*. Biophysical J 2007;93(9):3034–3045.

[35] Happe T, Mosler B, Naber JD. Induction, localization and metal content of hydrogenase in the green alga *Chlamydomonas reinhardtii*. Eur J Biochem 1994;222(3):769–774.

[36] Adams MW. The structure and mechanism of iron-hydrogenases. Biochim Biophys Acta 1990;1020(2):115–145.

[37] Ihara M, Nishihara H, Yoon K-S, Lenz O, Friedrich B, Nakamoto H, Kojima K, Honma D, Kamachi T, Okura I. Light-driven Hydrogen Production by a Hybrid Complex of a [NiFe]-Hydrogenase and the Cyanobacterial Photosystem I. Photochem Photobiol 2006;82(3):676.

[38] Yacoby I, Pochekailov S, Toporik H, Ghirardi ML, King PW, Zhang S. Photosynthetic electron partitioning between [FeFe]-hydrogenase and ferredoxin:NADP+-oxidoreductase (FNR) enzymes in vitro. Proc Natl Acad Sci U S A 2011;108(23):9396–9401.

[39] Lubner CE, Applegate AM, Knörzer P, Ganago A, Bryant DA, Happe T, Golbeck JH. Solar hydrogen-producing bionanodevice outperforms natural photosynthesis. Proc Natl Acad Sci U S A 2011;108(52):20988–20991.

[40] Posewitz MC. Discovery of Two Novel Radical S-Adenosylmethionine Proteins Required for the Assembly of an Active [Fe] Hydrogenase. J Biol Chem 2004;279(24):25711–25720.

[41] Posewitz MC, Dubini A, Meuser JE, Seibert M, Ghirardi ML. Hydrogenases, hydrogen production, and anoxia. The Chlamydomonas Sourcebook: Organellar and Metabolic Processes. Vol. 2. Elsevier, 2009.

Chapter 2

Studies on the phylloquinone cofactor of Photosystem I in *Chlamydomonas reinhardtii*

Selected figures used with permission from:

Interquinone Electron Transfer in Photosystem I As Evidenced by Altering the Hydrogen Bond Strength to the Phylloquinone(s). Stefano Santabarbara, Kiera Reifschneider, Audrius Jasaitis, Feifei Gu, Giancarlo Agostini, Donatella Carbonera, Fabrice Rappaport, and Kevin E. Redding. The Journal of Physical Chemistry B 2010 114 (28), 9300-9312.

Abstract

The binding pocket for the phylloquinone (PhQ) cofactor in Photosystem I (PSI) has been mutated, and the resulting strains exhibit accelerated oxidation kinetics from PhQ•- to F_X. Specifically, the leucine residue that provides a peptide nitrogen as a hydrogen bond donor to the keto-carbonyl of the phylloquinone has been modified. It has been hypothesized that the ability of the protein scaffold to stabilize the semiquinone form of the cofactor is important, and the insertion of residues with larger side chains than seen in the native system could result in the destabilization of the radical and thus provide a forward driving force for reduction of F_X. This is the first observation of accelerated oxidation kinetics from PhQ•- to F_X in *Chlamydomonas reinhardtii,* and the results obtained here present interesting possibilities for engineering photosynthetic organisms with increased electron transfer rates.

Introduction

A high-level introduction to photosynthesis as well as the structure and function of Photosystem I in green algae can be found in Chapter 1. Overall electron transfer is highlighted in Figure 1-2 therein. Here, the focus is narrowed to electron transfer within PSI, which catalyzes the light-driven oxidation of plastocyanin and reduction of ferredoxin. The majority of the electron transfer (ET) cofactors in PSI are bound noncovalently to the PsaA/PsaB heterodimer, which forms the reaction center (RC). The two terminal electron acceptors, the [4Fe-4S] clusters F_A and F_B, exist outside of the dimer and are bound to the subunit PsaC.

Phylloquinone is polycyclic aromatic ketone with a 2-methyl-1,4-naphthoquinone headgroup and a phytyl tail. It, or a slightly modified chemical species, acts as a secondary electron acceptor in PSI. It is reduced in less than 100 ps by the A_0 cofactor and the resulting radical PhQ•- is oxidized with polyphasic kinetics by the electron acceptor F_X, a [4Fe-4S] cluster[1-3]. The two branches of PSI appear structurally very symmetrical. While it has been shown that both the A and B branches participate in ET reactions[4], the two are not identical and differ in both kinetic properties and how often they are utilized. For example, the kinetics of the electron transfer rate from PhQ to F_X are described by a minimum of two exponential components, characterized by lifetimes of 10-25 and 200-300 ns, at room temperature[1,2]. By analyzing the effect of site-directed mutations in the PhQ binding sites, the approximately 250-ns phase was attributed to reactions involving the PsaA-bound PhQ (PhQ_A), and the 20-ns phase to PsaB-bound PhQ_B[4-6]. The precise origin of the 10- fold difference in rate is not currently known.

According to the crystallographic models[7,8], the edge-to-edge distance between PhQ and F_X in the A- and B-sides differ by only fractions of an angstrom, and the orientation of the electron donor and acceptor appear to be identical. Thus, it is likely that the difference in the oxidation rate of PhQ•- from each side arises from subtle protein-cofactor interactions and not structural differences. Modeling based on electron tunneling theory[2,9] and attempts to directly measure the redox potential of the PhQ[10] suggests a difference of approximately 40-100 mV between the standard redox potentials of the two phylloquinones. The PhQ_B•-/PhQ_B redox couple appears to be more electronegative, making F_X reduction by PhQ_B•- downhill in energy as compared to reduction by PhQ_A•-.

The protein framework surrounding the electron transfer cofactors can substantially tune the redox properties of the PhQ/PhQ- couple and consequently impact electron transfer rates. Here, the ability of the protein to stabilize the semiquinone form of the cofactor is of key importance. In PSI, the structural models suggest that the keto-carbonyl (position 2) of both PhQ_A and PhQ_B is asymmetrically hydrogen-bonded to the peptide nitrogen of the conserved leucine residues of PsaA-Leu722 and PsaB-Leu706 (Figure 2-1).

Here is reported an investigation of the PhQ binding site and electron transfer kinetics in *C. reinhardtii* PSI from the PhQ cofactor to F_X. Specifically, mutants in which the aforementioned conserved leucines have been replaced with either tyrosine (PsaA-L722Y, PsaB-L706Y) or threonine (PsaA-L722T) were analyzed. Note that the numbering system used is the same as in the *Thermosynechococcus elongatus* sequence to allow direct comparison with the crystallographic model[7]. It is shown that these mutations led to an acceleration of the electron transfer reactions involving either PhQ_A•- (PsaA-L722Y/T) or PhQ_B•- (PsaB-L722Y). This is in contrast with previous reports for other mutations of the PhQ binding sites[11].

Another interesting discovery from this mutant set was the apparent redistribution of oxidation phases of PhQ. Collaborator Stefano Santabarbara generated the interesting hypothesis that interquinone electron transfer occurs in PSI as a result of a low but unequal driving force for electron transfer reactions from PhQ_A•- and PhQ_B•- to F_X. His simulations and a detailed proposal of this energetic scenario will not be discussed in this dissertation, but is presented in detail in the literature[12].

Materials and Methods

Mutagenic PCR

Mutant strains were constructed as previously described[4,13] by the method of Picard[14]. Site-directed mutations were constructed by PCR using plasmids designed to reinsert the *psaA-3* or *psaB* genes[15].

Bioballistic chloroplast transformation

Transformation was performed by an adapted method of Boynton[16]. Each 1 μg of plasmid DNA was adsorbed onto 1-μm diameter tungsten nanoparticles (50 mg/mL, generous gift of J.D. Rochaix) in a mixture with $CaCl_2$ (1 M) and spermidine (20 mM). Recipient strains were prepared by first counting cells with a hemocytometer (Hausser Scientific), and concentrating by centrifugation to plate 10^7 cells per Tris-Acetate Phosphate (TAP)[17] plate. Each shot with a homemade helium-driven gene-gun delivered 10 μL of the DNA mixture (200 ng DNA) per plate. Plasmids bearing mutations in *psaA* exon 3 (*psaA*-3) were shot into strains KRC1001-11A (*psaA-3*Δ) and KRC91-1A (P71 *psbA*Δ *psaA-3*Δ*),* and *psaB* plasmids were shot into strains KRC1000-2A (*psaB*Δ) and KRC94-9A (P71 *psbA*Δ *psaB*Δ*)* followed by selection for resistance to spectinomycin (Gold Biotechnology) and streptomycin (Fisher Scientific). All strains were grown under low continuous illumination (~10 μE m^{-2} s^{-1}) on TAP medium.

Growth conditions for C. reinhardtii

All transformants selected by antibiotic resistance and the mutations confirmed by PCR were grown photoheterotrophically at 25 °C. Light sensitivity was tested as in 'Growth Assays' below, and light-sensitive strains were grown in the dark on acetate.

Thylakoid (TK) membrane preparation

TK membranes were prepared by an adapted method from Fischer[18]. Cells were harvested at 2-3x10^6 cells mL^{-1} by centrifugation and washed with buffer H1 (25 mM HEPES-KOH pH 7.5, 5 mM $MgCl_2$, 0.3 M sucrose). Pelleted cells were resuspended again in H1 to a concentration of 1.0x10^8 cell mL^{-1} and lysed by a French pressure cell press, by sonication, or by beating with glass beads. Figure 2-2 demonstrates three purification steps in the isolation of TK membranes and PSI particle preparations.

TK preparation by French Pressure cell

The French pressure cell press (Aminco) was applied at 2 tonnes pressure with a 1-inch piston. After lysis, the mixture was spun for 10 minutes at 20,000 x g at 4 °C in an SS-34 rotor. The pellet was resuspended in buffer H2 (5 mM HEPES-KOH pH 7.5, 5 mM $MgCl_2$, 10 mM EDTA and 0.3 M sucrose) and spun for 15 minutes at 70,000 x g at 4 °C in a KA40 rotor. A sucrose shock was used as needed to remove carotenoids: the pellet was resuspended using a paintbrush with ~15 mL H3 (5 mM HEPES-KOH pH 7.5, 5 mM $MgCl_2$, 10 mM EDTA and 1.8 M sucrose) per tube and homogenized. Remains of the pelleted cells were rinsed with H6 (25 mM HEPES-KOH pH 7.5, 5 mM $MgCl_2$ and 10 mM EDTA) into the tubes, filled to volume with H6 and mixed well. Tubes were spun

at 15 minutes at 70,000 x g at 4 °C in a KA40 rotor, and the process repeated. After this point, the supernatant containing the contaminating carotenoids was carefully removed, and the loose pellet components separated on a sucrose density gradient. The pellet was resuspended in 10 mL of buffer H3 and transferred at 10 mL per tube to six SW-28 swinging bucket centrifuge tubes. Carefully layered atop the lysed cells were two successive 10 mL quantities of buffers H4 (5 mM HEPES-KOH pH 7.5, 5 mM $MgCl_2$, 10 mM EDTA and 1.3 M sucrose) and H5 (5 mM HEPES-KOH pH 7.5, 5 mM $MgCl_2$, 10 mM EDTA and 0.5 M sucrose). The discontinuous gradient was spun for 90 minutes at 80,000 x g at 4 °C in an SW-28 rotor. The dark green layer at the interface was collected with a 16-20G needle. This fraction containing the TK membranes was resuspended in buffer H6 and spun for 45 minutes at 100,000 x g in a KA40 rotor to pellet the membranes. The supernatant was carefully removed, and the membranes resuspended as desired in H6+20% glycerol and homogenized >20x to evenly disperse the membranes. Chlorophyll concentration was determined by the method below, and samples were frozen in liquid nitrogen and stored at -80 °C.

TK preparation by sonication

Here, a protocol by Ohad[19] was adapted. After harvest, cells were resuspended in sonication buffer (50 mM HEPES pH 7.0, 20 mM NaCl, 10 mM $MgCl_2$) and washed twice in the same buffer. Afterward, the pellet was resuspended at 200-500 μg mL^{-1} chlorophyll in the same buffer. Using a sonicator microtip (Branson) operated at maximum power, the sample was sonicated 5 mL at a time (in a 10 mL tube kept in ice water) for 5 x 5 s with cooling intervals of 10 s. The sonicated suspension was diluted 5-

fold in cold buffer and centrifuged at 2,000 x g for 1 min at 4 °C. The pellet was discarded and the supernatant centrifuged at 15,000 x g for 10 min at 4 °C. For a crude TK, the pellet was removed with a soft brush (not disturbing the starch) and resuspended in the same buffer at a final concentration of 1-2 mg mL^{-1} chlorophyll. Further separation on a sucrose density gradient as above provided a cleaner preparation.

TK preparation by bead-beating

Here, the method followed the French pressure protocol in all steps save the cell lysis. In this protocol, cells were resuspended to 10^8 cells mL^{-1} in ~200 mL portions of H1. The cells were lysed in a bead beater (BioSpec) using an ice chamber and 0.5 mm glass beads (soda lime) with four 30-second bursts and 5-minute breaks between. The homogenate was decanted and the glass beads rinsed with H1 buffer. The remainder of the isolation protocol proceeded as in French pressure cell method above.

Photosystem I particle preparation

For experiments that required a more pure sample, Photosystem I particles were isolated. Thylakoid membranes prepared by any method above were diluted with 5 mM Tricine buffer to 0.8 mg mL^{-1} chlorophyll. To solubilize the membranes, β-dodecylmaltoside (βDDM, Dojindo) was added to a final concentration of 1%, mixed gently and allowed to stir in the dark and on ice for 30 minutes. Solubilized membranes were spun at 41,000 x g in a Ti70 rotor at 4 °C to pellet insoluble components. Cleared supernatant (5 mL) was loaded on top of pre-prepared gradient tubes (bottom to top: 10 mL (1.7 M sucrose, 5 mM Tricine, 0.05% βDDM), 5 mL (1.2 M sucrose, 5 mM Tricine,

0.05% βDDM), 10 mL (0.9 M sucrose, 5 mM Tricine, 0.05% βDDM)) and spun ≥12 hours at 200,000 x g in a 70 Ti rotor at 4 °C. The bottom band was collected and diluted with ≥4 volumes of 5 mM Tricine-KOH (pH 8.0)/0.03% βDDM, then spun ≥3 hr at 215,000 x g in a Ti70 rotor at 4 °C to collect particles. Supernatant was removed from the very loose pellet and the remainder resuspended with buffer (5 mM Tricine-KOH (pH 8.0)/0.03% βDDM). Chlorophyll determination was calculated as below, and the particles frozen in liquid nitrogen and stored at -80 °C.

Determination of chlorophyll concentration

The chlorophyll concentration of cell cultures, TK membranes, or PSI particle preparations was determined spectroscopically. For cell cultures, 1 mL of cell suspension was pelleted for 2 minutes at 25,000 x g, and the supernatant removed. Pellets were resuspended with 1 mL of 80% acetone and left to extract in the dark for two minutes. For TK membrane preparations or PS1 particles, 10 µL of the sample was added to 990 µL of 80% acetone. After the same dark extraction, all samples were spun again at 25,000 x g for two minutes and absorbance of the solvent-extracted pigments was measured at 750 nm, 663.6 nm and 646.6 nm. Absorbance values at 663.6 nm and 646.6 nm were corrected with the 750 nm value, then chlorophyll concentration was calculated according to the formulae presented in Porra *el al*[20].

Concentration of chlorophyll A (mM) = $0.01371\ A_{663.6} - 0.00285\ A_{646.6}$
Concentration of chlorophyll B (mM) = $0.02239\ A_{646.6} - 0.00542\ A_{663.6}$
Total chlorophyll concentration (mg/mL) = $0.01776\ A_{646.6} + 0.00734\ A_{663.6}$

Effect on exogenous quinone on reduction of P700+

Photosystem I particles of WT (JVD1B$^-$) and *menD*Δ[21] (generous gift of J.D. Rochaix) were prepared as above and diluted to 50 μM total chlorophyll (250 μL total volume) with N_2-bubbled JTS buffer (100 mM Tricine, 10 mM $MgCl_2$, 10 mM ascorbate, 0.03% βDDM). Vitamin K_1 (phylloquinone, Supelco) at 250 μg mL^{-1} in ethanol was added to the reaction mixture (0.55 nmol, 2.2 μM). Bleaching of P700+ was detected using a pulsed LED spectrometer (JTS-10, BioLogic) with the following detection sequence: 9(200msD) 20msI 10msJ 5(1msD) 5(3msD) 3(10msD) 5(30msD) 8(100ms) where D = detection flash, I = actinic light on, and J = actinic light off, was used. The actinic light in the above sequence was the only light the sample experienced. Samples were measured with and without PhQ, and the bleaching maxima were plotted against time to determine if an external quinone would stave off the PSI bleaching observed in the quinone precursor knockout strain *menD*Δ.

Quinone rescue growth assay

Three *C. reinhardtii* strains were examined: WT (137c genetic background), PsaA-L722Y, and PsaB-L702Y. All strains were grown in TAP media in dim light until reaching approximately mid-log phase (10^6 cells mL^{-1}). Exact cell culture concentrations were measured via hemocytometer (Hausser Scientific), and dilutions performed to 2.0×10^4 cells mL^{-1} into a sterile 12-well plate. For each strain, a concentration gradient of a vitamin K structural analogue (2-methyl-1,4-naphthoquinone, Acrōs Organics) was added at 0, 1, 5 and 25 μM in absolute ethanol (AAPER Alcohol). The 0 μM sample contained an equal volume of absolute ethanol to correct for solvent effects. The well-

plate was placed on an orbital shaker under constant (64μmol photons m^{-2} min^{-1}) light exposure for 6 days when growth patterns could be distinguished. A dark control containing the same components as the assay above was prepared and wrapped in aluminum foil to block out light, placed on the shaker, and monitored daily to distinguish growth patterns.

Light sensitivity growth assays

Strains were grown under low light conditions (≤1 μmol photons) in Tris- acetate-phosphate (TAP) medium[17]. Cultures were diluted to 1.0 x 10^6 and 1.0 x 10^5 cells mL^{-1} and 10 μL was spotted onto agar plates containing either TAP or a medium in which the acetate was replaced by 25 mM sodium bicarbonate (TBP). Plates were incubated at 25 °C in the dark (<0.1 μmol photons m^{-2} s^{-1}), low light (5 μmol photons m^{-2} s^{-1}), or high light (175 μmol photons m^{-2} s^{-1}) and photographed when growth had become apparent.

Immunoblots

Immunoblots were performed on solubilized thylakoid membranes, which were prepared by a modification of Fischer[18]. Here, cells were lysed using a bead beater (BioSpec) with 0.5 mm glass beads for five 30 s bursts separated by 5 minutes on ice. Prepared thylakoid membranes were diluted to approximately equal turbidity levels with buffer containing 5 mM HEPES- KOH (pH 7.5) and 10 mM EDTA, then combined with an equal volume of 2x Laemmli buffer and heated for 30 minutes at 40 °C. Solubilized membranes were cleared of insoluble material by centrifugation (5 minutes at 20,000 x g). Protein concentration of cleared lysates was measured using the bicinchoninic acid

assay (BCA) (Pierce Chemical Company). Samples were diluted to equal protein concentrations with 1x Laemmli buffer, dithiothreitol (DTT) was added to a final concentration of 2 mM, and the samples were heated for 10 minutes at 37 °C. Samples were loaded (30 µg total protein per well) on a 4-12% Bis-Tris gel (Invitrogen) and run as per the recommendations of the manufacturer. Gels were transferred onto 0.45-µm Immobilon-P polyvinylidene fluoride (PVDF) membranes (Millipore) and probed with an anti-PsaA antibody at 1:5,000 as described previously[15]. The secondary goat anti-rabbit HRP antibody was used at 1:10,000 (Bio-Rad), as was the StrepTactin-HRP conjugate for the chemiluminescent molecular weight standard (Bio-Rad). Blots were visualized with ECL (SuperSignal West Femto Chemiluminescent Substrate, Thermo) and imaged using an UltraLum Omega12iC imager. Immunoblot images were quantified with ImageJ software (NIH).

PSI quantification by Joliot-type spectroscopy

As another method of PSI quantification in addition to immunoblotting, P700 was quantified in cells, membranes and particles using a JTS-10 (BioLogic) pulsed LED spectrometer. Samples were diluted to 150 µg mL^{-1} chlorophyll in buffer (20 mM HEPES (pH 7.5), 20% Ficoll) containing 5 mM ascorbate and 10 µM 2,5-dibromo-3-methyl-6-isopropyl benzoquinone (DBMIB). Actinic light from LEDs (530 nm) induced P700 bleaching (oxidation), and measuring flashes (10-µs red LED passed through a 705-nm interference filter) monitored this oxidation and subsequent re-reduction of P700+. The extinction coefficient for P700 is 110,000 µAu μM^{-1} cm^{-1}[22]. Multiplication by 0.8

corrects for measuring at 705 nm while calculation of the literature extinction coefficient was done at 700 nm[23].

PSI purity determined by low temperature fluorescence

Free chlorophyll impurities from antennae in PSI preparations were detected by low temperature fluorescence. As per Henderson *et al.*[24], assays were normalized to 0.75 μg chlorophyll per assay in HE buffer (20 mM HEPES, 1 mM EDTA, pH 7.5) containing 50 ug mL^{-1} β-phycoerythrin as an internal standard and frozen in liquid nitrogen. Using a FluoroMax-3 fluorimeteter (Horiba Jobin Yvon, Middlesex, UK) and attached computer running DataMax v2.2, a scan was taken from 550 nm to 750 nm in 0.5 nm increments with an excitation wavelength at 430 nm or 470 nm. Data was exported to Excel (Microsoft) and plotted.

Time-resolved optical spectroscopy

Laser-flash induced difference absorption kinetics of the mutants were measured in whole cells by collaborator Stefano Santabarbara. Samples were prepared by concentrating the cells to an OD_{680nm} of ~1 by centrifugation followed by resuspension in a buffer of HEPES-NaOH, pH 7.0 and 20% Ficoll (Pharmacia) to prevent sedimentation. The uncoupler carbonylcyanide-*p*-trifluoro-methoxyphenylhydrazone was added to a final concentration of 10 μM to prevent the establishment of long-lived transmembrane electrochemical potentials, which would contribute additional electrochromic signals. Using a home-built pump-probe spectrometer[25,26], several sets of absorption-difference transients were obtained on different culture batches, and then simultaneously

globally fitted by a sum of exponential functions. Lifetimes were considered as global parameters, but pre-exponential factors (such as amplitude) were not globally constrained. The decay-associated spectra (DAS) presented in the Results section were obtained from a weighted average from the independent sets of measurements.

Results

Chemical identity of the C. reinhardtii PSI quinone cofactor

Early research efforts pursued the determination of the exact chemical identity of the quinone cofactor in *C. reinhardtii* PSI. High-performance liquid chromatography (HPLC) methods were developed to isolate the quinone and algal species with different quinones were identified, cultured, and the quinones extracted. However, prior to confirmation of the molecule identity by mass-spectrometry, it was revealed that another research group had identified the quinone as 5'-monohydroxyphylloquinone[27].

Mutants

From the quinone itself, focus was shifted to the binding pocket. The leucine at positions 722 and 706 of PsaA and PsaB, respectively, was mutated to the residues described in Table 2-1, and the change verified by PCR. Recipient strains *psaA-3*Δ and *psaB*Δ were PSI knockouts of the A- and B- sides respectively that were complemented by the appropriate introduced plasmid. For experiments requiring the absence of spectroscopically-confounding extra chlorophylls, the recipient strains P71 *psbA*Δ *psaA-3*Δ and P71 *psbA*Δ *psaB*Δ were used. These strains were PSIΔ, PSIIΔ, and contained low levels of light harvesting complex (LHC). Note that the numbering system used here

reflects that of *Thermosynechococcus elongatus*, to allow for direct comparison with the crystallographic model[7]. It was hypothesized that the leucine to threonine mutation might perturb the position of the quinone headgroup, and that mutations to the larger tryptophan and tyrosine might generate a steric clash and evict at least some fraction of the endogenous quinone.

Effect of an exogenous quinone on P700+re-reduction

The mutant library generated here focused on modifications to the PhQ binding pocket. Out of curiosity, the effect of adding an exogenous quinone to TK membranes of a quinone biosynthesis mutant (*menD1*) was tested. The *menD1* strain is deficient in MenD, which encodes 2-succinyl-6-hydroxy-2,4-cyclohexadiene-1-carboxylate synthase, an enzyme that catalyzes the first step of the phylloquinone biosynthetic pathway in *C. reinhardtii*[21]. In this strain under native conditions, plastoquinone (PQ) is recruited to the empty PhQ binding site. However, PQ is not as effective as an electron transfer intermediate as PhQ. Work by Lefebvre-Legendre and colleagues showed that the addition of exogenous quinone could restore growth of *menD1* under high light on TAP. Figure 2-3 suggests that the addition of exogenous PhQ to *menD1* also ameliorates the loss of P700+ bleaching seen in *menD1*. This initial observation was substantially expanded and published by colleagues who observed that addition of exogenous quinone to already photoinactivated PSI can restore activity and confer resistance to further photoinactivation[28]. While the cited work focused on the observation of a double-reduced quinone in samples experiencing photon bombardment far above any possible

native circumstance, it further bolstered the literature examples of PSI utilizing non-native or exogenous secondary electron acceptors[29,30].

Quinone rescue growth assay

Preliminary results using pump-probe spectroscopy suggested that the proposed steric clash in the PsaA-L722Y mutant between the tyrosine side chain and the native phylloquinone (Table 2-2) led to an eviction of the cofactor in up to 40% of the binding sites[12]. Later observation by FDMR of increased triplet yield in this mutant indicated charge recombination from the [$P700^+A_0^-$] radical pair and supported the preliminary results[12]. With this partially vacant binding site in mind as well as the indiscriminate nature of the PhQ binding site verified above, the possibility of growth-rescue of the photosensitive PsaA-L722Y mutant with an exogenous quinone was pursued.

After seven days of growth under exposure to consistent 64 μmol photons m^{-2} min^{-1} light and varied concentrations of 2-methyl-1,4-naphthoquinone, the growth pattern in Figure 2-4 was observed. It appeared that the PsaA-L722Y mutant was rescued by the addition of the quinone. In the light assay, the PsaA-L722Y mutant with no exogenous quinone showed no growth. In the corresponding dark assay, growth was observed. The addition of 1 μM quinone rescued growth in light for the PsaA-L722Y mutant.

PsaB-L706Y was less light sensitive than PsaA-L722Y as evidenced by its slight growth in the absence of added quinone in the light and similar growth patterns in the dark. This corroborates with later plate-spotted growth assays in Figure 2-5. The addition of 2-methyl-1,4-naphthoquinone here did little to affect the growth of PsaB-L706Y as seen by comparison of the control (0 μM) with the low (1 μM) quinone conditions. It also

appeared that high concentrations of 2-methyl-1,4-naphthoquinone were lethal for the alga, in both light and dark conditions. An interesting observation is the death of WT and PsaB-L706Y cultures in the 5 μM and 25 μM quinone concentration, when compared to the strong growth of the PsaA-L722Y at 5 μM quinone, suggesting that uptake of the molecule (i.e. into the PhQ_A site) reduced the concentration of free quinone.

TK membrane and Photosystem I particle preparation

As was the case with the P700+ re-reduction experiment above, further experimentation on the PhQ binding site mutants required not only cells, but also isolated TK membranes or purified PSI particles. It is known that transformation of either of the parent deletion strains (Table 2-1) with the WT plasmid will fully generate the WT photosynthetic growth phenotype and PSI accumulation[15]. However, mutants PsaA-L722W and PsaB-L722W could not grow photoautotrophically, demonstrated severe light sensitivity, and did not accumulate PSI when assayed by immunoblot (data not shown). They were thus dropped from further analysis. Strains from Table 2-1 that were able to accumulate PSI protein were cultured in large volume and either TK membranes or PSI particles were prepared (Figure 2-2 for preparation images).

Light sensitivity growth assays and immunoblots

Prior to looking at electron transfer from PhQ to F_X, mutants in the WT background (Table 2-1) were assayed for light sensitivity and the amount of PSI accumulation determined by immunoblot.

For the light sensitivity growth assay, cells grown heterotrophically in low light were spotted onto agar plates and then grown under (photo)heterotrophic or photoautotrophic conditions (Figure 2-5). Cells without PSI (*psaAΔ*) are unable to grow under high light, and cannot grow photosynthetically, while WT cells are able to do both. The PsaA-L722T mutant behaved like WT, while the PsaA-L722Y mutant grew barely better than the PSI null mutant. The PsaB-L706Y mutant was intermediate, in that it grew photoheterotrophically under high light, but could not grow photoautotrophically under the same conditions.

The growth characteristics were largely mirrored by the accumulation of PSI, as detected by immunoblot analysis of the PsaA core subunit (Figure 2-6).

One exception to the growth assay and immunoblot correlation is the PsaA-L722Y mutant. Based on PSI accumulation, its growth would have been expected to be close to the WT strain, if the PSI it possessed were equally active. This is the case with the PsaB-L706Y strain. With PsaA-L722Y, it is possible that the increased triplet yield[12] makes the strain less viable in high light.

A similar immunoblot to the one in Figure 2-6 was generated from the P71 Fud7 background (Table 2-1), as the biophysical analyses were completed with this mutant set. The PSI levels seem to be somewhat higher than seen in the WT background, but the results were similar (data not shown). Immunoblot results in both backgrounds were mirrored by P700 quantification by LED pump-probe spectrometry (data not shown).

Time-resolved optical spectroscopy

Summarized in Table 2-3 is the kinetics of PhQ oxidation in the mutant set. The lifetimes τ_1 and τ_2 correspond to transfer in the fast (PhQ_B) and slow (PhQ_A) branches respectively. This data was extracted from kinetic data at selected wavelengths (Figure 2-7) fitted to extract the decay-associated spectra (DAS) (Figure 2-8). Fitting was satisfactory using three experimental functions: the two lifetimes in the submicrosecond timescale, and the nondecaying component reflecting electron transfer reactions involving diffusible electron transport carriers in addition to cytochrome b6f. In order to compare the DAS, they were normalized to maximal bleaching at 430 nm (P700). From Table 2-3, it can be seen that the PsaA-L722T/Y mutants demonstrated a significant acceleration in the kinetics of oxidation on the A-side. The PsaB-L706Y mutant also showed acceleration of oxidation kinetics, especially the B-side. So, in the three mutants, at least one of the two sub-µs components was significantly accelerated.

Discussion

Addition of exogenous quinones restores photosynthetic function in deficient strains

In line with the literature, addition of an exogenous quinone can allow recovery of electron transfer and light-sensitivity issues deriving from hampered electron flow through PSI in deficient strains. Accordingly, it appeared that the light sensitivity of the PsaA-L722Y mutant could be rescued by addition of a vitamin K structural analogue. This is perhaps due to reconstitution of the purportedly partially-vacant PhQ binding site and restoration of forward electron transfer under conditions of high light. In a similar vein, it appears that addition of exogenous quinone to a strain with no quinone present

(*menD*Δ) restored P700+ bleaching not observed in the original *menD*Δ mutant. Disappearance of the P700+ signal can occur as a result of back-reaction when the next electron transfer cofactor (PhQ) is unable to receive and transfer electrons. The native quinone can be replaced fairly promiscuously to allow the photosystem to cope with high light and high electron throughput conditions.

Acceleration of PhQ oxidation kinetics

It is likely that in the mutants, the insertion of larger or more branched side chains than existing in the native site leads to steric hindrances with the phytyl tail of the adjacent PhQ. Since the peptide nitrogen of the residue appears to act as a donor to the C_2-keto oxygen of the phylloquinone on both sides, disruption in this association may result in changes to the stability of the cofactor, and consequently changes in oxidation kinetics. Interestingly, all mutants previously made had only caused retardation of oxidation kinetics[2,11].

In this research, an acceleration of the kinetics of oxidation of either PhQ_A•- or PhQ_B•- was observed in mutants of the conserved Leu residue involved in H-bonding to the respective quinone. In *Synechocystis* sp. PCC 6803, the analogous Leu was mutated to a bulky Trp[31]. The result was a transient EPR spectrum of the P700•+ A_1•- radical pair indicating that the spin density distribution on the phyllosemiquinone was altered in a way consistent with hydrogen-bond weakening. The increase in oxidation kinetics seen here was also interpreted in terms of a weakening of the H-bond to either PhQ_A or PhQ_B. The electron withdrawing character of a hydrogen bond between the peptide nitrogen and the keto-carbonyl would ordinarily stabilize the semiquinone. This would lead to a more

oxidizing midpoint potential. Disruption of the hydrogen bond strength by the addition of the bulky residue would destabilize the PhQ•- anion, shift the reduction potential toward the negative, and increase the kinetics of oxidation. Provided that the selected mutation did not modify the standard midpoint potential of the F_X, there exists a larger forward driving force for PhQ to F_X. Interestingly, it was recently suggested, based on EPR analysis, that the PsaA-L722T mutation results in introduction of an additional hydrogen bond between the PhQ_A and the threonine side chain OH group[32]. It appears that the resulting increase in midpoint potential of the quinone and subsequent increase in activation energy is offset by a slightly stronger electronic coupling between PhQ_A to F_X, explaining the overall increase in rate.

Here it has been demonstrated that the quinone cofactor is an essential, yet readily modified PSI electron transfer component. The identification of accelerated oxidation kinetics in this mutant set are the first presented in this organism, and raise an interesting challenging to increase electron transfer rates with additional novel destabilizing mutations.

Table 2-1: Mutants constructed to have an effect on the PhQ binding pocket.

A-side	Recipient strain	B-side	Recipient strain
PsaA-L722T	*psaA-3*Δ	--	--
PsaA-L722W	*psaA-3*Δ	PsaB-L706W	*psaB*Δ
PsaA-L722Y	*psaA-3*Δ	PsaB-L706Y	*psaB*Δ
PsaA-L722T	P71 *psbA*Δ *psaA-3*Δ	--	--
PsaA-L722W	P71 *psbA*Δ *psaA-3*Δ	PsaB-L706W	P71 *psbA*Δ *psaB*Δ
PsaA-L722Y	P71 *psbA*Δ *psaA-3*Δ	PsaB-L706Y	P71 *psbA*Δ *psaB*Δ

Table 2-2: Projected result of mutations.

Mutation	Relevant amino acid	Predicted result on incorporation
PsaA-L722T	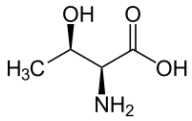	Perturb the position of the quinone headgroup.
PsaA-L722W	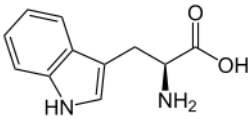	Steric clash, evict the endogenous quinone.
PsaA-L722Y	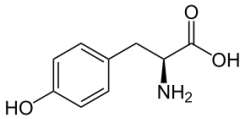	Steric clash, evict the endogenous quinone.
PsaB-L706W	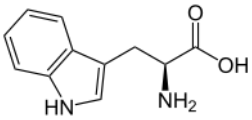	Steric clash, evict the endogenous quinone.
PsaB-L706Y	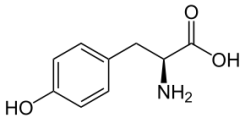	Steric clash, evict the endogenous quinone.

Table 2-3: Fit parameters describing the kinetics of ET in WT and mutant PS I

	lifetimes[a]		
	τ_1 (ns)	τ_2 (ns)	τ_3 (μs)
control	22±2	256±12	6.2±0.4
PsaA-L722T	24±2	171±10	6.4±0.3
PsaA-L722Y	18±3	205±22	6.4±0.6
PsaB-L706Y	11±4	197±15	5.7±0.8

[a]Lifetimes of the three exponential decay components obtained by global fitting of ET kinetics in whole cells expressing WT and mutant PSI.

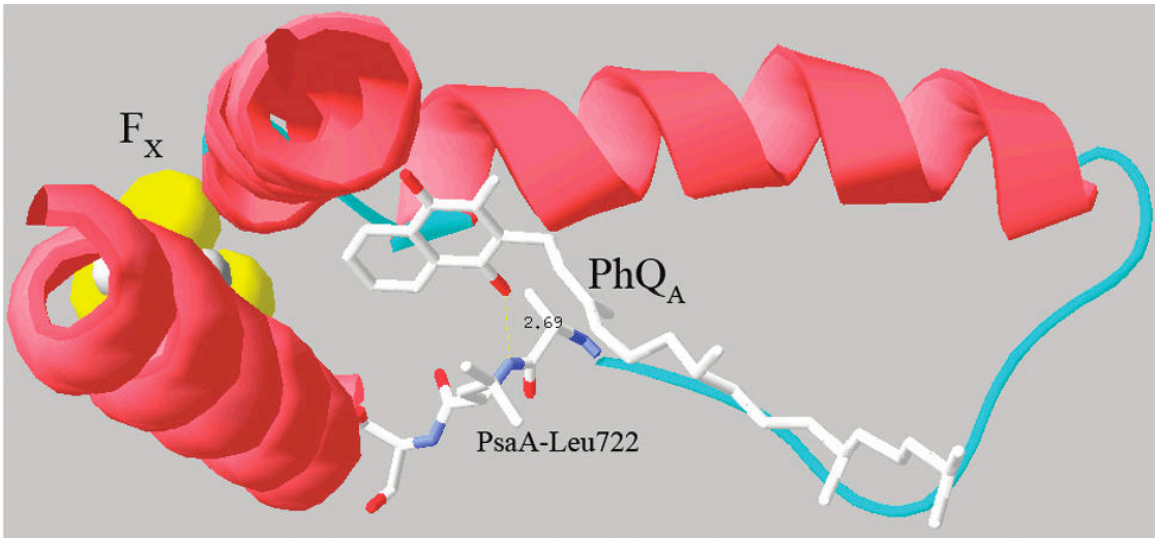

Figure 2-1: The PhQ_A binding site and targeted residue. The binding site is seen from 'above' the PhQ, with the residue (PsaA-Leu722) targeted in this study (along with the residues immediately before and after) shown as stick figures. Figure made by Swiss-PDBViewer derived from the 2.5-Å crystal structure coordinates of PS I from *T. elongatus* (1JB0)[7]. The putative H-bond involving Leu722 and PhQA is shown as a dotted yellow line (distance of 2.69 Å). This figure is unmodified from reference[12].

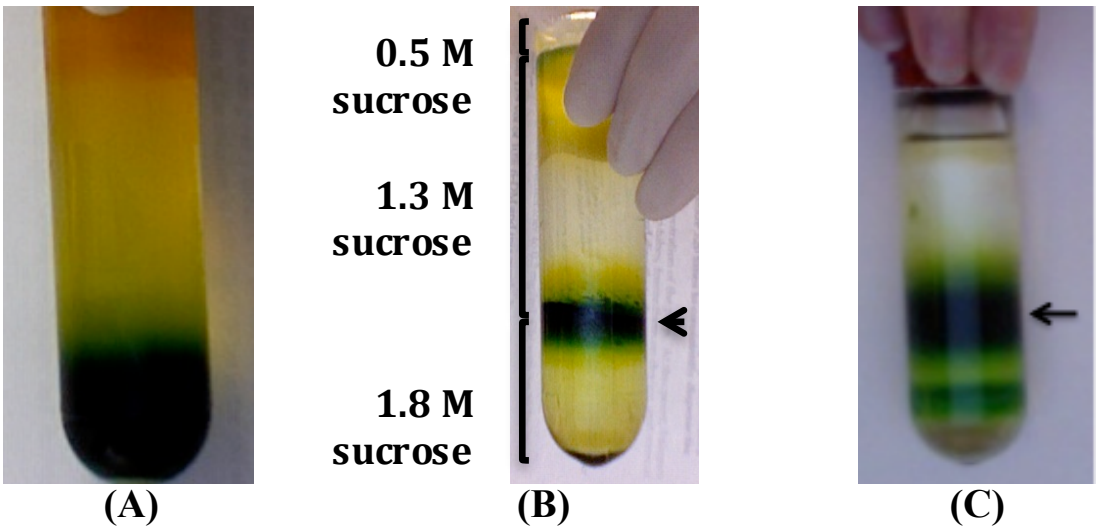

Figure 2-2: Purification of thylakoid (TK) membranes and Photosystem I (PSI) particles. (A) Washes remove carotenoids (orange) from crude TK membranes. (B) TK membrane separation occurs on a discontinuous sucrose gradient. (C) Isolation of PSI particles is performed on a continuous sucrose gradient.

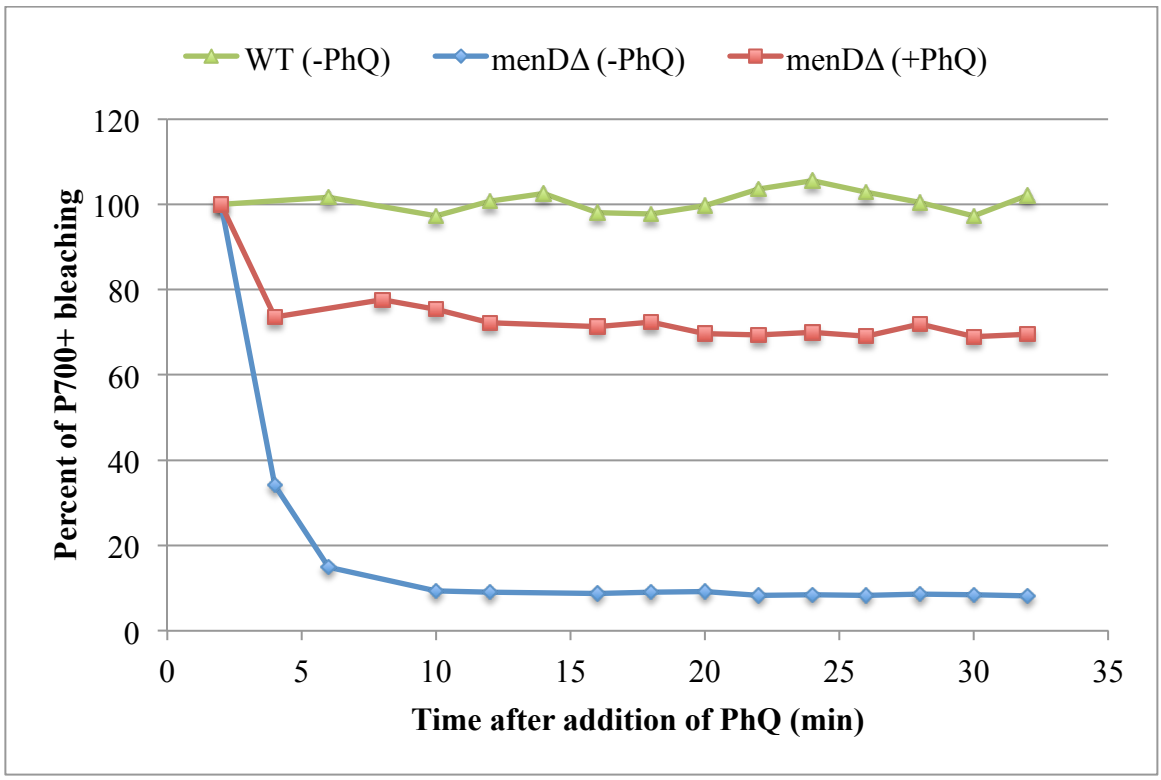

Figure 2-3: Addition of PhQ to PSI particles from a *menD*Δ strain ameliorates the loss of P700+ bleaching seen in the native state. PSI particles were diluted to 50 µM total chlorophyll and photobleaching of P700+ was detected using a pulsed LED spectrometer. Where required, phylloquinone in ethanol was added at 2.2 µM. The loss of P700+ bleaching was plotted against time after adding PhQ.

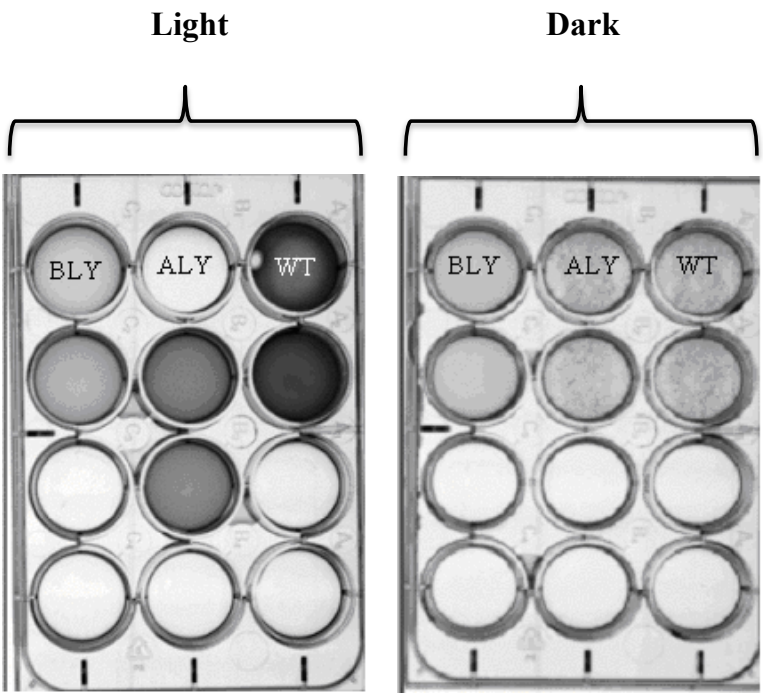

Figure 2-4: Quinone rescue growth assay. For rows top to bottom, cultures of equal cell density contain 0, 1, 5, and 25 μM 2-methyl-1,4-naphthoquinone in absolute ethanol and were cultured in light or dark conditions as noted.

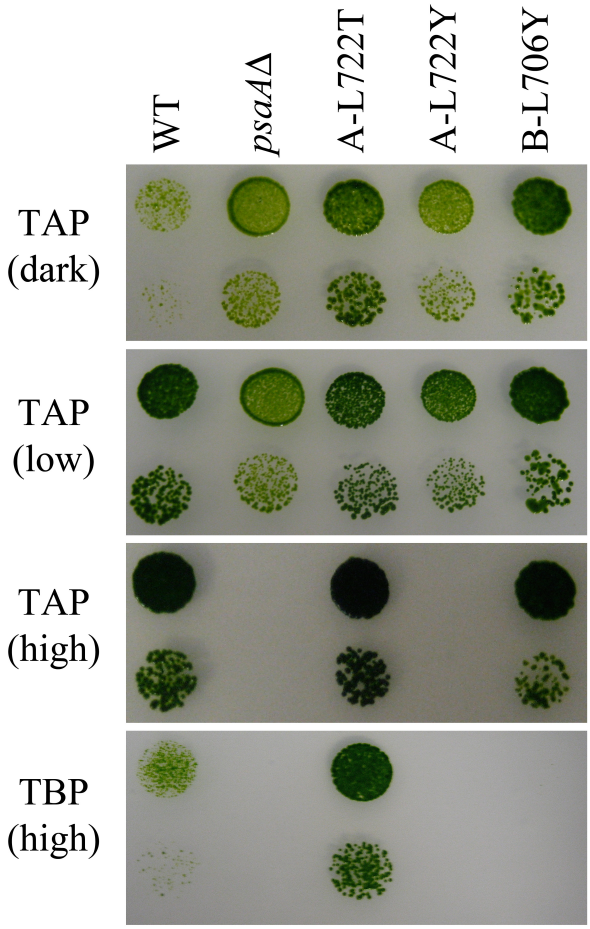

Figure 2-5: Growth tests of PhQ binding site mutants. Cultures grown to late log phase in TAP medium under low illumination were spotted onto agar plates (10 µL) containing acetate (TAP) or bicarbonate (TBP) as carbon sources. After drying, plates were transferred to different light conditions: dark (<0.1 µEinstein m^{-2} s^{-1}), low light (~5 µEinstein m^{-2} s^{-1}), and high light (~175 µEinstein m^{-2} s^{-1}).

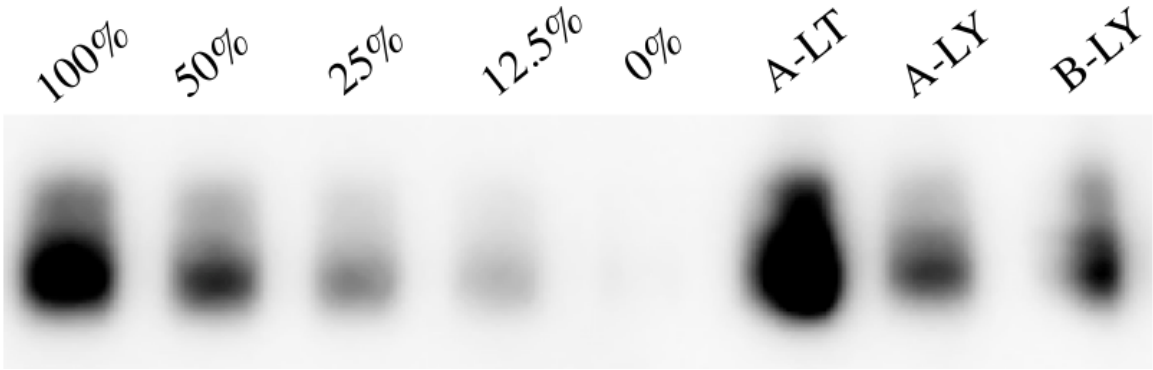

Figure 2-6: PsaA immunoblot for the estimation of cellular PSI accumulation. The same strains as shown in Figure 2-5 were grown further in liquid TAP medium under low light, harvested, washed, and lysed. Crude cellular membranes were separated from soluble components and solubilized by heating with 2% SDS. Each well was loaded with 30 μg of solubilized membrane protein. A standard series was created by serial 2-fold dilutions of the WT extract (100%) into the *psaAD* extract (0%). The gel was blotted and probed with an anti-PsaA antibody. A standard curve based on quantification of the PsaA band allowed estimation of PsaA levels in the PsaA-L722T (147%), PsaA-L722Y (50%) and PsaB-L706Y (47%) mutants.

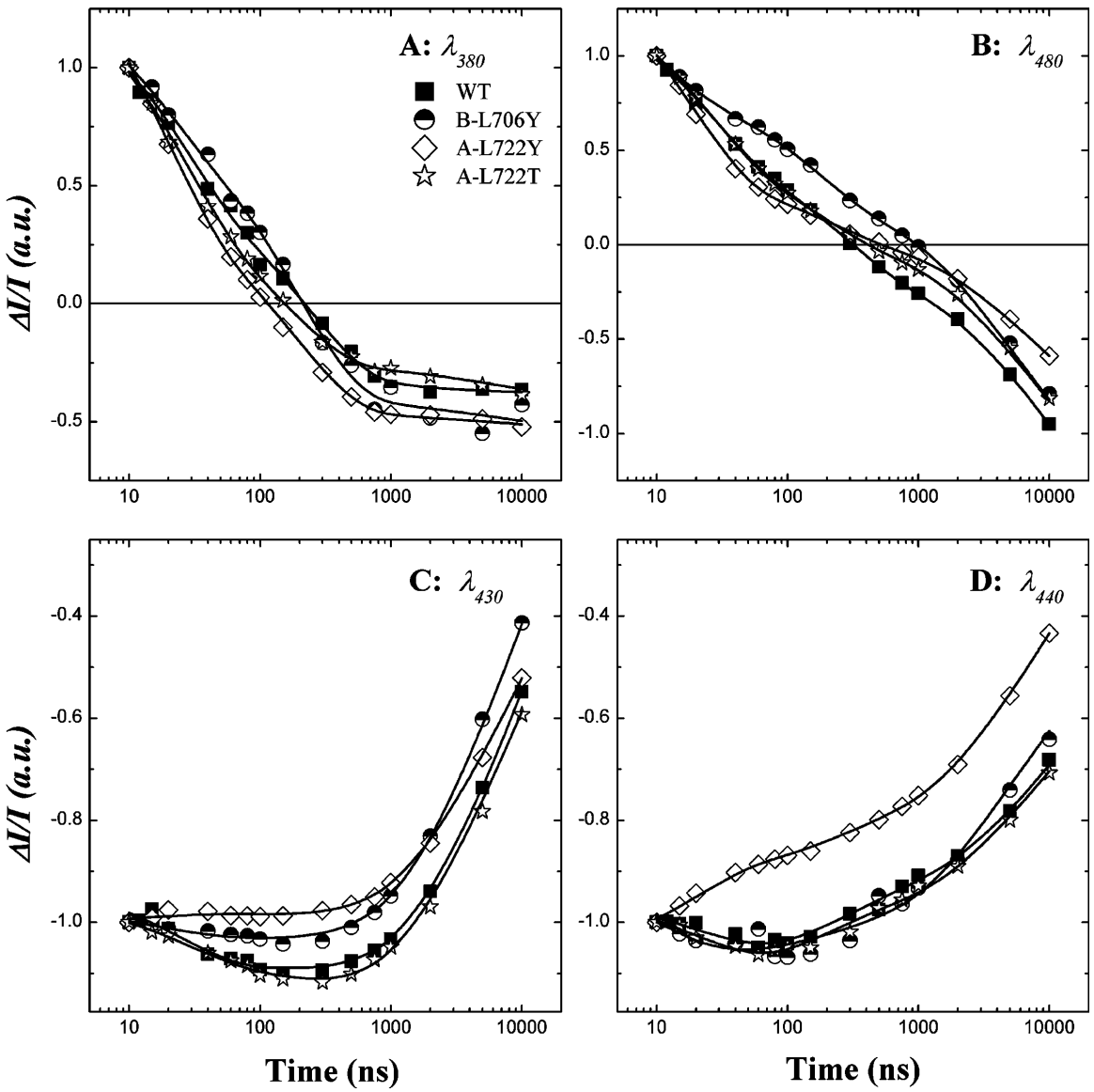

Figure 2-7: Kinetics of laser-flash photolysis in the B-LY, A-LY and A-LT mutants. Values in mutants were compared to WT and recorded at different observation wavelengths. WT = square, B-LY = circle, A-LY = diamond, and A-LT = star. Solid lines are lines of best fit, and all kinetics are normalized on initial amplitude while maintaining the original polarization (bleach/rise). Figure is inserted unmodified from cited paper[12].

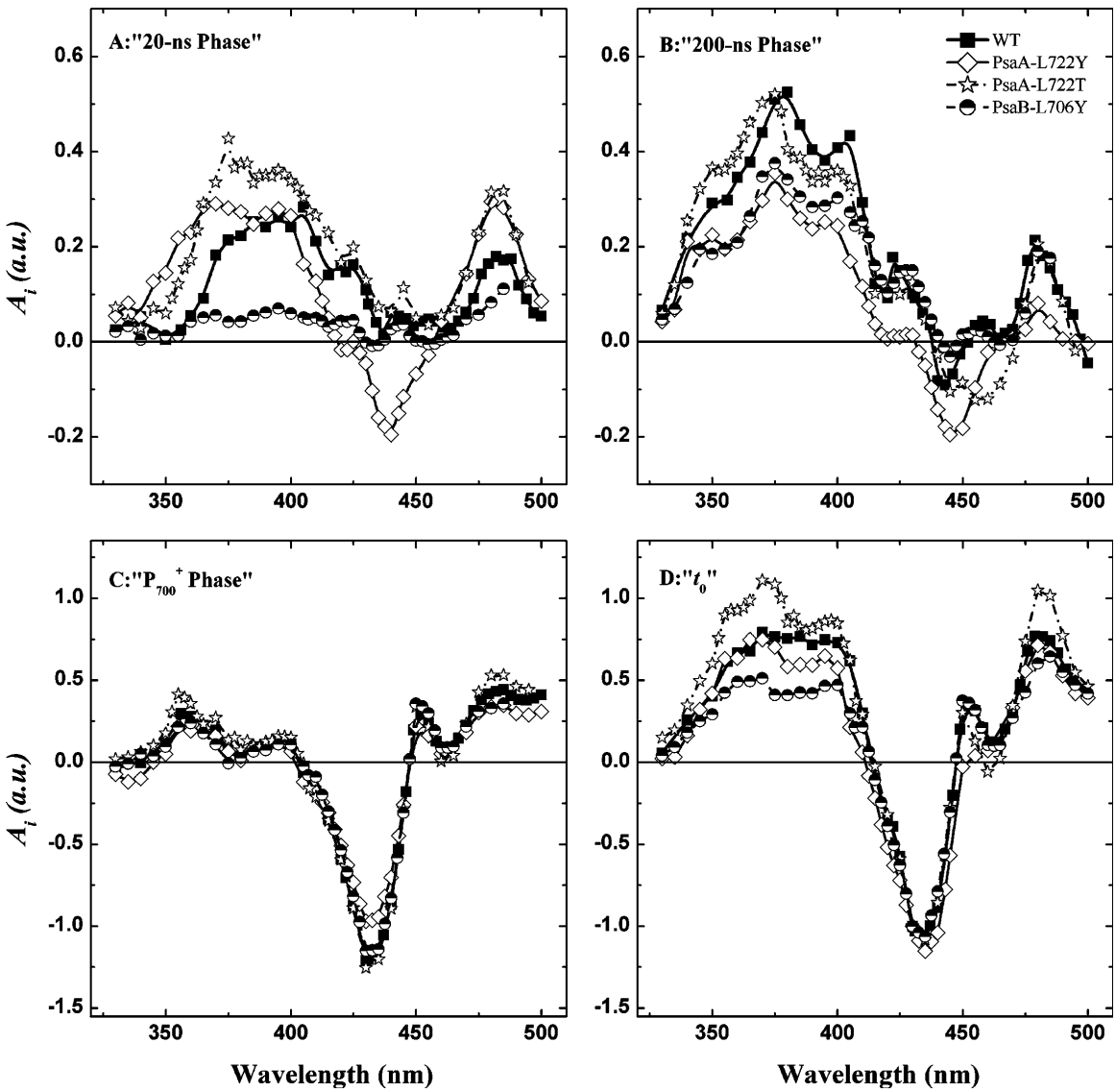

Figure 2-8: Decay-associated spectra (DAS). Shown are τ_1 = 10-30 ns (A), τ_2 = 150-260 ns (B), τ3 = 6 µs (C), extrapolation at t_0 of the decaying components (D). Control: thick, solid lines. A-LY = open diamonds, dashed lines. A-LT = open stars, dashed-dotted lines. B-LY = solid circles, dotted lines. Spectra were internally normalized on bleaching (430 nm) of the t = 0 spectrum. Figure is inserted unmodified from cited paper[12].

References

[1] Brettel K, Leibl W. Electron transfer in Photosystem I. Biochim Biophys Acta 2001;1507(1-3):100–114.

[2] Santabarbara S, Heathcote P, Evans MCW. Modelling of the electron transfer reactions in Photosystem I by electron tunnelling theory: The phylloquinones bound to the PsaA and the PsaB reaction centre subunits of PS I are almost isoenergetic to the iron–sulfur cluster F_X. Biochim Biophys Acta 2005;1708(3):283–310.

[3] Srinivasan N, Golbeck JH. Protein–cofactor interactions in bioenergetic complexes: The role of the A_{1A} and A_{1B} phylloquinones in Photosystem I. Biochim Biophys Acta 2009;1787(9):1057–1088.

[4] Guergova-Kuras M, Boudreaux B, Joliot A, Joliot P, Redding K. Evidence for two active branches for electron transfer in Photosystem I. Proc Natl Acad Sci U S A 2001;98(8):4437–4442.

[5] Li Y, van der Est A, Lucas M-G, Ramesh VM, Gu F, Petrenko A, Lin S, Webber AN, Rappaport F, Redding K. Directing electron transfer within Photosystem I by breaking H-bonds in the cofactor branches. Proc Natl Acad Sci U S A 2006;103(7):2144–2149.

[6] Byrdin M, Santabarbara S, Gu F, Fairclough WV, Heathcote P, Redding K, Rappaport F. Assignment of a kinetic component to electron transfer between iron–sulfur clusters F_X and $F_{A/B}$ of Photosystem I. Biochim Biophys Acta 2006;1757(11):1529–1538.

[7] Jordan P, Fromme P, Witt HT, Klukas O, Saenger W, Krauss N. Three-dimensional structure of cyanobacterial Photosystem I at 2.5 angstrom resolution. Nature 2001;411(6840):909–917.

[8] Ben-Shem A, Frolow F, Nelson N. Crystal structure of plant Photosystem I. Nature 2003;426(6967):630–635.

[9] Moser C, Dutton PL. Application of Marcus Theory to Photosystem I Electron Transfer. In: Advances in Photosynthesis and Respiration, Golbeck J, editor. Vol. 24. Springer Netherlands, 2006. p. 583–594.

[10] Munge B, Das SK, Ilagan R, Pendon Z, Yang J, Frank HA, Rusling JF. Electron Transfer Reactions of Redox Cofactors in Spinach Photosystem I Reaction Center Protein in Lipid Films on Electrodes. J Am Chem Soc 2003;125(41):12457–12463.

[11] Rappaport F, Diner BA, Redding K. Optical measurements of secondary electron transfer in Photosystem I. In: Photosystem I. Springer, 2006. p. 223–244.

[12] Santabarbara S, Reifschneider K, Jasaitis A, Gu F, Agostini G, Carbonera D, Rappaport F, Redding KE. Interquinone Electron Transfer in Photosystem I As Evidenced by Altering the Hydrogen Bond Strength to the Phylloquinone(s). J Phys Chem B 2010;114(28):9300–9312.

[13] Li Y, Lucas MG, Konovalova T, Abbott B, MacMillan F, Petrenko A, Sivakumar V, Wang R, Hastings G, Gu F, van Tol J, Brunel LC, Timkovich R, Rappaport F, Redding K. Mutation of the Putative Hydrogen-Bond Donor to P700 of Photosystem I. Biochemistry 2004;43(39):12634–12647.

[14] Picard V, Ersdal-Badju E, Lu A, Bock SC. A rapid and efficient one-tube PCR-based mutagenesis technique using Pfu DNA polymerase. Nucleic Acids Res 1994;22(13):2587–2591.

[15] Redding K, MacMillan F, Leibl W, Brettel K, Hanley J, Rutherford AW, Breton J, Rochaix J-D. A systematic survey of conserved histidines in the core subunits of Photosystem I by site-directed mutagenesis reveals the likely axial ligands of P700. EMBO J 1998;17(1):50–60.

[16] Boynton JE, Gillham NW, Harris EH, Hosler JP, Johnson AM, Jones AR, Randolph-Anderson BL, Robertson D, Klein TM, Shark KB. Chloroplast transformation in *Chlamydomonas* with high velocity microprojectiles. Science 1988;240(4858):1534–1538.

[17] Harris EH, Stern DB, Witman G. The *Chlamydomonas* Sourcebook. San Diego: Academic Press, 1989.

[18] Fischer N, Sétif P, Rochaix JD. Targeted mutations in the *PsaC* gene of *Chlamydomonas reinhardtii*: preferential reduction of F_B at low temperature is not accompanied by altered electron flow from Photosystem I to ferredoxin. Biochemistry 1997;36(1):93–102.

[19] Ohad I, Adir N, Koike H, Kyle DJ, Inoue Y. Mechanism of photoinhibition *in vivo*. A reversible light-induced conformational change of reaction center II is related to an irreversible modification of the D1 protein. J Biol Chem 1990;265(4):1972–1979.

[20] Porra RJ, Thompson WA, Kriedemann PE. Determination of accurate extinction coefficients and simultaneous equations for assaying chlorophylls a and b extracted with four different solvents: verification of the concentration of chlorophyll standards by atomic absorption spectroscopy. Biochim Biophys Acta 1989;975(3):384–394.

[21] Lefebvre-Legendre L, Rappaport F, Finazzi G, Ceol M, Grivet C, Hopfgartner G, Rochaix JD. Loss of phylloquinone in *Chlamydomonas* affects plastoquinone pool size and Photosystem II synthesis. J Biol Chem 2007;282(18):13250-13263.

[22] Krabben L, Schlodder E, Jordan R, Carbonera D, Giacometti G, Lee H, Webber AN, Lubitz W. Influence of the Axial Ligands on the Spectral Properties of P700 of Photosystem I: A Study of Site-Directed Mutants. Biochemistry 2000;39(42):13012–13025.

[23] Gulis G, Narasimhulu KV, Fox LN, Redding KE. Purification of His_6-tagged Photosystem I from *Chlamydomonas reinhardtii*. Photosynth Res 2008;96(1):51–60.

[24] Henderson JN. Disassembly and Degradation of Photosystem I in an *in vitro* System Are Multievent, Metal-dependent Processes. J Biol Chem 2003;278(41):39978–39986.

[25] Santabarbara S, Jasaitis A, Byrdin M, Gu F, Rappaport F, Redding K. Additive effect of mutations affecting the rate of phylloquinone reoxidation and directionality of electron transfer within photosystem I. Photochem Photobiol 2008;84(6):1381–1387.

[26] Béal D, Rappaport F, Joliot P. A new high-sensitivity 10-ns time-resolution spectrophotometric technique adapted to *in vivo* analysis of the photosynthetic apparatus. Rev Sci Instrum 1999;70(1):202–207.

[27] Ozawa SI, Kosugi M, Kashino Y, Sugimura T, Takahashi Y. 5'-Monohydroxyphylloquinone is the Dominant Naphthoquinone of PSI in the Green Alga *Chlamydomonas reinhardtii*. Plant Cell Physiol 2012;53(1):237–243.

[28] McConnell MD, Cowgill JB, Baker PL, Rappaport F, Redding KE. Double Reduction of Plastoquinone to Plastoquinol in Photosystem 1. Biochemistry 2011;50(51):11034–11046.

[29] Itoh S, Iwaki M, Ikegami I. Modification of Photosystem I reaction center by the extraction and exchange of chlorophylls and quinones. Biochim Biophys Acta 2001;1507(1-3):115–138.

[30] Biggins J. Evaluation of selected benzoquinones, naphthoquinones, and anthraquinones as replacements for phylloquinone in the A1 acceptor site of the Photosystem I reaction center. Biochemistry 1990;29(31):7259–7264.

[31] Srinivasan N, Karyagina I, Bittl R, van der Est A, Golbeck JH. Role of the Hydrogen Bond from Leu722 to the A_{1A} Phylloquinone in Photosystem I. Biochemistry 2009;48(15):3315–3324.

[32] Mula S, McConnell MD, Ching A, Zhao N, Gordon HL, Hastings G, Redding KE, van der Est A. Introduction of a Hydrogen Bond between Phylloquinone PhQ Aand a Threonine Side-Chain OH Group in Photosystem I. J Phys Chem B 2012;116(48):14008–14016.

Chapter 3

Expression of the [FeFe]-hydrogenase in the chloroplast of *Chlamydomonas reinhardtii*

Abstract

Biologically generated hydrogen from phototrophic organisms is a promising source of renewable fuel. The nuclear-expressed [FeFe]-hydrogenase from *Chlamydomonas reinhardtii* has an extremely high turnover rate, and so has been a target of intense research. Here, it is demonstrated that a codon-optimized native hydrogenase can be successfully expressed in the chloroplast. At the same time, a curiously strong negative selective pressure was observed against unregulated hydrogenase expression in this location. Successful management of the system was attained with a vitamin-sensitive gene repression system. This represents the first example of a nuclear-expressed, chloroplast-localized metalloprotein being synthesized *in situ.* Control of this process opens up several bioengineering possibilities for the production of biohydrogen fuel.

Introduction

There is a need for clean, renewable, and domestically sourced energy. Research efforts toward this goal have been both varied and substantial, with the generation of fuel from algal species considered a viable option. Compared to other biological sources, algae have a space-efficient growth habit, do not compete for agricultural land, and possess the ability to co-produce high value products that can subsidize initial energy production efforts. Green algae have demonstrated their efficiency in producing biodiesel[1], but there is also substantial interest in using green algae for the production of H_2. Green algae contain a native enzyme capable of producing H_2 using only protons, electrons, and energy derived from water and solar radiation.

Hydrogenases

There are two main classes of hydrogenases that catalyze the reversible oxidation of H_2 ($H_2 \leftrightarrows 2H^+ + 2e^-$). The [NiFe]- and [FeFe]-hydrogenases are so named for the metals in their enzyme active sites[2,3]. The nickel-iron [NiFe]-hydrogenases can be larger than the [FeFe] class, are often multimeric, and readily catalyze the oxidation of H_2. Of interest here is the [FeFe]-hydrogenase. These frequently small and simple enzymes often possess a bias toward rapid H_2 production. Rates upwards of 50 to 100 times that of [NiFe]-hydrogenases have been measured in [FeFe] enzymes[2,4-7]. As such, they are model candidates for engineering efforts. The [FeFe] enzyme in the green algae *Chlamydomonas reinhardtii* is among the smallest hydrogenases characterized to date. It lacks the additional [4Fe-4S] clusters seen in bacterial [FeFe]-hydrogenases that hypothetically function in electron transfer to and from redox mediators or the physiological partner[8,9]. Its reaction rate does not appear to suffer, however, and its simplicity makes it an ideal candidate for study. The catalytic centre of the enzyme (the 'H-cluster') consists of a binuclear iron subcluster with three CO ligands, two CN ligands, and a bridging azadithiolate. The nature of the bridging atom in the dithiolate has been hotly contested, with initial structural interpretations from *Desulfovibro desurfuricans* indicating that it was carbon-based[9,10]. However, later structural interpretations supported the presence of a nitrogen bridgehead[11,12], and this was further reinforced by new research showing activation of the apoprotein only by using an active site mimic containing a nitrogen bridgehead in the dithiolate ligand[13,14]. In the natural system, the catalytically active 2Fe subcluster is linked to a [4Fe-4S] cluster via a single bridging cysteine.

One hypothesized mechanism for the generation of hydrogen proceeds by a catalytic cycle [15-19] wherein one turn results in restoration of the starting $Fe_P(I)Fe_D(II)$ state and the release of H_2. Unfortunately for production goals, [FeFe]-hydrogenases are quickly and irreversibly inactivated by oxygen. Bound O_2 at the distal Fe of the subcluster is hypothesized to be converted to superoxide by a one electron reduction, and either migrates the short distance to oxidize the $[4Fe\text{-}4S]^{2+}$ cluster, or stays bound and destroys the cluster via a through-bond electron transfer from the $[4Fe\text{-}4S]^{2+}$ cluster[20,21]. The mechanism of destruction of the cluster by O_2 was only recently elucidated, but the inhibitory effect of oxygen on hydrogen production has been known since the uptake and evolution of hydrogen in green algae was first observed by Gaffron and Rubin over seventy years ago[8,22-27]. Among other hypotheses, computational and experimental studies have suggested that the substantial difference in O_2 stability between [NiFe]- and [FeFe]-hydrogenases is in part due to differences in size and polarity of gas channels in the different proteins[28,29]. Significant effort is being applied to the understanding and remediation of oxygen sensitivity in the [FeFe]-hydrogenases as some degree of oxygen stability will likely be required for feasible commercial-scale hydrogen production.

In the time since Gaffron and Rubin first observed hydrogen production in green algae, substantial progress has been made in untangling the genetics, biochemistry and metabolic networks involved[15,30].

Genetics and expression of hydrogenase

In the model organism *Chlamydomonas reinhardtii*, two [FeFe]-hydrogenases have been identified: HydA1 and HydA2. HydA2 is 74% similar and 68% identical to HydA1[22,31]. Both hydrogenases are able to catalyze H_2 production from either fermentative or photosynthetic pathways, but HydA1 is the dominant isoform. Photoproduction of H_2 from HydA2 is approximately 25% of that from HydA1[23,25].

Both HydA1 and HydA2 are encoded in the nucleus, but function in the chloroplast[25,32]. The *HYDA1* gene codes for a mature protein of 441 amino acids. As the 56 N-terminal amino acids are not found in the purified protein, this region likely functions as a transport peptide. In addition, a putative peptidase cleavage site (VACA) is located at the end of the fragment [33-37]. The residues here are also rich in hydroxylated and basic amino acids, a property that has been seen in chloroplast-transit peptides[36,37], further supporting chloroplast import.

Maturation of the hydrogenase appears to be a highly choreographed process involving at least three additional protein cofactors: HYDE, HYDF and HYDG. In *C. reinhardtii*, the HYDEF protein contains two regions that are homologous to two separate bacterial proteins. In *C. reinhardtii*, HYDEF and HYDG both contain transit peptides[30,38], indicating that they are also brought into the chloroplast to function in *in situ* maturation of a functional hydrogenase. A crystal structure of the *C. reinhardtii* hydrogenase apoprotein prepared in the absence of maturation factors shows the presence of the [4Fe-4S] cluster, but not the 2 Fe subcluster moiety, suggesting stepwise assembly of the H-cluster[39,40] with the [4Fe-4S] moiety being inserted prior to the 2Fe subcluster. The [4Fe-4S] unit does not appear to require the assistance of the maturases,

and is likely assembled by native iron-sulfur machinery that is not hydrogenase-specific[20,41-44]. The same apoprotein can be activated to full H_2 production functionality with only a 2Fe subcluster mimic [45].

Assembly and transport of the di-iron subcluster then is the job of the maturases. Maturases HydE and HydG are radical S-adenosyl methionine (SAM) proteins[46] that build the Fe subcluster and synthesize its attendant CO and CN ligands. HydF is actually a GTPase, and appears to act as a scaffolding protein during the construction process[20,47-49].

Electron sources for hydrogenase

Once the enzyme is constructed and functional, electrons for photosynthetic H_2 production can be obtained from the light-driven oxidation of water at PSII. It was observed however, that *C. reinhardtii* is also able to produce hydrogen in the presence of the PSII-inhibitor 3-(3,4-dichlorophenyl)-1,1-dimethylurea (DCMU)[43,50], indicating that there is a source of electrons in addition to those derived from water-splitting. Electrons for PSII-independent hydrogen production likely derive from catabolic fermentative processes[2,25,51-55]. Reducing equivalents coming out of Glycolysis or the Citric Acid Cycle appear to donate their electrons to the photosynthetic electron transport chain[56,57]. It is interesting to note that no H_2 photoproduction is observed in the presence of cytochrome b_6f inhibitor 2,5-dibromo-3-methyl-6-isopropyl benzoquinone (DBMIB), suggesting that this additional source of electrons must enter the chloroplast electron transport chain before cytochrome b_6f. Electrons from Glycolysis and the Citric Acid Cycle are thought to enter at the Q-cycle by way of an NAD(P)H

reductase[58,59]. Figure 1-2 in Chapter 1 presents a relevant general electron transfer schematic.

Physiological role of hydrogenases

In the absence of oxygen, algae switch their metabolism to fermentation[60,61]. In the light, they degrade starch via Glycolysis, and hydrogen gas is evolved as a byproduct[20,62]. The persistence of the anaerobically induced hydrogenase in largely aerobic organisms is likely because the enzyme ensures organism survival under transiently experienced anaerobic conditions. Under anaerobic conditions, H_2 evolution appears to be a primary way of maintaining electron transfer, and thus proton pumping, and hence the production of ATP [2,10,25,63]. As oxygen is the terminal electron acceptor for respiration, accumulated reducing equivalents under anaerobic conditions cannot be oxidized without hydrogenase. The hydrogenase thus appears to act as a bleed valve and oxidizes excess reducing equivalents. H_2 is a nontoxic and highly diffusible means of disposing of excess electrons[64].

Current methods of algal H_2 production

Hydrogen production from green algae is stimulated *in vivo* by inducing an anaerobic state. Early work used nitrogen or argon to physically flush oxygen from cultures, while maintaining the samples in the dark to prevent any photosynthetic O_2 evolution. An additional method was developed when a lack of sulfur in growth media was observed to result in a decrease in the rate of oxygenic photosynthesis[65] due to degradation of PSII, while at the same time maintaining the rate of mitochondrial

respiration[2]. As a result, electrons from residual PSII activity still feed the hydrogenase [53,55,66-69], but anaerobiosis is maintained by consumption of PSII-generated O_2, and the hydrogenase is active under light conditions. Under these conditions, low-level hydrogen production has been sustained in the light over several days[2]. This is a significant improvement over the hydrogenase inactivation in a matter of minutes when a dark and anaerobic culture is exposed to light[8]. Under those conditions, the burst of hydrogen produced from electrons from PSII is almost immediately inactivated by the O_2 also produced at PSII.

Unfortunately, the sulfur-deprivation process is not without flaws. Temporal separation of photosynthetic oxygen evolution and carbon accumulation from metabolite catabolism and H_2 production addresses the vexing problem of oxygen sensitivity of the [FeFe]-hydrogenase, but the adaptation is time-intensive, and the absence of sulfur is detrimental to production of cellular proteins[10] and eventually lethal for the cells.

In order to circumvent some of the difficulties inherent in natural systems, some researchers have pursued *in vitro* fusion concepts. Ihara and colleagues were successful in creating a hydrogen-producing fusion between PsaE of the cyanobacterium *Thermosynechococcus elongatus* and the membrane-bound [NiFe]-hydrogenase from the bacterium *Ralstonia eutropha*[11]. Yacoby and colleagues circumvented the significant loss of photosynthetic electrons toward NADPH production by directly fusing the *C. reinhardtii petF* ferredoxin gene to *HYDA1* with a linker peptide and expressing the fusion in *E. coli*[13]. Lubner and colleagues obtained outstanding hydrogen production rates by using a 1,6-hexanedithiol 'wire' to link the [FeFe]-hydrogenase enzyme from

Clostridium acetobutylicum to PSI from the same organism[16] or from *Synechococcus* sp. PCC 7002[18,70] in the presence of artificial electron donors.

In Appendix 2 of this dissertation, the design of an *in vivo* fusion of the PsaC subunit of *C. reinhardtii* PSI with the native hydrogenase is described. In this arrangement, the substantial electron flow coming out of PSI would be routed through a fused hydrogenase and used to make biohydrogen. This system has the benefit of functioning *in vivo* and requiring only native components. If successful, this would present a system amenable to scalable hydrogen production. In order to proceed with the fusion however, demonstration of the feasibility of expressing a hydrogenase in the chloroplast was required. The biosynthesis of metalloproteins, of which hydrogenase is one type, often includes a complicated network of transport peptides, cofactors, maturases and chaperones. The chloroplast expression and functionality demonstrated here with the *C. reinhardtii* hydrogenase presents the first example of synthesis and function of a transported metalloprotein *in situ*.

Materials and Methods

Growth conditions

Unless otherwise noted, *C. reinhardtii* strains FUD50 (Institut de Biologie Physico-Chimique, Paris)[15], A31 (Silvia Ramundo, Université de Genève)[20], *hydA1-1 hydA2-1* (Matthew Posewitz, Colorado School of Mines)[23], and a 137c wild type (WT) were cultured in Tris- acetate- phosphate (TAP) media[25,71] under ambient light with agitation. The minimal media Tris- bicarbonate- phosphate (TBP) was prepared as for TAP but replaced acetic acid with 25 mM bicarbonate and was titrated to pH 7.0.

Where required, the antibiotics ampicillin (Fisher) and spectinomycin (Gold Biotechnology) were used at 100 mg L^{-1} unless otherwise noted. Vitamins B_1 (Acros) and B_{12} (Sigma Aldrich) were used at 50 μM and 37 nM respectively.

Construction of cphydA plasmids pKTR1 and pKTR3

Two plasmids were constructed to introduce the chloroplast codon-optimized *HYDA1* gene (henceforth cp*hydA*) into the chloroplast of a recipient algal strain. Both are depicted in Figure 3-1. Plasmid pKTR1 and pKTR3 share the hydrogenase gene, as well as the regions of chloroplast homology to guide directed insertion by homologous recombination. Plasmid pKTR3 contains an aminoglycoside resistance cassette (*aadA*), which eliminates the need for co-transformation with a selectable marker that was required with the first iteration of the construct (pKTR1).

Construction of pKTR1

Plasmid pKTR1 (Figure 3-1) was constructed by cutting the codon-optimized *HYDA1* gene out of its pET-Duet vector (modified from the original[27,72] by and obtained by us from Matthew Posewitz, National Renewable Energy Lab) with complete BglII and partial NcoI digestions. This gene codes for the sequence of the mature hydrogenase protein, with an N-terminal hexahistidine (His_6) tag replacing the signal peptide. The chloroplast expression vector cg13 containing the *atpB* locus and flanking areas (provided by Jörg Nickelsen, Ludwigs-Maximilians Universität München) was cut with BamHI and NcoI. Ligation of the linearized cg13 and pETDuet-*HYDA1* insert was performed with the USB Ligate-IT kit then transformed into chemically competent cells

(NEB). Colonies selected on ampicillin (100 mg L^{-1}) were test digested and submitted for sequencing (ASU DNA Laboratory).

Construction of pKTR3

Plasmid pKTR1 was linearized with EcoRV, which cuts between the 5'-*psbD* UTR and *atpB* flanking region. An internal spectinomycin cassette (*aadA*) flanked by direct repeats of the *psbC*-promoter/5'-UTR (untranslated region) was excised from plasmid pKR102[22,40] with ClaI and SphI. The *aadA* cassette and repeats fragment was blunted using 'Quick Blunting Kit' (NEB) followed by blunt-end ligation with EcoRI-linearized pKTR1 at a insert:vector molar ratio of 3:1 and transformed into NEB5α (NEB). Colonies selected on ampicillin (100 mg L^{-1}) and spectinomycin (100 mg L^{-1}) were submitted for sequencing (ASU DNA Laboratory).

Bioballistic chloroplast transformation

Transformation was performed by an adapted method of Boynton[28,42,44]. For transformation of the *atpB*Δ recipient strains initially developed by Woessner[15,73] (FUD50.02+ and FUD50.21+, obtained from the Institut de Biologie Physico-Chimique, Paris), each 1 µg of plasmid pKTR1 was adsorbed onto 1-µm diameter tungsten nanoparticles (50 mg mL^{-1}, generous gift of J.D. Rochaix) in a mixture with $CaCl_2$ (1 M) and spermidine (20 mM). Recipient strains were prepared by first counting cells with a hemocytometer (Hausser Scientific) and then concentrating by centrifugation to plate ~10^7 cells per plate containing Tris-Bicarbonate-Phosphate medium (TBP). Next, each plate was shot with a homemade helium-driven gene-gun delivering 200 ng of the DNA

mixture per plate. Transformants were screened under high light (175 μmol photons m^{-2} s^{-1}) for photosynthetic ability. For co-transformations, 1 μg of plasmid pKTR1 was mixed with pORF472::*aadA*[22] at a molar ratio of 5:1, processed in the manner above, transformed into a back-crossed 137c WT strain, plated on TAP plates containing 100 mg L^{-1} ampicillin and 100 mg L^{-1} spectinomycin and maintained under ambient light. The *hydA1-1 hydA2-1* double hydrogenase mutant (obtained from Matthew Posewitz, Colorado School of Mines) was transformed with plasmid pKTR3, plated onto TAP containing 100 mg L^{-1} ampicillin and 100 mg L^{-1} spectinomycin and maintained in the dark. The vitamin-repressible strain A31 (obtained from Silvia Ramundo, Université de Genève) was transformed with plasmid pKTR3 and was most successful with pre-adaptation of the recipient strain with vitamins (50 μM B_1 and 37 nM B_{12}) in liquid TAP culture. Transformants were shot onto TAP plates containing 100 mg L^{-1} ampicillin, 100 mg L^{-1} spectinomycin, 50 μM B_1 and 37 nM B_{12}. Transformants were maintained in the dark on alternating vitamin and antibiotic plates of either 500 mg L^{-1} spectinomycin or 150 mg L^{-1} streptomycin.

Inducing a genetic bottleneck by nitrogen starvation

Nitrogen starvation induces a decrease in chloroplast copy number[25]. A31[cp*hydA*] transformants close to homoplasmicity (>75% homoplasmic) were struck on TAP media containing 1/10 the amount of nitrogen in the form of NH_4Cl_2 in addition to 500 mg L^{-1} spectinomycin, 50 μM B_1 and 37 nM B_{12} and were maintained in the dark. Once growth was apparent, the strains were transferred back to full-nitrogen TAP plates

with 500 mg L^{-1} spectinomycin, 50 μM B_1 and 37 nM B_{12}. Homoplasmicity of the strains was then quantified by polymerase chain reaction (PCR) as outlined below.

Detection and homoplasmicity PCRs and primers

Schematic representation of the primer annealing locations and amplicon sizes for the cp*hydA* detection and homoplasmicity PCR reactions is presented in Figure 3-2. Presence of the cp*hydA* gene was detected in genomic DNA by PCR for 25 cycles: 94 °C denaturation for 30 s, 50 °C annealing for 30 s, 72 °C elongation for 30 s. Primers were designed to anneal within the chloroplast codon-optimized *hydA* gene (*HYDA1*-as: CAGCTGGTAAACATCGGCA), and upstream in the 5'-*psbD* region (*psbD*-5'-UTR-s: ATAATAAATTTAACGTAACGATGAG). This arrangement does not amplify the native hydrogenase gene and results in a 439 base pair (bp) product from the cp*hydA* gene. Homoplasmicity was quantified using a primer set in the *atpB* region (*atpB*-3'-s: TACTTAGTAGGTAACATTACAGAAGC), and in the *atpB* flanking region (*atpB*-3'-UTR2: ATTATTAAATACACGTTTAA). In the absence of the cp*hydA* gene, a 219-bp product results. With the cp*hydA* insertion, the product is 1.6 kbp, and detection of this longer product was precluded by the PCR conditions used. Amplified products were visualized on a 1% TAE gel with ethidium bromide staining, and the relative amounts were quantified using the ImageJ program (NIH).

Growth assays

Strains were grown under low light conditions (5 μmol photons m^{-2} s^{-1}) in TAP medium[25]. Cultures were diluted to 1.0 x 10^6 cells mL^{-1} and 8 μL was spotted onto agar

plates containing TAP either with, or without, vitamins B_1 (10 or 50 μM for 1x and 5x) and B_{12} (7.4 or 37 nM for 1x and 5x), as noted. Antibiotics (spectinomycin or streptomycin) were added at 100, 200, or 500 mg L^{-1} as noted. Plates were incubated at 25 °C under ambient light (10 μmol photons m^{-2} s^{-1}) and were photographed after 10 days.

Reverse-transcriptase PCR

The cp*hydA* gene was designed to mimic the mature hydrogenase: coding regions only, no promoter region or N-terminal transit peptide sequence. As such, primers cannot be designed to span introns, and primers for the detection of the inserted cp*hydA* mRNA by reverse-transcriptase PCR would also detect minute amounts of contaminating DNA present in the RNA prep. This confounded attempts to quantify relative levels under different conditions. The first reverse-transcriptase PCR attempted used a β-tubulin loading control whose primers (F: CTACCATGGCGACTCAGACC, R: CAGGCTCCAGGTCCATCA) span an intron of 259-bp. If contaminating DNA were present in the reaction mixture, a 366-bp product would result in addition to the 107-bp mRNA product.

Desiring a more defined result, a selective RNA amplification using dUMP-containing primers and Uracil-DNA Glycosylase (UDG) was used[34,74]. Cells were lysed using either bead beating (ZR BashingBead™, Zymo Research) or sonication. RNA was prepared using the RNeasy Prep Kit (QIAGEN) following manufacturer instructions. A dUMP adapter primer (cp*hydA*-adapt: GUCUCCAUCUCUGCAGUCAUAAUAAAUUUAACGUAACGAUGAG) was

hybridized to RNA, followed by first strand synthesis with Reverse Transcriptase (Tetro, Bioline). RNA was degraded with RNAse H (New England Biolabs) and the gene-specific primer (cp*hydA*-GSP: CAGCTGGTAAACATCGGCA) hybridized to the now-exposed first strand. Second strand synthesis proceeded and the adapter primer was degraded with UDG (New England Biolabs). The amplification primer (cp*hydA*-amp: GTCTCCATCTCTGCAGTC) annealed to the region cleared by degradation of the adapter primer by UDG, and standard PCR amplification resulted in a 455-bp product. The product was visualized on a 1% TAE gel with ethidium bromide staining, and the relative amounts were quantified using the ImageJ program (NIH).

Expression and purification of rHydA

An *E. coli* expression vector containing cp*hydA* (pET-Duet-*HYDA1*, provided by Matthew Posewitz, Colorado School of Mines) was transformed into strain BL21(DE3) (New England Biolabs) and transformants were selected on ampicillin at 100 mg L^{-1}. Protein expression was induced in culture at 0.5 OD_{600} with 400 μM isopropyl β-D-1-thiogalactopyranoside (IPTG, Sigma) for 3 hours at 37 °C. After lysis by sonication, cleared (soluble) lysate was bound to Ni-NTA (nitrilotriacetic acid) resin (Invitrogen) equilibrated with 5 column volumes of Native Binding Buffer (50 mM NaH_2PO_4, 500 mM NaCl, pH 8.0), washed 5 column volumes of the same including 20 mM imidazole, and eluted with 4 column volumes of 250 mM imidazole. SDS-PAGE followed by Coomassie staining was used to confirm desired product size. To verify protein identity, purified protein samples were run with equal protein on a 10% SDS Tris-Glycine gel (4% stacking), then processed as in the section on immunoblotting below.

Crude lysate from induced C. reinhardtii

Anaerobic induction was achieved by either four hours of nitrogen flushing or a 30-minute argon purge at room temperature followed by four hours of sealed shaking in the dark. All procedures after induction were performed inside an anaerobic chamber (Coy). Cells were pelleted and then lysed by sonication on ice (5, 5-second pulses at maximum power with 10 second rests between) in 50 mM phosphate buffer (pH 8.0) containing 10 μL mL^{-1} water-soluble serine, cysteine and metalloprotease inhibitors (P2714 cocktail, Sigma). The supernatant was clarified by centrifugation (2,500 x g for 2 minutes), was concentrated by acetone precipitation and solubilized by heating in lithium dodecyl sulfate (LDS) sample buffer (Invitrogen) at 75 °C for 10 minutes. Total protein was quantified by the bicinchoninic acid (BCA) assay (Pierce). Samples were reduced with 5% β-mercaptoethanol at 75 °C for 10 minutes, then separated by SDS-PAGE on a 4%/10% (stacking/resolving) Bis-Tris gel with MOPS buffer (50 mM MOPS, 50 mM Tris Base, 0.1% SDS, 1 mM ethylenediamine tetraacetic acid (EDTA), pH 7.7). Samples destined for immunoblotting (described below) were run with chemiluminescent molecular weight standards (Precision Plus Protein™ WesternC™ Standards, Bio-Rad).

IMAC purification of cpHydA from induced C. reinhardtii

After induction as above, cells were lysed as before but in binding buffer (50 mM phosphate buffer (pH 8.0), 300 mM NaCl and 10 μL mL^{-1} protease inhibitors). Clarified supernatant was loaded on a Ni-ITA (iminodiacetic acid) column (800 μg binding capacity, Affymetrix). The column was washed with 620 μL binding buffer, and protein eluted with 720 μL of the same buffer containing 250 mM imidazole. Fractions were

concentrated and desalted through a 5-kDa molecular weight cut off spin filter (Corning). All steps were carried out an anaerobic chamber. SDS-PAGE separation was carried out as above, and immunoblotting as described below. For analysis, samples were heated in a lithium dodecyl sulfate (LDS) sample buffer (Invitrogen) containing 5% β-mercaptoethanol at 75 °C for 20 minutes, run on a 4%/10% (stacking/resolving) Bis-Tris gel with MOPS buffer (50 mM MOPS, 50 mM Tris Base, 0.1% SDS, 1 mM EDTA, pH 7.7) and either Coomassie stained, or processed as in the section on immunoblotting below.

Immunoblotting

SDS-PAGE separation was followed by protein transfer to 0.45-µm Immobilon-P polyvinylidene fluoride (PVDF) membranes (Millipore) with Bis-Tris/Bicine transfer buffer (25 mM Bicine, 25 mM Bis-Tris, 1 mM EDTA, pH 7.2). Blots were blocked in 5% nonfat dry milk in TBST (20 mM Tris-HCl (pH 7.5), 500 mM NaCl, 0.05% Tween-20) overnight then probed with a primary antibody, either anti-HydA at 1:1000 (Agrisera) or anti-His_6 at 1:1000 (Genscript). The secondary goat anti-rabbit HRP conjugate was used at 1:10,000 (Bio-Rad), as was the StrepTactin-HRP conjugate (Bio-Rad) for the chemiluminescent molecular weight standard. Blots were visualized with an enhanced chemiluminescent (ECL) substrate (SuperSignal West Femto Chemiluminescent Substrate, Thermo) and imaged using an UltraLum Omega12iC imager.

Fluorescence measurements

Freshly-cultured cells were grown to active mid-log phase and normalized to 6 µg mL^{-1} total chlorophyll as detailed below. After a dark adaption period of one minute, a JTS-10 (BioLogic) pulsed LED spectrometer was used to measure chlorophyll fluorescence with the following pulse sequence: 5(1sD) 919msE 80msF 200µsD 5(1sD). Here, D = detection, and E and F are a light bank on at high intensity and off respectively. The F_0 parameter is automatically measured from the initial zero-fluorescence baseline and F_M, the maximum fluorescence, is defined as the peak on illumination. The fluorescent parameter F_V/F_M is calculated as $(F_M-F_0)/F_M$.

Determination of chlorophyll concentration

The chlorophyll concentration of cell cultures was determined spectroscopically. Cell culture (1 mL) was pelleted for 2 minutes at 25,000 x g, and the supernatant removed. Pellets were resuspended with 1 mL of 80% acetone and left to extract in the dark for two minutes. The sample was then spun again at 25,000 x g for two minutes and absorbance of the solvent-extracted pigments was measured at 750 nm, 663.6 nm and 646.6 nm. Absorbance values at 663.6 nm and 646.6 nm were corrected with the 750 nm value, and chlorophyll concentration was calculated according to the formulae presented in Porra *el al*[36].

Concentration of chlorophyll A (mM) = $0.01371\ A_{663.6} - 0.00285\ A_{646.6}$
Concentration of chlorophyll B (mM) = $0.02239\ A_{646.6} - 0.00542\ A_{663.6}$
Total chlorophyll concentration (mg/mL) = $0.01776\ A_{646.6} + 0.00734\ A_{663.6}$

Determination of starch in whole cells

Starch granules in whole cells were qualitatively imaged by staining with 10 µL Lugol's iodine solution (Sigma) per 90 µL of cells and photographed through an optical oil-immersion lens (Fisher Scientific) with a 5-megapixel CCD camera (Apple, iPhone). In quantitative determination of starch content, cell cultures were concentrated and normalized to 10^8 cells mL^{-1}. Pigment extraction with 80% acetone left a pellet that was assayed for either protein (BCA, Pierce) or starch as follows. Sodium acetate buffer (100 mM, pH 4.8) was added to the pellet and autoclaved for 15 minutes at 120 °C to solubilize. From that sample, 200 µL was removed to a microplate and 5 µL of Lugol's iodine added. The samples were immediately read at 580 nm on a microplate reader and the starch content determined from a standard curve generated from soluble starch in sodium acetate buffer.

Catalase activity assay

Catalase activity was determined by an adaptation of the method of Beers and Sizer[33]. Cells were grown to mid-log phase and transferred to the dark for 16 h. At that point, cell density was determined using a hemocytometer, and the chlorophyll concentration determined by the method of Porra[36]. A cell pellet containing $2x10^8$ cells was resuspended in 200 µL of 50 mM potassium phosphate buffer (pH 7) and lysed by two freeze/thaw cycles using liquid nitrogen and a 37°C heat block. Protein was quantified in the clarified supernatant and 50 µg of total protein was mixed with 60 mM H_2O_2 in the same phosphate buffer as above in a total reaction volume of 1 mL.

Consumption of H_2O_2 by catalase in the cell lysate was measured spectroscopically by monitoring the drop of absorbance at 240 nm.

Ascorbate peroxidase activity assay

Ascorbate peroxidase activity was also assayed spectroscopically[38] (at 290 nm) using cell extract (prepared in the same manner as the Catalase assay, but using 20 mM phosphate buffer) with a final protein concentration of 5 μg mL^{-1} (BCA assay, Pierce), containing 500 μM ascorbate and 1 mM H_2O_2 as substrates. Consumption of H_2O_2 was monitored by the disappearance of the ascorbate signal at 290 nm. Rates were normalized to chlorophyll concentration, and a molar absorptivity of 2.8 mM^{-1} cm^{-1} was used for ascorbate[39].

Total dark anaerobic hydrogen evolution from cell culture

Anaerobically-adapted cell cultures were assayed for total dark anaerobic hydrogen production by gas chromatography (GC) headspace analysis. Cell culture at 200 μg mL^{-1} Chl (400 μg total) was induced in the dark in the reaction vessel as in '*Crude lysate from induced C. reinhardtii'* above. After 24 hours under anaerobic conditions in the dark, hydrogen in the headspace gas was measured from an injection of 200 μL into a SRI model 310C Gas Chromatograph with a helium mobile phase. Total headspace was calculated by the subtraction of the total volume of reaction mixture from the total internal volume of the reaction vessel, determined by water displacement. All transfers of cells and gases were performed using argon-flushed, gas-tight syringes (Hamilton Company).

Hydrogen evolution from detergent-permeabilized cells

Anaerobically-adapted cell cultures were assayed for maximum hydrogen production by a method adapted from Happe[41]. Induced cell culture at 200 μg mL^{-1} Chl (40 μg total) was added to the reaction vessel containing a solution of methyl viologen (10 mM) in 50 mM potassium phosphate buffer (pH 6.9) containing 0.2% Triton-X (1.2 mL total). To this mixture, 200 μL of 100 mM sodium dithionite in 30 mM sodium hydroxide was added and the sample was incubated at 37 °C for 15 minutes. As above, hydrogen in the headspace gas was measured from an injection of 200 μL into a SRI model 310C Gas Chromatograph with a helium mobile phase. All transfers of cells, solutions, and gases were performed using argon-flushed, gas-tight syringes (Hamilton Company).

Results

Test transformation of atpBΔ strains: complementation of atpBΔ

Targeted gene insertion is possible in the chloroplast if regions of chloroplast homology flank the gene of interest. The chloroplast transformation vectors pKTR1 and pKTR3 (Figure 3-1) were designed to complement the *atpB*Δ genotype and restore phototrophic (PS+) growth. Algal strains lacking the chloroplast ATP synthase are unable to grow photosynthetically, and therefore complementation to a photosynthetic phenotype (PS+) may be used as a transformation selection. To test transformation effectiveness, FUD50 (*atpBΔ*) was transformed with the plasmid cg13 (Jörg Nickelsen, Ludwigs-Maximilians Universität). The plasmid contains a *psbD*(promoter+5'-UTR)-*aadA*(ORF)-*rbcL*(3'-UTR) inserted into atpB-int vector (Figure 3-3A). This is the parent plasmid used

as the backbone for pKTR1 and pKTR3, wherein the *aadA* from cg13 is switched out for cp*hydA*. Transformants with cg13 showed the PS+ growth phenotype after complementation (Figure 3-3B) with high transformation efficiency.

Transformation of atpBΔ strains with pKTR1

Schematics of plasmids pKTR1 and pKTR3 can be found in Figure 3-1. Both plasmids contain a chloroplast codon-optimized *HYDA1* gene (cp*hydA*). The changed codon bias reflects the relatively AT-rich composition of the chloroplast genome compared to that of the nucleus. In addition, the sequence coding for the 56 amino-acid putative chloroplast import peptide found on *HYDA1* was removed and replaced with a His_6 tag. As a result, the gene product resembles that of the mature, or processed HydA. In both plasmids, cp*hydA* was placed behind the constitutive *psbD* promoter and 5'-UTR. The UTR later becomes essential when vitamin-mediated gene repression is utilized. Transformations of FUD50 under the same conditions as the complementation above were performed with the pKTR1 plasmid. Here, complementation of the photosynthetic (PS+) phenotype would be expected in addition to the introduction of the chloroplast codon-optimized hydrogenase gene into the chloroplast. From thirty-six independent transformations with pKTR1 into two different FUD50 strains, no PS+ transformants were generated (Table 3-1).

The identity and *atpBΔ* phenotype of the recipient strains were confirmed by PCR and integrity of the plasmids were reconfirmed by test digest and sequencing. Neither algae nor DNA showed unexpected changes that would explain the abject failure in transformation.

Co-transformation of WT with pKTR1 and aadA

Twelve independent co-transformations of the WT KRC1-4A+ with pKTR1 and the spectinomycin resistance cassette *aadA* selected on spectinomycin in ambient light resulted in numerous dark green colonies that were screened for the cp*hydA* insertion by PCR (Table 3-1). Gene copy number was quantitated by a combination of cp*hydA* detection, and homoplasmicity detection PCR (Figure 3-2). In the cp*hydA* detection PCR, only the chloroplast hydrogenase gene (cp*hydA*) is detected, not the nuclear *HYDA* genes. PCR reactions normalized to total genomic DNA can track the enrichment or disappearance of the cp*hydA* band over generations.

The *C. reinhardtii* chloroplast contains ~80 copies of the genome[43]. Homoplasmicity refers to a state in which all copies of the genome contain the insertion. Immediately after transformation, very few copies in the chloroplast genome will contain the introduced gene. During subsequent cell divisions, the number of copies of the modified genome will increase or decrease in daughter cells due to unequal inheritance. The homoplasmicity detection PCR uses primers in the *atpB* and *atpB* flanking regions. In the absence of the cp*hydA* insertion, a ~200 bp product is formed. On successful insertion of the cp*hydA* gene, the span between the primers becomes too large to amplify under the set experimental conditions, and a product is no longer observed for that fraction of the population. So, the cp*hydA* and homoplasmicity detection PCR results are inversely related and may be used to track retention of the gene over generations (Figure 3-4). Until the insertion becomes homoplasmic (i.e. all copies of the genome are replaced), the risk of reversion to the untransformed state is high, especially in the presence of a negative selective pressure.

PCR screening of WT[cp*hydA*] colonies initially yielded positive results, but the transformants did not maintain the gene in subsequent generations. Several thousand transformants were screened, but only one transformant maintained the gene, and eventually became >99% homoplasmic as determined by PCR.

Table 3-1 summarizes the numerous transformation attempts. Each transformation comprised >10 shots and independent plate selections. Details for each specific transformation may be found in the Materials and Methods for this section or in the related subsections above.

Unfortunately, in the WT background, without positive selective pressure to maintain the hydrogenase gene, even a >99% homoplasmic transformant quickly divested itself of the gene. This is demonstrated in Figure 3-5.

The collective result of obtaining no colonies from the transformation of FUD50 with pKTR1 with selection by phototrophic growth, and few stable WT[cp*hydA*] transformants from the co-transformation with the spectinomycin resistance-conferring pORF472::*aadA* and pKTR1, motivated the redesign of plasmid pKTR1 in order to more closely link selection ($Spec^R$) with the hydrogenase gene.

Redesign of the transformation vector

Construction of plasmid pKTR3 is described in detail in Materials and Methods. In brief, the plasmid maintains the *atpB* regions of homology that allow insertion into the chloroplast genome (seen in pKTR1), but adds an aminoglycoside resistance cassette (*aadA*) upstream of the hydrogenase. The *aadA* gene is flanked by 5'-*psbC* repeats that allow selectable marker recycling when antibiotic selective pressure is dropped. In

essence, plasmid pKTR3 has a tightly-linked antibiotic resistance marker near the cp*hydA* gene, eliminating the need to perform co-transformations.

Transforming a double hydrogenase knockout with pKTR3

In order to simplify downstream experiments and assays with the hydrogenase, transformation of a hydrogenase double knockout strain with the pKTR3 plasmid was attempted. In line with the difficulties observed previously with the transformation of the WT with pKTR1, it is unsurprising that transformants in this background could not be maintained. There appears to be a significant selective pressure against expressing the hydrogenase in the chloroplast.

Vitamin repression with A31

It was hypothesized that unregulated expression of the cp*hydA* gene was in some way deleterious to growth, thereby generating negative selective pressure against the presence of the gene. To test this idea, a vitamin-mediated gene repression system was used[20].

The vitamin-mediated gene repression system makes use of the native function of the Nac2 protein (Figure 3-6), which stabilizes the chloroplast *psbD* mRNA encoding the PSII polypeptide D2[75,76]. Nac2 binds to the *psbD* 5'UTR. In the A31 strain, a mutant *nac2* allele was complemented with a gene putting *NAC2* under control of a vitamin B_{12}-responsive promoter and a TPP riboswitch. The native *psbD* gene is also placed under the *psaA* promoter and UTR, so its expression no longer requires the Nac2 protein. In the presence of vitamins, the vitamin B_{12}-responsive promoter decreases transcription of the

gene placed behind the *psbD* 5'UTR and promoter. If any transcript is made, a TPP-riboswitch induces alternate splicing of the mRNA (prematurely adding a stop codon)[20], thus forming a truncated and nonfunctional processed Nac2 transcript which further tightens the repression (Figure 3-7A and B).

Test transformation of A31 with aadA

In order to test the repressive ability of the A31 strain, it was first transformed with plasmid pKR152 (*aadA* cassette behind a *psbD* promoter)[47]. Hydrogenase expression is not trivial to assay, but spectinomycin resistance is simple to observe in a test-transformed strain. Thus, in the absence of vitamins, the transformants should exhibit a spectinomycin-resistant phenotype. When vitamins are added, the transformed strains should become sensitive to spectinomycin.

The bottom row of Figure 3-8 demonstrates this: a spectinomycin-sensitive phenotype is observed at the 500 mg L^{-1} concentration of spectinomycin. The apparent lack of repression at lower antibiotic levels may be due to leaky repression. In this case, differences in growth are observable only at high levels of antibiotics.

Transformation of A31 with pKTR3

After the test transformation, the expression of cp*hydA* was placed under control of the TPP riboswitch and B_{12}-responsive promoter. In keeping with the regulation described above, in the absence of vitamins, Nac2 stabilizes the mRNA and the HydA1 gene product is made (Figure 3-7A). In the presence of vitamins and absence of Nac2, the

cp*hydA* mRNA is not stabilized and no gene product should result, effectively repressing chloroplast hydrogenase expression (Figure 3-7B).

With the apparent potential for vitamin control of gene expression, conditions for generation and maintenance of hydrogenase transformants were optimized.

Keeping transformants in the dark.

Chlamydomonas strains grow more rapidly in the light than the dark, and as the recipient strain exhibited no apparent light-sensitivity, initial screening of the transformants was performed under ambient light. However, when the copy number of cp*hydA* was tested by PCR in colonies grown in both light and dark conditions, a substantial drop in copy number was observed for strains maintained in the light. This rapid loss of the introduced gene appeared to be an issue only in the highly heteroplasmic or low homoplasmicity strains (Figure 3-9).

Pretreating A31 with vitamins and select on vitamin-containing media.

Growing the recipient A31 strain in TAP media with vitamins B_1 and B_{12} for at least 48 hours prior to transformation, as well as shooting onto plates containing both spectinomycin (100 mg L^{-1}) and vitamins resulted in a greater number of colonies maintaining the cp*hydA* gene (Table 3-2).

Maintaining transformants on vitamin-containing media until homoplasmic.

To demonstrate the importance of vitamins in maintaining the cp*hydA* copy number, a single subclone that had been maintained on vitamins and in the dark was

cultured in the dark and in the absence or presence of vitamins ("G_1" of Figure 3-10A and 3-10B, respectively). In the continued presence of vitamins, the cp*hydA* abundance increased (Figure 3-10B, "G_2"), only to decrease when vitamin control was removed (Figure 3-10B, "G_3"). The strong initial growth on vitamins was in stark contrast to the level of cp*hydA* after subculturing in the absence of vitamins once (Figure 3-10A, "G_1"). When this subclone was returned to vitamin-containing media, the cp*hydA* copy number was maintained (Figure 3-10A, "G_2 (S+V)"). In contrast, a second generation in the absence of vitamins resulted in the drop of cp*hydA* below detection limits (Figure 3-10A, "G_2 (S)"). This is a striking demonstration of the strong selective pressure against expression of the cp*hydA* gene. After this discovery, strains were maintained only in the dark and on vitamin-containing media.

Using a genetic bottleneck to accelerate attaining a homoplasmic state

As mentioned briefly above, the *C. reinhardtii* chloroplast contains ~80 copies of the genome[43]. A homoplasmic state occurs when all of the copies contain the modification of interest. Until homoplasmic, reversion to the WT genotype can readily occur, especially if there is selective pressure against the modification. All transformants containing the cp*hydA* were persistently unstable with respect to the gene and maintained a heteroplasmic state. Several times, it was observed that strains would increase cp*hydA* copy number and move closer to homoplasmicity, only to revert shy of complete homoplasmicity. A method was required to 'push them over the edge' into a stable state. It is known that nitrogen starvation induces a decrease in chloroplast copy number[25]. Once released to nitrogen-replete conditions, the strains go through a genetic bottleneck.

This provided a method to generate more homoplasmic clones. Strains at >75% homoplasmicity were cultured on TAP media containing 1/10 the amount of nitrogen in the form of NH_4Cl_2, and then moved back to nitrogen-replete media. PCR results for the detection of cp*hydA* and homoplasmicity show an increase in cp*hydA* copy number and homoplasmicity after 1/10 nitrogen treatment when compared to its prior condition (Figure 3-11). It appears that this method can generate strains homoplasmic to >99%, the detection limit for the amplification protocol.

Homoplasmic strains verified by PCR were followed through several generations and it appears that once >99% homoplasmicity is obtained, both vitamins and the need for dark conditions became less essential (data not shown). However, they have been maintained under those conditions for redundant protection.

Reverse-transcriptase PCR

As determined by PCR, the cp*hydA* gene was present in the A31 transformants. A strong selective pressure against maintaining the gene was also apparent. It is then reasonable to hypothesize that a gene product with some deleterious effect may be produced. The cp*hydA* gene in both pKTR1 and pKTR3 is behind the strong constitutive promoter *psbD*. Not entirely unexpectedly then, reverse-transcriptase PCR showed production of the cp*hydA* transcript, even under aerobic conditions (Figure 3-12). This reaction was saturated, owing to the initial hypothesis that levels under aerobic conditions may be so low as to need as much amplification as possible. This is clearly not the case. Note that the primers used specifically amplify the cp*hydA* transcript and the β-tubulin control shows equal RNA loading that is free from contaminating DNA.

When transcript levels under vitamin repression were examined, it was observed that the vitamin repression system was indeed functional, and that under aerobic (growth) conditions, the quantity of transcript was reduced to 50 percent of the unrepressed state when vitamins were added (Figure 3-13). A similar knockdown was observed under anaerobic conditions.

Interestingly, it appears that there was a significant difference in transcript level between aerobic and anaerobic growth conditions under non-saturating experimental conditions (Figure 3-13). It is likely that this is related to promoter function under the different conditions. This hypothesis was supported by a replicate of the spectinomycin-resistance growth assay shown in Figure 3-8, this time cultured under both aerobic and anaerobic conditions (Figure 3-14). That the spectinomycin-resistant WT control as well as the A31[*aadA*] transformants grew on spectinomycin under aerobic conditions, but failed to do so under anaerobic conditions, indicates that expression from the *psbD* promoter driving both the *aadA* cassette in this strain and the cp*hydA* gene in A31[cp*hydA*] may be substantially hindered under anaerobic conditions.

Expression and purification of recombinant HydA

With the presence of the cp*hydA* transcript verified, evidence of expression of the cpHydA polypeptide under different conditions was pursued. Initial difficulties in optimizing immunoblot conditions for detecting cpHydA in cell lysates required the generation of a positive control in order to develop experimental protocols. Recombinant HydA (rHydA) was isolated. This is the *C .reinhardtii* codon-optimized hydrogenase expressed in an *E. coli* expression vector.

As detailed in the Materials and Methods, a PCR-verified clone was used to transform an *E. coli* expression strain. Induction time and IPTG concentrations were optimized for maximum protein yield. The protein was then purified by ion-metal affinity chromatography (IMAC) and resolved by SDS-PAGE as seen in Figure 3-15. The predominant band migrates at 47.6 ± 3.6 kDa, close to the sequence-calculated molecular weight of 49.3 kDa. The same band reacted with both anti-HydA and anti-His_6 antibodies. Conditions for immunoblotting developed here were applied to algal cell lysates and purified protein.

Purification of cpHydA from induced C. reinhardtii

Using similar methods to those employed in the isolation and detection of the recombinant HydA above, the cpHydA protein was isolated from an induced *C. reinhardtii* A31[cp*hydA*] transformant and probed with anti-HydA and anti-His_6 antibodies. As seen in Figure 3-16, the predominant band after SDS-PAGE separation migrates at 48.5 ± 1.0 kDa, within range of the 49.3 kDa calculated MW of the apopolypeptide of cpHydA. Concentrated, partially purified cpHydA showed reactivity with both anti-HydA and anti-His_6 antibodies. Densitometric analysis of the Coomassie-stained SDS-PAGE separation estimates the cpHydA to comprise approximately 30% of the total loaded protein.

Immunoblot of cpHydA polypeptide

With the above conditions developed for the recombinant protein and tested on partially-purified algal cpHydA, we examined clarified algal cell lysates for the presence

of the cpHydA polypeptide. The possibility of a constitutively-expressed hydrogenase localizing in inclusion bodies was initially considered, but immunoblotting with both anti-HydA and anti-His_6 antibodies on soluble, detergent soluble, and insoluble cell fractions revealed that this was not the case (data not shown). The chloroplast codon-optimized hydrogenase appeared in the soluble fraction of the cell lysate, as is observed for the native protein[52].

The striking feature of the immunoblot in Figure 3-17 is the production of anti-His_6 cross-reactive protein under both aerobic and anaerobic conditions, and only in the cp*hydA*-transformed strain. The presence of slightly more cpHydA polypeptide in the aerobic conditions compared to the anaerobic conditions reflects the pattern seen in the reverse transcriptase PCR data. There is also no anti-His_6-reactive protein present in A31[*aadA*] or the double hydrogenase knockout preparations. As was the case with the purified cpHydA protein (Figure 3-16), the cell extract also contained polypeptide of the same molecular weight that reacted with anti-HydA antibodies. The cp*hydA* transformant produced more anti-HydA reactive polypeptide under anaerobic conditions, consistent with an additional contribution of the native HydA polypeptide (data not shown).

Immunoblotting of samples under +/- vitamin conditions show no attenuation of protein levels under vitamin repressible conditions (data not shown). This indicates that the approximately 50% transcript attenuation observed under vitamin-cultured conditions in the RT-PCR is still saturating for translational purposes.

The key evidence obtained from the immunoblotting is the identification of an anti-HydA and anti-His_6 reactive polypeptide present in the A31[cp*hydA*] transformant, observed under both aerobic and anaerobic conditions. Unfortunately, the aerobic

production of hydrogenase may be problematic and is possibly a source of the large selective pressure against constitutively expressing a hydrogenase in the chloroplast.

Morphological and biochemical characterization of A31[cphydA]

Growth and basic metabolism in the cp*hydA* transformants was probed, resulting in the identification of some interesting differences when compared to parent, control transformants, and other WT strains.

Photosynthetic ability

An early growth assay on the A31 parent strain revealed, very unexpectedly, that the strain was unable to grow photoautotrophically (data not shown). No light sensitivity was observed in the strain, and there was no indication it would be photosynthetically impaired. After the vitamin-mediated hydrogenase strain was developed, it was revealed that the vitamin-repressible strain A31 lacks a pyrenoid, which was discovered by electron microscopy screening (Jean-David Rochaix, personal communication). This revelation may explain some of the aberrant characteristics of the parent strain as compared to 137c-type WT strains.

Considering the physiological defect of the parent strain being unable to fix carbon at low CO_2 concentrations, photosynthetic performance was measured. Minimal differences were observed between the transformants and control strains. Using chlorophyll fluorescence as a measure of photosynthetic yield, a 137c-derived WT strain exhibited F_v/F_m ratio as expected for healthy cells with functioning PSII, about 0.7. The

parent strain A31 showed diminished PSII quantum yield compared to the WT, but the cp*hydA* transformant was not markedly different from its parent (Table 3-3).

Starch content

During a routine microscopic examination of cells, Lugol's iodine was used to fix the cells (preventing movement and simplifying observation). In addition to killing the cells, the I_5^- present in the solution intercalates with the amylose helix[54] in starch, producing a colored adduct. Unexpectedly, it was observed that the strain containing cp*hydA* appeared to accumulate more starch than the control (Figure 3-18).

A more quantitative starch assay revealed a substantial difference in the amount of soluble starch (detected spectroscopically by association with iodine) in the transformant as compared to the parent and control strains (Table 3-4). A linear standard curve was constructed from serial dilutions (100 to 0 μg mL^{-1}) of soluble starch mixed with Lugol's iodine. A negative control of glucose showed no color response when mixed with the iodine. The values obtained for A31 and A31[*aadA*] were higher than would be expected for mixotrophic growth in light; however, they do closely resemble numbers obtained for stressed or nutrient-deprived cells[51]. Subsequent assays did not always yield such a large magnitude of difference between the parent or control and the transformant, and it is likely that starch quantity may depend heavily on growth conditions and/or cell cycle.

Reactive oxygen species (ROS)

As starch accumulation is sometimes an indicator of stress, it is not unreasonable to consider the presence, and deleterious effect, of reactive oxygen species (ROS). Here, the activity of two prominent antioxidant enzymes, catalase (CAT) and ascorbate peroxidase (APX), were assayed.

Quantification of CAT activity in cell lysate was accomplished by spectroscopically measuring the disappearance of H_2O_2 added to cell lysate mixtures. APX activity measurements were based on the spectroscopic disappearance of exogenously-added ascorbate. This occurs in the process of detoxifying added H_2O_2 to cell lysates. From Table 3-5, it can be observed that for the CAT assay, the hydrogenase transformant appeared to exhibit an increase in activity over the parent strain (A31) and the test transformant (A31[*aadA*]). Despite the large error in a few of the catalase assays (later determined to be due to insufficient mixing of the reaction mixture prior to spectrophotometric monitoring), the values were within reported literature values for *C. reinhardtii* grown phototrophically or photoheterotrophically[56].

For APX activity, as seen for the CAT system, an elevation in the enzyme activity in the cpHydA transformant was observed, although it was a more modest increase than in the CAT system. The observed values are slightly lower, but similar to those reported in the literature[58]. Interestingly, a growth assay of WT, control and A31[*aadA*] and A31[cp*hydA*] transformed strains on TAP containing 0.8 mM H_2O_2 showed that the A31 lineage in general coped very poorly when tasked with detoxifying ROS as compared to the WT (data not shown). This possibly contributed to the lower than expected baseline activity levels observed in the parent.

The elevation of these two antioxidant enzyme systems in the hydrogenase transformant (Table 3-5) appear to confirm that the system is under stress. The negative selective pressure associated with expressing a hydrogenase in the chloroplast was demonstrated in the gene copy number drop, and appears to be manifested in stress-specific physiological responses. A direct link between the presence of a chloroplast-expressed hydrogenase and the generation of excess ROS requires additional investigation.

Hydrogen generation in detergent-permeabilized cells

In order to test the hypothesis that the cp*hydA* gene was expressing an active hydrogenase enzyme, hydrogen production in the cp*hydA* transformant and control strains was measured. Total dark anaerobic hydrogen production *in vivo* using electrons from fermentation in A31[cp*hydA*] was twice that of the controls (Table 3-6 and Figure 3-19). However, given the higher starch content in the A31[cp*hydA*] strain, and the role of starch fermentation in dark production of hydrogen[60], it would be difficult to isolate the expression of cpHydA as the primary cause of the higher dark H_2 production *in vivo*.

An anaerobically-adapted cell culture permeabilized with Triton-X detergent is able to use reduced methyl viologen as an electron donor for hydrogen evolution. In Table 3-7 and Figure 3-20, it is shown that transformants with cpHydA evolved approximately twice the amount of hydrogen as the control strains. In contrast, MV-mediated H_2 production in the A31[*aadA*] control transformant was indistinguishable from that of the parent. Hydrogen production in the A31 background was also about the same as in a non-engineered wild-type strain (137c background), indicating that the

increase in production in the cp*hydA* transformant was not due to reversion of a low-H_2 production phenotype in the parental strain.

Discussion

Indicators of selective pressure against a chloroplast-expressed hydrogenase

Chloroplast transformation, unlike the random insertion observed in nuclear transformation, can be directed. Regions of homology in the transformation vector ensure the insertion of the desired gene at a specified location. After substantial time invested in experimental troubleshooting, it became apparent that while FUD50 (*atpBΔ*) strains could be complemented with the cg13 *atpB* integration vector containing the *aadA* cassette to photosynthetic competency as demonstrated by high light screening, introduction of a chloroplast codon-optimized hydrogenase gene replacing the *aadA* cassette in the same transformation vector (pKTR1) was not tolerated. When pKTR1 was co-transformed along with a plasmid conferring aminoglycoside resistance into a wild-type background strain and colonies selected on the basis of spectinomycin resistance in the dark, colonies were observed. While an improvement, the strains demonstrated short-lived retention of the gene as determined by PCR. There was an early indication of a light dependent, but otherwise uncharacterized negative selective pressure against expressing a hydrogenase in the chloroplast.

Redesign of the transformation vector to the form in pKTR3 more closely linked the spectinomycin resistance phenotype with the presence of the hydrogenase gene. In a co-transformation, the antibiotic resistance gene, lacking regions of homology, inserts randomly into the genome. This presents the possibility of a $Spec^R$ phenotype, without

the insertion of the cp*hydA* gene. However, placing the two genes in the same transformation vector more tightly links the presence of $Spec^R$ with the presence of the cp*hydA* gene.

With the newly designed plasmid, an effort was mounted to create a strain containing the chloroplast-expressed hydrogenase as the sole hydrogenase. Unfortunately, transformation of plasmid pKTR3 into a double hydrogenase knockout strain resulted in no colonies that could retain the hydrogenase gene.

At this point, it may be helpful to reiterate that transformation of the chloroplast, while assisted immensely by homologous recombination, must also contend with the issue of obtaining that homoplasmicity. As detailed in the Results section previous, the *Chlamydomonas* chloroplast contains approximately 80 copies of the genome. In order for a strain to be more stable, all 80 copies must contain the modification of interest, lest ready reversion to the wild type genotype occur. Particularly under conditions of negative selective pressure, homoplasmicity is both essential and difficult to obtain. The highly heteroplasmic state of new transformants is especially vulnerable to reversion in the face of negative selective pressure. After observation of the consistent inability of varied recipient strains to maintain the cp*hydA* gene, the possibility of a deleterious effect caused by the hydrogenase gene product was seriously considered.

Managing the selective pressure against a chloroplast-expressed hydrogenase

As detailed in the Results section, the addition of vitamins B_1 and B_{12} to a culture of a transformed A31 strain results in targeted gene repression. Expression of the gene placed behind the *psbD*-5'UTR can be controlled by way of both a TPP riboswitch, and a

B_{12}-responsive promoter[20]. It must be noted here that the result was not a complete knockdown. Test transformations with the spectinomycin-resistance cassette *aadA* placed behind the *psbD*-5'UTR and promoter demonstrate this in Figure 3-8 where high levels of antibiotics are required to observe the differences in growth with and without vitamins.

In developing conditions for the successful maintenance of the hydrogenase gene, it was determined that the presence of vitamins during the transformation process is essential, indicating that the hydrogenase should be shut off from an early state, and that this requirement persists through generations as each division is an opportunity for a decrease in copy number and reversion to the WT state. While strains maintained on vitamins and in the dark were able to keep their copy numbers higher than those with no vitamin treatment, they were still observed in a persistent heteroplasmic state. Starving the cells for nitrogen has been demonstrated to decrease the copy number of the chloroplast[25], doubtlessly due to nutrient management by the cell. As a result, moving strains from nitrogen deplete to replete conditions passes them through a genetic bottleneck which proved helpful in creating strains with greater than 99 % homoplasmicity, as detected by PCR.

Transcript production of cphydA in the transformant

With a more stable gene construct in place, cp*hydA* transcript levels could subsequently be analyzed. For RT-PCR and other RNA analyses, primers are often designed to span introns, to eliminate the confounding effect of contaminating DNA. Unfortunately, our construct was designed to mimic the mature HydA protein, and so contains no introns. As an additional challenge here, polyadenylated mRNA that may be

cleanly separated from DNA and total RNA by affinity chromatography is not often found in the chloroplast, and when it is, is readily degraded in that location[63]. In order to confront DNA contamination of the RNA preparations, a RNA-targeted amplification method was used (see Materials and Methods).

As seen in Figure 3-12, a saturated reverse transcriptase PCR shows constitutive production of the cp*hydA* transcript under both anaerobic and aerobic conditions. This is relevant because, while details are scarce, it appears that regulation of the native hydrogenase is tightly controlled, and occurs at the level of transcription[67,77,78].

In wild-type *Chlamydomonas*, H_2 production has been observed to correspond directly with an increase of *HYDA* mRNA[67]. In addition, a dramatic change in the hydrogenase transcript level has been observed during the shift from an aerobic to an anaerobic atmosphere, indicating very rapid regulation of transcription by the oxygen status of the cells[67]. Recently published work also indicates the role of chromosome conformation in structurally blocking transcription under aerobic conditions[69]. Evidence for this extremely rapid and sensitive regulation of the native system may indicate that unchecked transcription and translation of the hydrogenase under aerobic conditions is deleterious for the organism, and thus tightly controlled. As a result, it may be expected that by circumventing this native control system, unexpected and possibly negative effects may be observed.

A second, and more sensitive RT-PCR design testing vitamin supplementation under both aerobic and anaerobic growth conditions revealed an interesting pattern (Figure 3-13). While both aerobic and anaerobic transcription of the gene still appear to occur, and the addition of vitamins resulted in an approximately 50 percent knockdown in

transcript levels, the anaerobic chloroplast hydrogenase transcript level is observed to be actually lower than that seen under aerobic conditions. The reactions are normalized to RNA loading and a β-tubulin control confirmed equal loading, so the observed result likely derives from a regulatory effect. A growth assay looking at spectinomycin-resistant mutants driven by the *psbD* promoter bore out a surprising but consistent result. It appears that gene expression driven by the *psbD* promoter/5'-UTR is down-regulated under anaerobic conditions (Figure 3-14). This does not appear to be addressed in the literature and appears puzzling from a metabolic standpoint. Despite this unexpected wrinkle, the observed production of the cp*hydA* transcript under aerobic conditions leads naturally to questions about the production of the cpHydA polypeptide under the same conditions.

Isolation of the chloroplast-expressed hydrogenase from induced C. reinhardtii

After immobilized metal affinity chromatography (IMAC), SDS-PAGE separation revealed a strong band migrating at the expected molecular weight for a native hydrogenase less the transit peptide, but with an added six-histidine tag at the N-terminal end. When probed with anti-HydA and anti-His_6 antibodies, the band was reactive. With the conditions developed for semi-purified protein, the cpHydA polypeptide was also identified in clarified cell lysates. Reflecting the RT-PCR data from Figure 3-12, an anti-His_6 reactive polypeptide was identified under both aerobic and anaerobic conditions, and only in the transformed strain. Evidence of an aerobically-expressed gene product leads to questions about the possible role of aerobic cpHydA in the strong selective pressure against gene retention.

As prepared, in the presence of 10 mM sodium dithionite, UV-visible spectroscopic analysis of the IMAC-purified protein revealed a shoulder at 430 nm generally attributed to the ligand-metal charge transfer of the iron-sulfur clusters[66] (data not shown). On overnight oxidation of the sample in air, the 430-nm signal increases by approximately 50% at the maximum difference point, as is noted in the literature[66,79]. When a sample of the oxygen-exposed frozen protein was thawed, the 430-nm signal does not reappear, suggesting destruction of the cluster. Further, treatment of the same sample with sodium dithionite also does not regenerate the signal, indicating that it is not likely a heme-containing contaminant that would be stable in an O_2 environment and would be expected to yield a 430-nm signal upon re-reduction. Unfortunately, chlorophyll co-purification with tagged hydrogenases is currently a problem in the field (Paul W. King, personal communication), so the contribution of chlorophyll absorbance to the 430-nm signal cannot be ruled out. Cells have been provided to collaborators at the National Renewable Energy Lab (Golden, Co) to pursue Fourier-transform infrared spectroscopy (FT-IR) with an aim to identify CO and CN ligands, and thus confirm full structural assembly of the chloroplast-expressed hydrogenase.

That said, from the presented results it can be concluded that removal of the native promoter and UTR regions in the construct, as well as changing its location from the nucleus to the chloroplast, has replaced the native regulatory control with an engineered one responsive to an orthogonal exogenous signal – the presence of B_{12} and TPP. The cp*hydA* gene is transcribed in the chloroplast and the transcript is translated

there as well. The cpHydA polypeptide is thus present under both aerobic and anaerobic conditions and it carries the introduced His_6-tag.

Characterization of transformants

Parallel to transcript and gene product analysis, a more broad characterization of the transformed strains was undertaken. As seen in Table 3-3, a diminished maximum quantum yield of PSII was observed in both the A31 parent strain, and the cp*hydA* transformant. The low F_V/F_M seen in the A31 transformants may be a function of the higher levels of starch observed therein. Starch degradation in the dark could result in a reduced PQ pool, which would play out as a higher F_0 and therefore higher F_V and lower F_V/F_M than otherwise expected. This said, while an explainable difference in PSII fluorescence is observed between A31 and a WT strain, there is little difference between A31 and A31[cp*hydA*]. The presence of the hydrogenase does not appear to affect primary photochemistry.

No light sensitivity is observed in the A31-derived strains, but it was later revealed that the A31 strain appears to lack a pyrenoid (Silvia Ramundo and Jean-David Rochaix, personal communication). The pyrenoid is a structure that contains enzymes involved in carbon fixation and the dark reactions of photosynthesis. This explained an extremely perplexing growth assay wherein A31 appeared to grow well on acetate-containing media in the light, but could not grow anaerobically on the same, or aerobically on a minimal media requiring CO_2 fixation (data not shown). Lack of a pyrenoid does not completely preclude carbon fixation however; the literature supports carbon fixation at high levels of CO_2[80,81].

An unexpected discovery during routine microscopic examination of cells was a visible difference in coloration in parent and transformant cells fixed with Lugol's iodine (Figure 3-18). As iodine interacts with starch to form a deeply colored complex, this observation suggested starch accumulation in the transformant. A more quantitative analysis supported the first observation (Table 3-4). Starch accumulation is an indicator of growth under stress conditions[70], and metabolic evidence of stress supported initial suspicions of manifestation of a negative selective pressure. While far from proven, an origin of stress in the cells was tentatively hypothesized to be due to the generation of reactive oxygen species (ROS) on or near a partially-formed aerobically expressed hydrogenase.

Possible origins of the negative selective pressure

It is unlikely that a fully functional hydrogenase is expressed under aerobic conditions. The synthesis and assembly of the 2Fe subcluster of the H-cluster requires the presence of maturase proteins HydEF and HydG [49,82]. While the enzymes may show slight baseline levels of transcript under aerobic conditions, compared to their anaerobic partners, the transcripts are strongly reduced in the presence of O_2[71]. In addition, the HydG-catalyzed AdoMet radical chemistry required for the generation of the CN ligands on the this subcluster[72] is unlikely to occur under aerobic conditions.

However, expression of the native *C. reinhardtii* HydA apoprotein in the absence of maturase enzymes was shown to produce a product containing a [4Fe-4S] cluster[40]. This cluster is likely constructed using native cluster-making machinery[42,44], which is functional under aerobic conditions. Several interactions between the cluster and oxygen

could be envisioned. The stoichiometric production of superoxide from the cluster similar to that observed for FNR is possible[73]. Also possible and potentially more dangerous to the cell is the donation of excess electrons directly from ferredoxin to molecular oxygen in the Mehler reaction. Production of superoxide here could attack the exposed [4Fe-4S] cluster in the nascent chloroplast hydrogenase (and other clusters, for that matter) and the resulting constant recycling of the pool of damaged polypeptides could be taxing to the cell. ROS-scavenging enzymes are abundant in the cell, as unmitigated generation of ROS can cause significant damage to cellular components. As seen in Table 3-5, a slight elevation in the ROS-detoxifying catalase and ascorbate peroxidase activities in the cp*hydA* transformant are observed.

ROS have been recently characterized as essential stress signaling molecules[58,83]. The presence of ROS is a regulated balance between signaling for recruitment of stress-management systems, and inflicting actual cellular damage. This suggests again, like in many cellular interfaces, that interactions are an exquisitely balanced system of checks, balances, and feedback mechanisms. That said, new research indicates that molecular hydrogen is involved in stress response in plants. Exposure of plants to H_2-saturated water triggered expression and increased the activity of plant catalase and ascorbate peroxidase enzymes[74]. So, the slight baseline elevation of ROS-detoxifying enzymes could support the moderate suggestion that the transformed system exists in a stressed condition, or it may recommend a more direct link with the aerobic expression of the chloroplast hydrogenase.

Production of hydrogen in the cp<u>hydA</u> transformant

In order to test the hypothesis that the cp*hydA* gene was expressing an active hydrogenase enzyme, hydrogen production was measured in the cp*hydA* transformant and control strains. In order to measure the maximum H_2 evolution activity, reduced methyl viologen (MV) was used as an electron donor in detergent-permeabilized cells. This removes variations due to *in vivo* changes of electron transfer sources and sinks, and the measurement of evolved H_2 should be limited only by the amount of hydrogenase activity. MV-mediated H_2 generation in the A31[cp*hydA*] strain was slightly more than twice that of the A31 parent strain, which was indistinguishable from the A31[*aadA*] control transformants. Hydrogen production in the A31 background was also about the same as in a non-engineered wild-type strain (137c background), indicating that the increase in production seen in the cp*hydA* transformant was not due to reversion of a low-H_2 production phenotype in the parental A31 strain arising during the numerous genetic modifications it underwent.

Increased H_2 generation in the chloroplast hydrogenase transformants may present the first example of a nuclear-expressed, chloroplast-localized metalloprotein successfully synthesized and functioning *in situ*. This proof-of-concept now encourages work on the designed PSI-hydrogenase fusion for continuous photo-production of hydrogen. That said, the demonstrated difficulties in maintaining the chloroplast expression of hydrogenase point to the importance of native regulation in energetic systems. Progression through the new research will need to remain mindful of the possible challenges in the high-risk and high-reward project ahead.

Table 3-1 Summary table of independent control and cp*hydA* transformations. Chloroplast bioballistic transformation was performed as in Materials and Methods. A ✓ indicates that colonies were obtained under the listed selection conditions. A ✗ indicates that no colonies were obtained. See the text for more detail.

#	Recipient strain	Recipient trait	Type	Plasmid	Notes	Screen for	Result
10	FUD50.02 or FUD 50.21	*atpBΔ*	control	cg13 or cg20	complete *atpB*	PS+	✓
36	FUD50.02 or FUD 50.21	*atpBΔ*	cp*hydA*	pKTR1	complete *atpB*	PS+	✗
12	KRC1-4A	WT	cp*hydA*	pKTR1 + pORF472 :: *aadA*	Co-transform with $Spec^R$ cassette	$Spec^R$	✓

Table 3-2: Effect of vitamins on transformation yields. This table is a summary of initial growth and subsequent PCR-positive colonies obtained under different pretreatment conditions. Results are the average of two independent transformations. Samples denoted +V were supplemented with 10 μM B_1 and 7.4 nM B_{12} and spectinomycin was used at 100 mg L^{-1}.

Pretreatment	Plates	Colonies	Colonies picked and restruck	PCR-positive colonies after restreak
none	TAP +Spec^{100}	17	17	0
+V	TAP +Spec^{100} +V	100s	16	16

Table 3-3: Maximum quantum yield of PSII (F_v/F_m) in cp*hydA* transformant. The parameter F_v/F_m can be described by F_m-F_o/F_m, where F_v is the variable fluorescence, or difference between F_m (maximum fluorescence) and F_o (zero fluorescence level).

Strain	F_v/F_m
WT	0.67 ± 0.01
A31 (parent strain)	0.54 ± 0.01
A31[cp*hydA*] (transformant)	0.53 ± 0.01

Table 3-4: Quantitative iodine starch assay. Cultures of A31, A31[*aadA*], and A31[cp*hydA*] were subcultured several times under ambient light to attain similar cell concentrations and growth phases. Soluble starch in aliquots of cell culture was assayed colourimetrically. The data are presented as the mean ± standard deviation (n=3).

Strain	ID	Starch (μg/10^6 cells)
A31	Parent strain	12 ± 6
A31[*aadA*]	Control transformant (+*aadA*)	7 ± 4
A31[cp*hydA*]	Hydrogenase transformant (+cp*hydA*)	127 ± 16

Table 3-5: ROS-detoxifying enzyme activities. Catalase (CAT) and ascorbate peroxidase (APX) activities were measured in the A31 parental strain and the *aadA* and cp*hydA* transformants (see Material and Methods for details).

Strain	ID	CAT (U/mg protein)	APX (μmol min^{-1}mg chl^{-1})
A31	Parent strain	81.9 ± 21.9	--
A31[*aadA*]	Control transformant (+*aadA*)	63.4 ± 39.8	4.01 ± 0.70
A31[*hydA*]	Hydrogenase transformant (+cp*hydA*)	157 ± 7.10	6.71 ± 1.13

Table 3-6: Total dark anaerobic H_2 production in cell cultures. Hydrogen production was measured in anaerobically-adapted cells that were allowed to accumulate H_2 for 24 hours in the dark. The following strains were assayed: the hydrogenase double mutant (-*hydA1*-*hydA2*), a 137c wild-type strain (WT), the A31 parental strain, and the A31[*aadA*] and A31[cp*hydA*] transformants.

Strain	**Type**	**H_2 produced (nmol H_2 mg chl^{-1})**
-hydA1-1 -hydA2-1	Double *hydA* KO	4 ± 0
WT	Wild type	112 ± 1
A31	Vitamin-repressible	109 ± 1
A31[*aadA*]	A31 with Spec^R cassette under vitamin control	94 ± 6
A31[cp*hydA*]	A31 with cp*hydA* gene under vitamin control	237 ± 8

Table 3-7: MV-mediated H_2 production in permeabilized cells. Hydrogen production was measured in anaerobically-grown cells that were permeabilized by detergent and provided reduced methyl viologen as electron donor to hydrogenase (see Materials and Methods for details). The following strains were assayed: the hydrogenase double mutant (-*hydA1*-*hydA2*), a 137c wild-type strain (WT), the A31 parental strain, and the A31[*aadA*] and A31[cp*hydA*] transformants.

Strain	**Type**	**H_2 produced (μmol H_2 mg chl^{-1} h^{-1})**
-hydA1-1 -hydA2-1	Double *hydA* KO	none detected
WT	Wild type	59 ± 4
A31	Vitamin-repressible	79 ± 13
A31[*aadA*]	A31 with Spec^R cassette under vitamin control	73 ± 16
A31[cp*hydA*]	A31 with cp*hydA* gene under vitamin control	151 ± 12

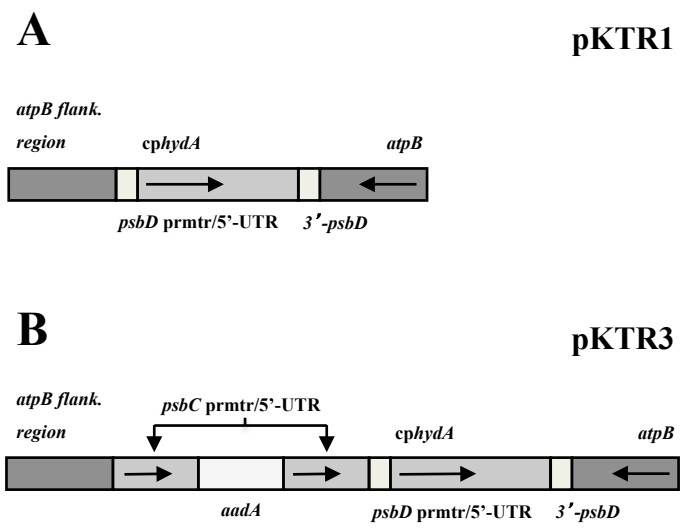

Figure 3-1: Schematic representation of plasmids pKTR1 and pKTR3. In both plasmids, the hydrogenase gene (cp*hydA*) is controlled by the *psbD* promoter and 5'-UTR (*psbD* prmtr/5'-UTR) and is bordered by the 3'-end of *atpB* and a portion of the *atpB* flanking region to direct homologous recombination in the chloroplast. Plasmid pKTR3 contains an *aadA* (aminoglycoside resistance) cassette upstream of the 5'-*psbD* UTR and it is controlled by the *psbC* promoter and 5'-UTR. The *psbC* repeat allows excision of the *aadA* gene by homologous recombination and subsequent loss after selection for antibiotic-resistance is released.

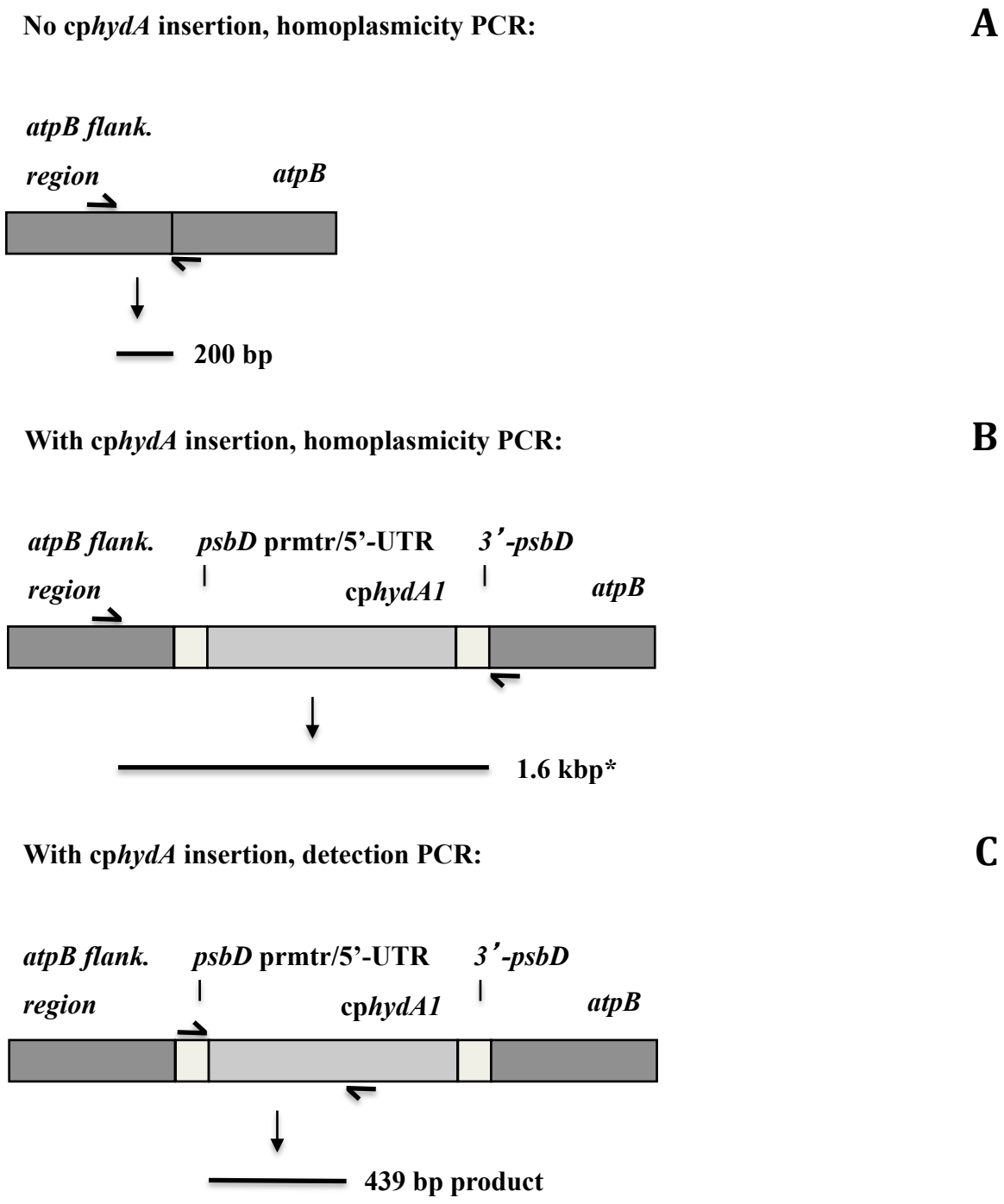

Figure 3-2: **Primer annealing locations and predicted product sizes for cp*hydA* detection and homoplasmicity PCR reactions.** *Formation of the 1.6kbp product is precluded by experimental conditions.

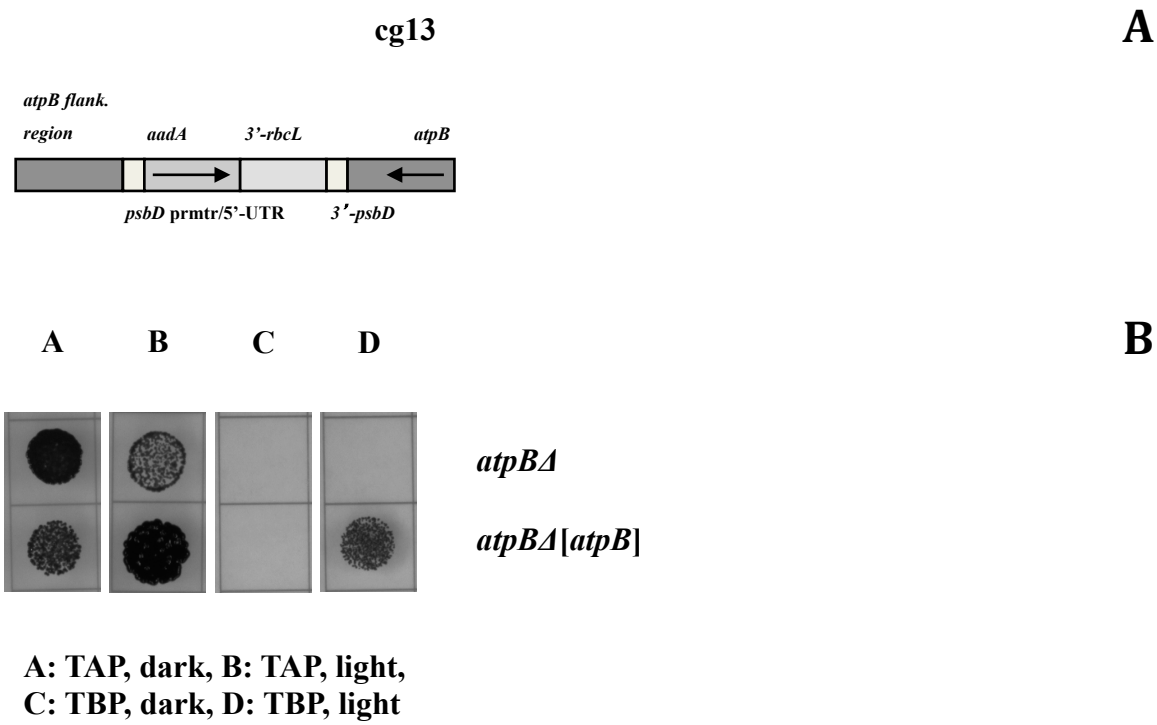

Figure 3-3: Plasmid cg13 complements an *atpB*Δ genotype and restores phototrophic growth. Panel A: plasmid cg13, forming the backbone for the pKTR1 and pKTR3 plasmids, is shown. The 3' end of *atpB* and its flanking region direct chloroplast insertion by homologous recombination. Panel B: Cultures of *atpB*Δ and the *atpB*-complemented strain (FUD50 and FUD50[cg13] respectively) were grown to mid-log phase under low illumination. Equal numbers of cells were spotted onto agar plates (8 µL) containing acetate (TAP) or bicarbonate (TBP) as carbon sources. After drying, plates were transferred to dark (<0.1 µEinstein m^{-2} s^{-1}) or light (~175 µEinstein m^{-2} s^{-1}) conditions.

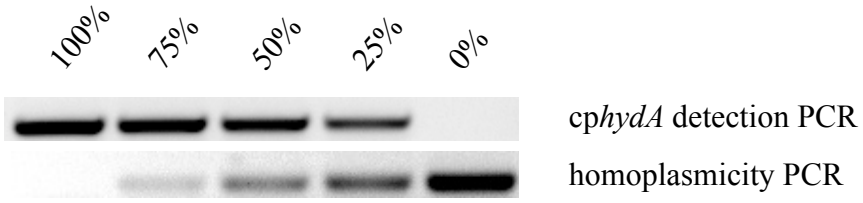

Figure 3-4: Inverse relationship between cp*hydA* detection and homoplasmicity PCR results. Using the primers diagrammed in Figure 3-2, DNA from WT[cp*hydA*] was diluted into DNA from the double hydrogenase knockout (-*hydA1-1* -*hydA2-1*) and amplified as per conditions in Materials and Methods. All reactions were normalized to 20 ng/reaction total genomic DNA.

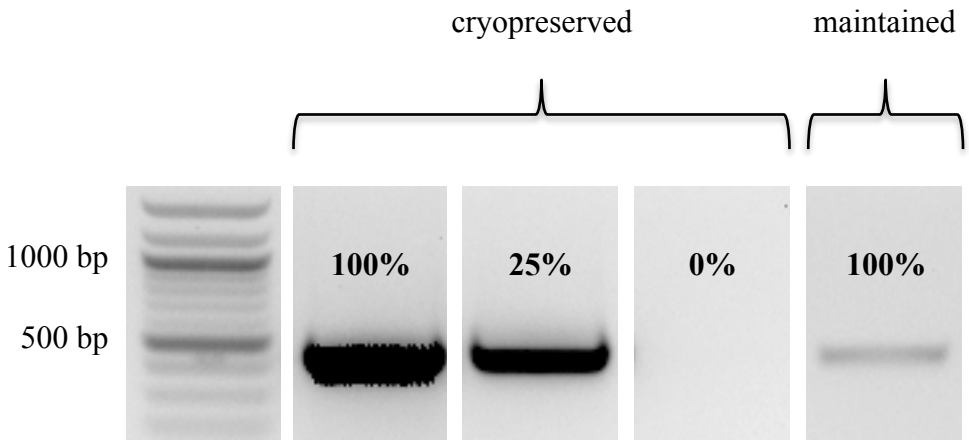

Figure 3-5: Without vitamin gene repression, cp*hydA* copy number drops over time. Using identical clones of a greater than 99 percent homoplasmic WT[cp*hydA*] transformant maintained under different conditions, one clone was cryopreserved immediately after homoplasmicity was confirmed, while a replicate was maintained on TAP agar plates in the dark for one year. In the cryopreserved sample, DNA was prepared after thawing and minimal culturing. All reactions were normalized to 20 ng/reaction total genomic DNA. Genomic DNA of the cryopreserved strain was diluted 4-fold into genomic DNA of the double hydrogenase knockout strain ("0%") to produce the "25%" quantification standard.

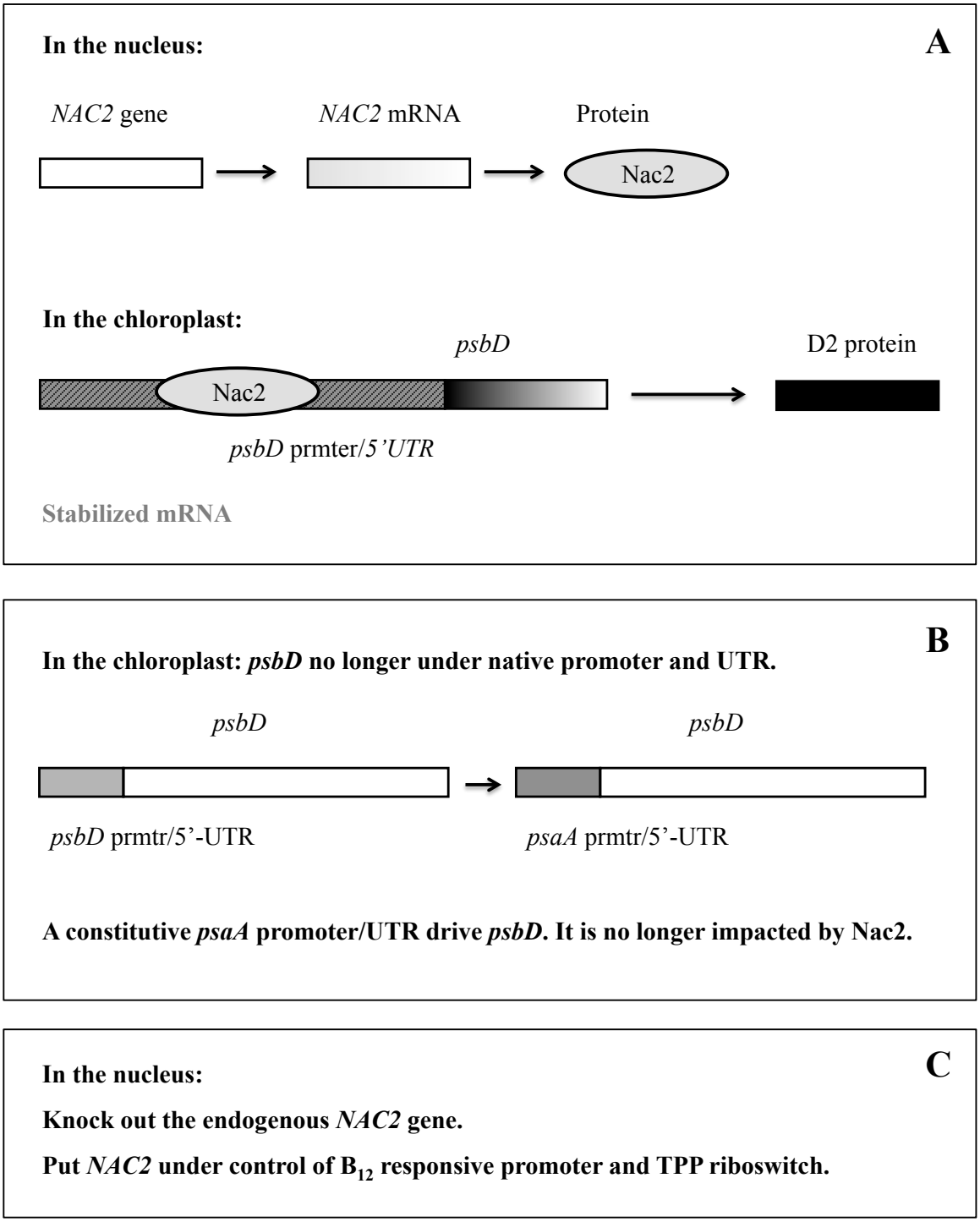

Figure 3-6: Native function of the Nac2 protein and genetic changes in A31. Panel A shows the stabilizing effect of Nac2 on *psbD* mRNA in the native system. Panels B and C show the genetic changes in A31 resulting in the constitutive expression of *psbD* and the control of *NAC2* expression via a B_{12}-responsive promoter and TPP riboswitch.

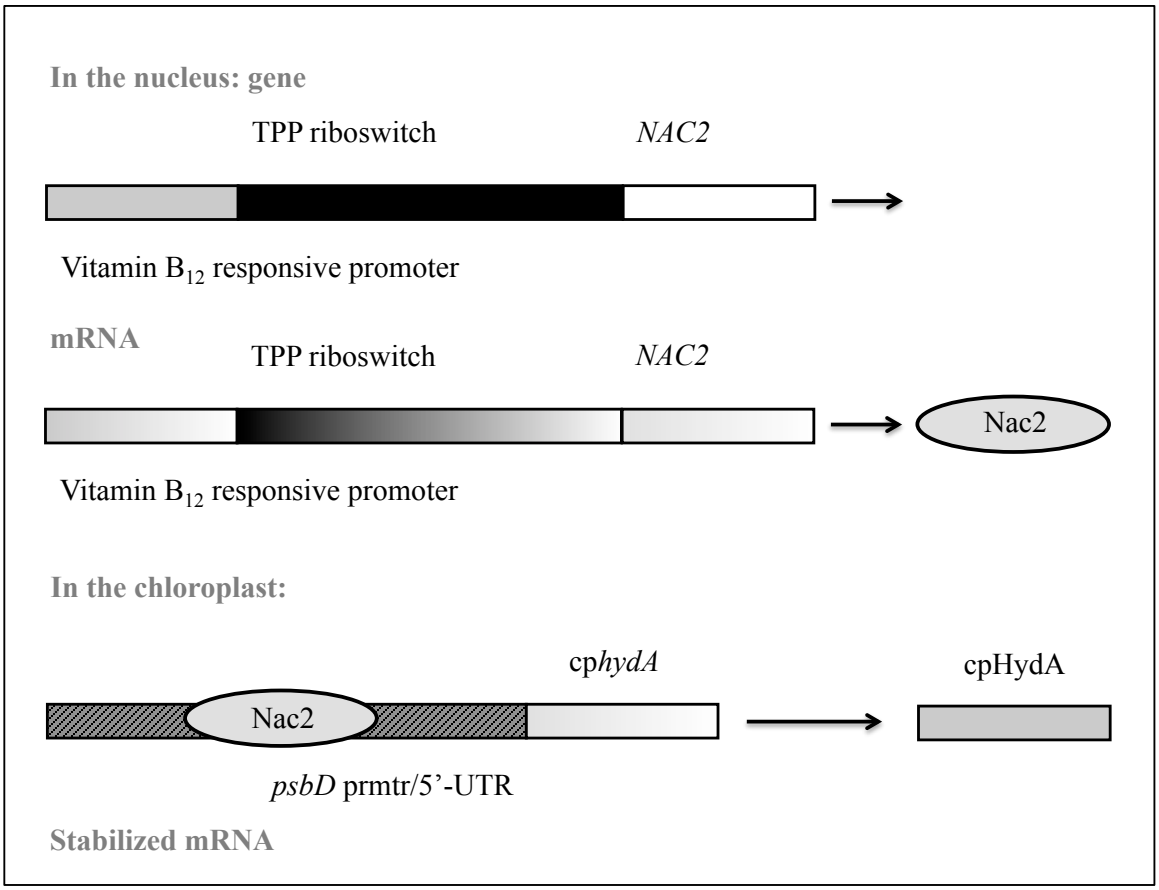

Figure 3-7A: Schematic of vitamin-mediated gene repression in A31 (no vitamins). Schematic shows the function of the vitamin repressible system in the absence of vitamins and the effect on cpHydA expression.

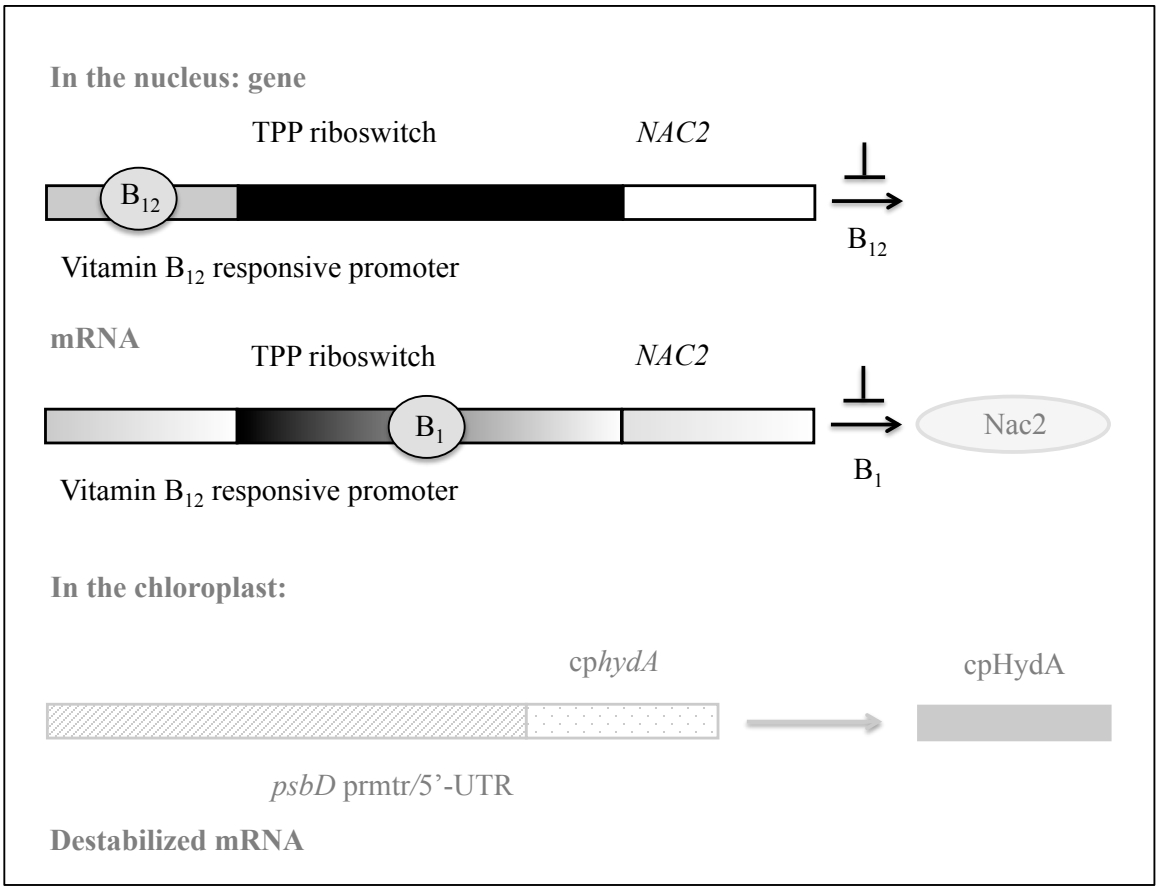

Figure 3-7B: Schematic of vitamin-mediated gene repression in A31 (vitamins present). Schematic shows the function of the vitamin repressible system in the presence of vitamins and the effect on cpHydA expression.

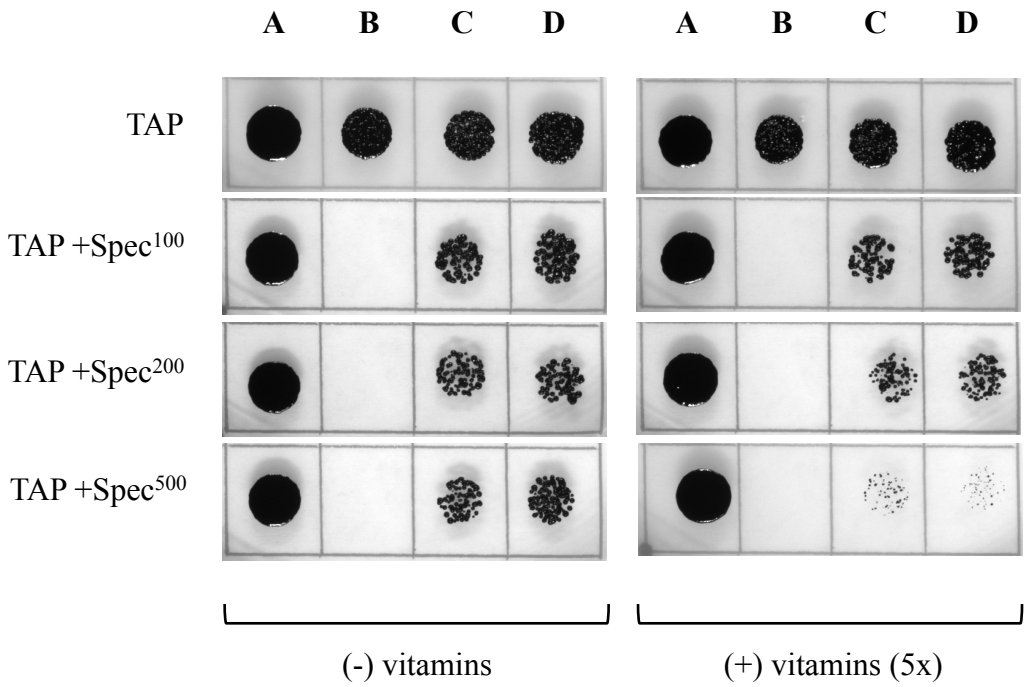

Figure 3-8: Growth assay of test transformants demonstrating vitamin-mediated repression of the *aadA* gene. The following strains were grown in liquid TAP medium under low illumination and spotted on agar plates without (TAP) and with (TAP + Spec) spectinomycin at 100, 200 and 500 mg L^{-1}. Vitamins were B_1 and B_{12} at 50 µM and 37 nM respectively. After drying, plates were grown under ambient light (~75 µEinstein m^{-2} s^{-1}). **A:** spectinomycin-resistant control (*psbD*-driven *aadA* in a 137c strain); **B:** A31 parental strain; **C** and **D:** Independent A31[*aadA*] transformants.

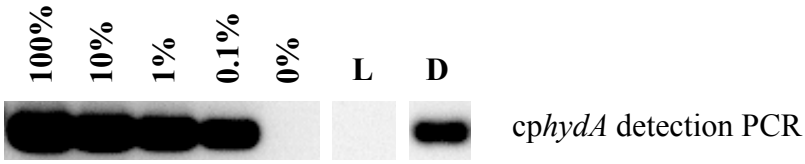

Figure 3-9: Detection PCR shows a light-dependent loss of copy number. The same heteroplasmic subclone was cultured on TAP with spectinomycin (100 mg L^{-1}) and 50 µM B_1 and 37 nM B_{12} in either the light (L) or the dark (D). After sub-culturing in the light (75 µEinstein m^{-2} s^{-1}), PCR-detectable cp*hydA* was no longer present. A serial dilution of genomic DNA from a cryopreserved positive homoplasmic cp*hydA* transformant was into genomic DNA from the double hydrogenase knockout strain to allow estimation of gene copy. Each reaction used 20 ng genomic DNA as template.

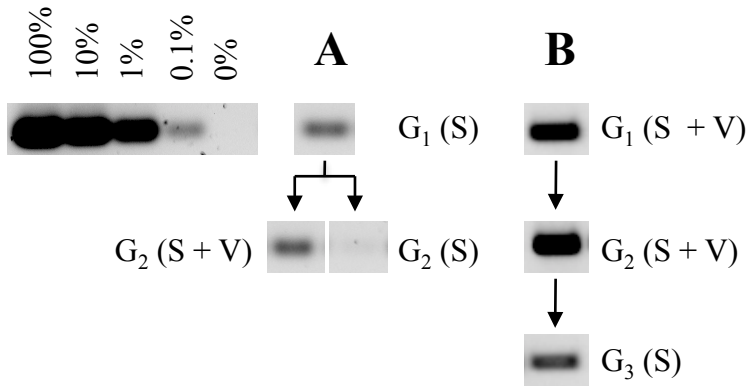

Figure 3-10: Loss of cp*hydA* gene upon cessation of vitamin-mediated repression. Each band shows the abundance of the cp*hydA* gene visualized by cp*hydA*-specific detection PCR after growth conditions as follows. All strains were grown in the dark. From the same initial colony of A31[cp*hydA*] grown on media containing spectinomycin (S) at 500 mg L^{-1} and vitamins B_1 and B_{12} (V, 50 µM and 37 nM respectively), Panel A G_1 (S) shows the result of culturing on spectinomycin only, in the absence of vitamins. That cultured strain was differentially grown again on spectinomycin only G_2 (S), or returned to a vitamin-containing media in G_2 (S+V). In Panel B, the strain was maintained on vitamin containing media for G_1 (S+V), and again for G_2 (S+V). Removal of vitamin conditions is shown in G_3 (S).

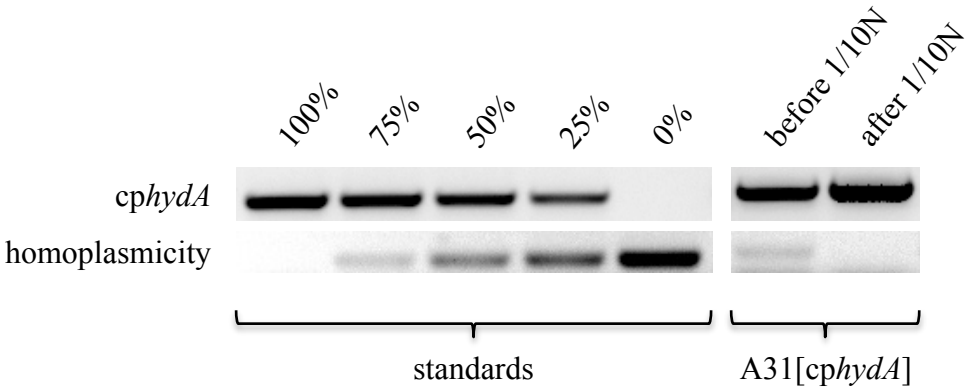

Figure 3-11: Homoplasmicity can be attained by nitrogen depletion followed by repletion. Detection PCR for both cp*hydA* and homoplasmicity was performed on a representative strain. Genomic DNA was prepared before the strain was moved to TAP media containing 1/10 the amount of nitrogen in the form of NH_4Cl_2, and after the strain had been cultured on 1/10 N and returned to growth on nitrogen-replete TAP media. Each reaction used 20 ng genomic DNA as template.

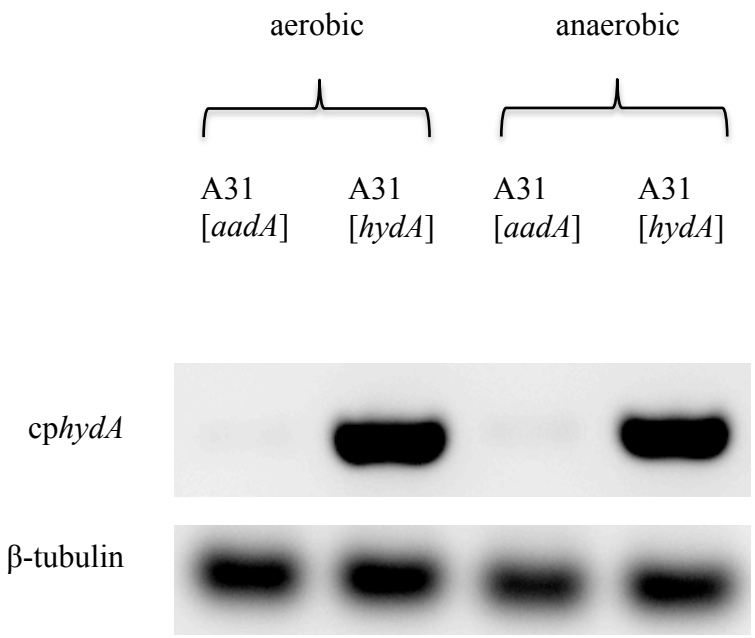

Figure 3-12: Reverse-transcriptase PCR shows constitutive expression of cp*hydA* mRNA. The mRNA levels of cp*hydA* and beta-tubulin (as control) were assessed by an RT-PCR protocol (see Materials and Methods for details). RNA was isolated from the A31[*aadA*] and A31[cp*hydA*] transformants that had been grown aerobically or anaerobically.

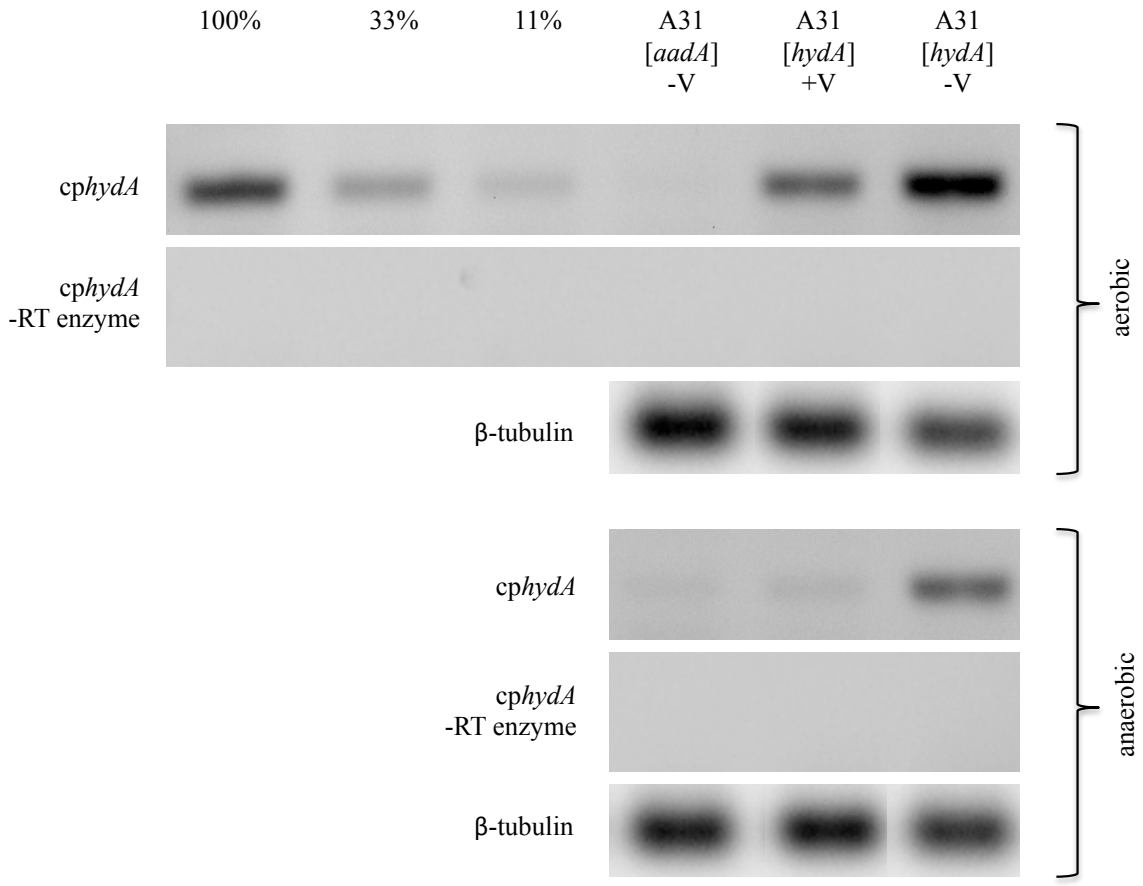

Figure 3-13: Reverse-transcriptase PCR shows partial vitamin-repression of transcription. The mRNA levels of cp*hydA* and beta-tubulin (as control) were assessed by an RT-PCR protocol (see Materials and Methods for details). RNA was isolated from strains grown aerobically or anaerobically in absence or presence of vitamins B_1 and B_{12} (V). The first 3 lanes are RT-PCR results using RNA isolated from anaerobically-grown A31[cp*hydA*] cells diluted into RNA isolated from the A31[*aadA*] strain (at the same concentration) at 1/3 or 1/9 to allow quantification of the cp*hydA* mRNA.

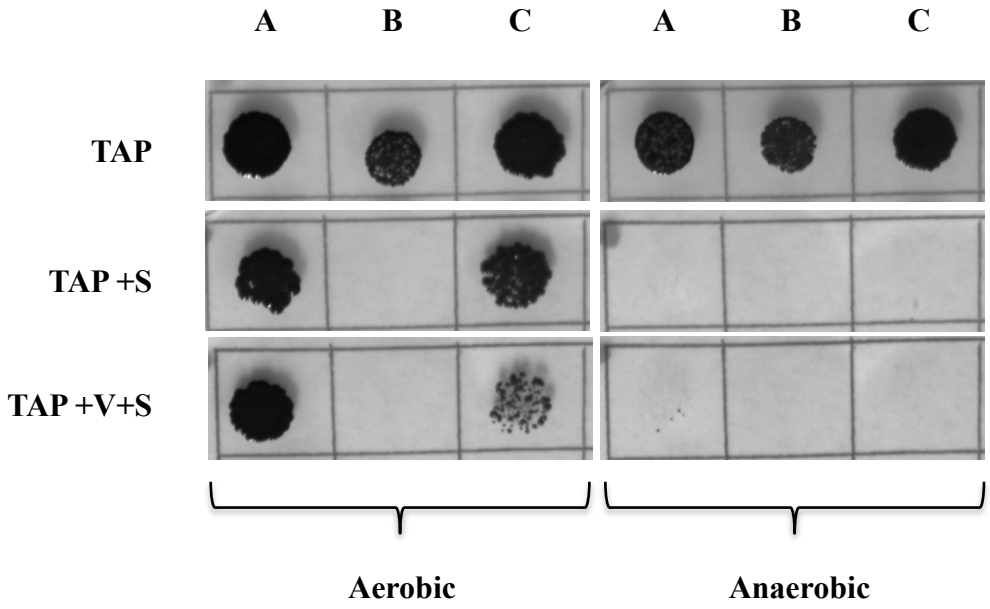

Figure 3-14: Growth assay showing the sensitivity of the *psbD* promoter or 5'-UTR to the anaerobic state of the cells. Culture A is a spectinomycin-resistant WT transformant containing the *aadA* cassette behind the *psbD* promoter. Culture B is A31. It is sensitive to spectinomycin and here acts as a negative control. Culture C is the A31[*aadA*] transformant. Here, expression of the aminoglycoside resistance cassette is vitamin-repressible, utilizing the *psbD* promoter and 5'-UTR (see Figures 3-6 and 3-7 for reference). Cultures were grown to late log phase in TAP medium under low illumination and spotted onto agar plates (10 µL) containing acetate (TAP) and the combinations of antibiotics and vitamins as noted. Vitamin concentrations were at 50 µM B_1 and 37 nM B_{12} and spectinomycin was used at 500 mg L^{-1}. After drying, plates were grown under ambient light (~75 µEinstein m^{-2} s^{-1}) under either aerobic or anaerobic conditions (Bio-Bag, B-D).

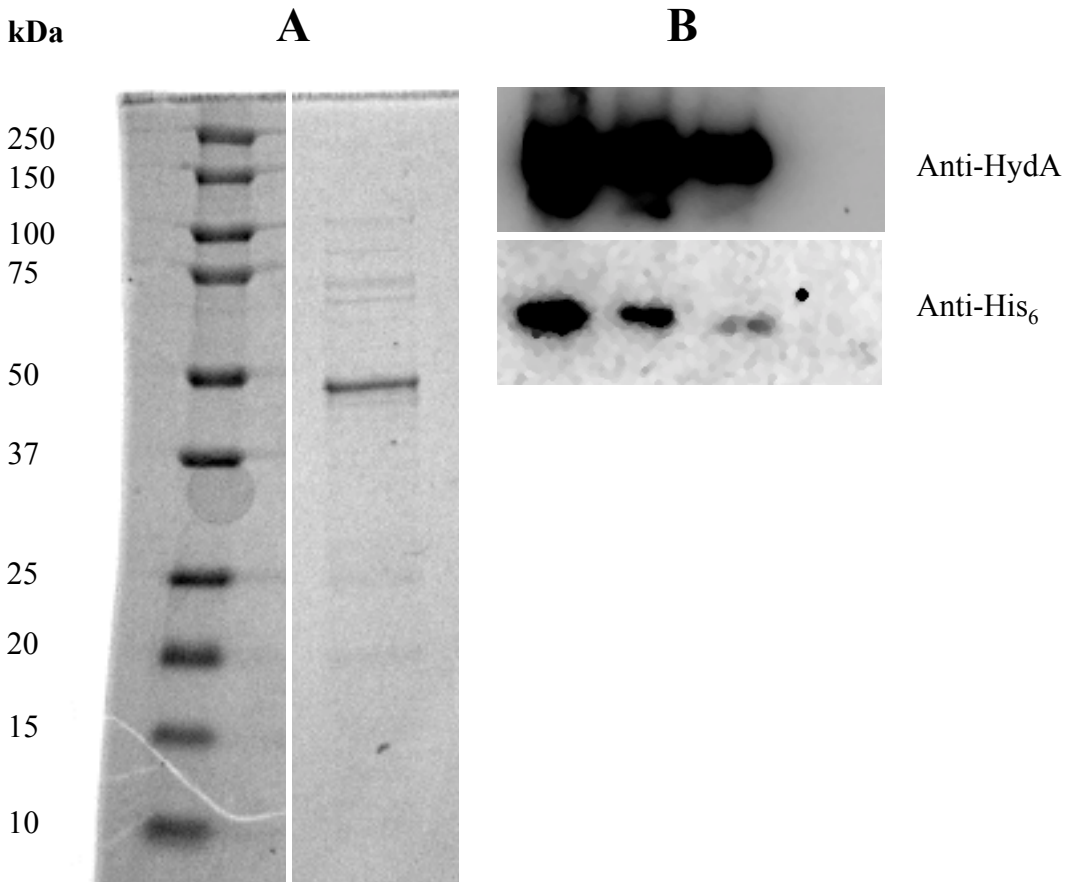

Figure 3-15: Purification of recombinant HydA (rHydA) for the optimization of immunoblot conditions. Cloned, induced and purified rHydA from *C. reinhardtii* expressed in *E. coli* assisted in the development of immunoblot conditions suitable for detection of protein from algal samples. The rHydA protein was isolated by IMAC as described in the text. The preparation was subjected to (A) SDS-PAGE and (B) immunoblots with anti-HydA and anti-His_6 antibodies. For immunoblots, the concentration of protein was (from left to right): 1000, 500, 250 and 0 ng per well.

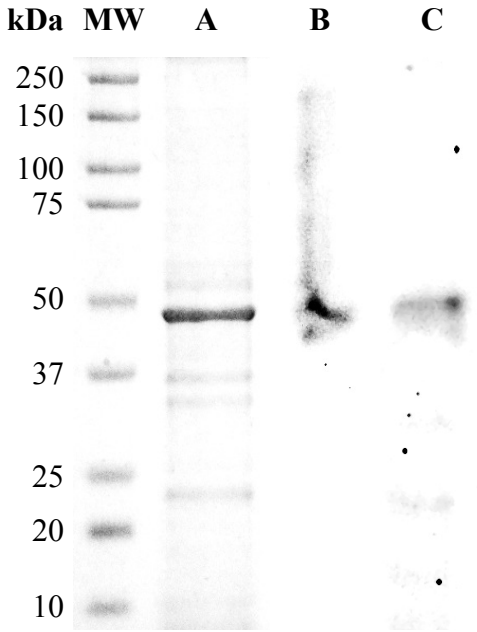

Figure 3-16: Partial purification of the cpHydA apoprotein by IMAC. The cpHydA protein was isolated by IMAC as described in the text. The preparation was subjected to SDS-PAGE (A) and immunoblotting with anti-HydA (B) and anti-His_6 (C) antibodies.

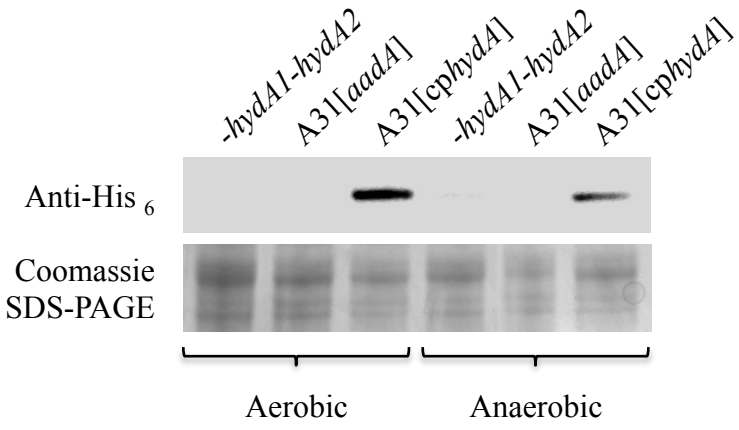

Figure 3-17: Expression of cpHydA apoprotein under aerobic and anaerobic conditions. Clarified cell extracts from the hydrogenase double mutant (*-hydA1-1 -hydA2-1*), A31[*aadA*], and A31[cp*hydA*] strains grown aerobically or anaerobically were separated by SDS-PAGE and immunoblotted with the anti-His_6 antibodies as in Figure 3-16. (A separate gel run the same way and Coomassie-stained is shown below to assess protein loading.)

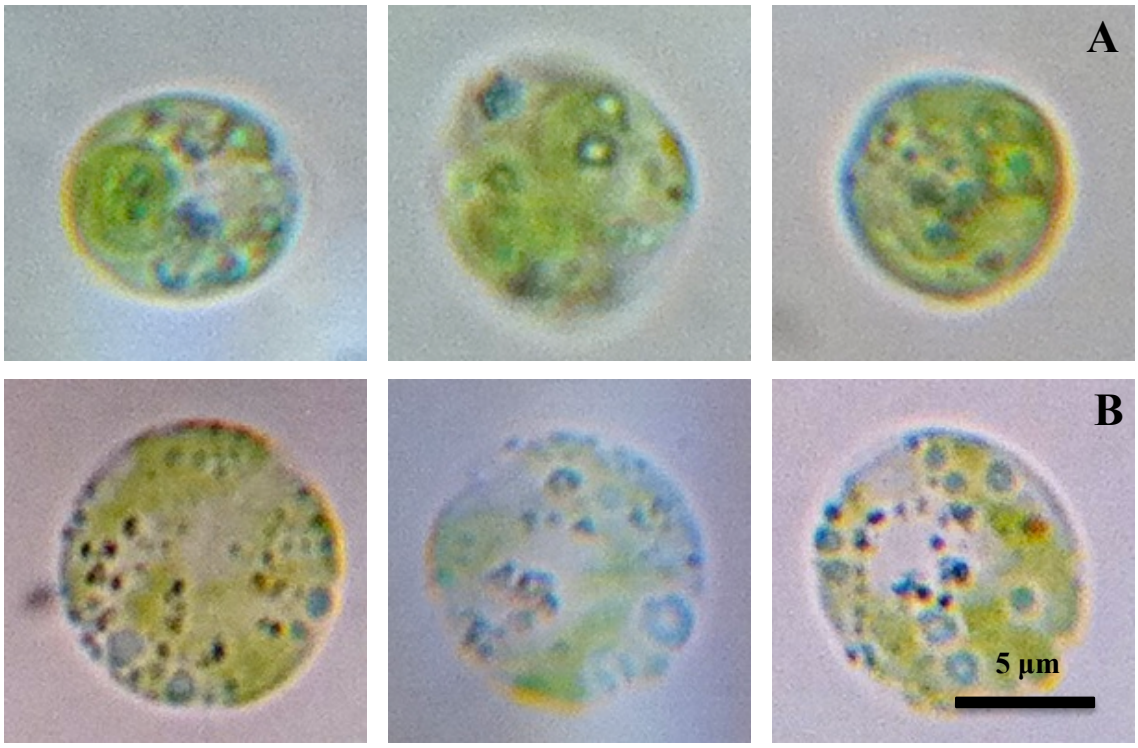

Figure 3-18: Qualitative observation of starch staining in the cp*hydA* transformant. Cultures of A31[*aadA*] in (A) and A31[cp*hydA*] in (B) were subcultured several times under ambient light to attain similar cell concentrations and growth phases. Aliquots of cell culture were fixed with Lugol's iodine and viewed through an optical oil-immersion lens.

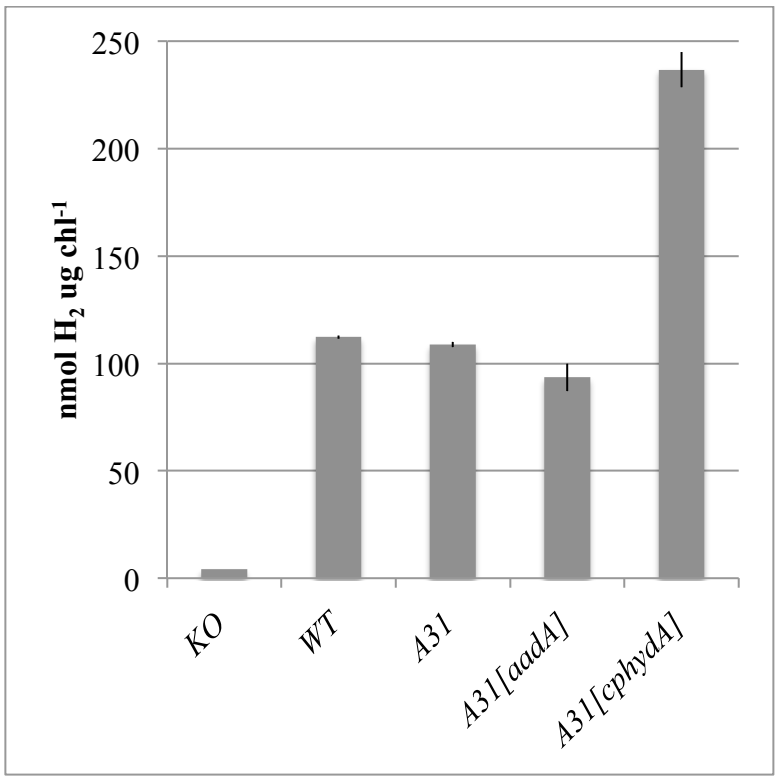

Figure 3-19: Total dark anaerobic H_2 production in cell cultures. Hydrogen production was measured in anaerobically-adapted cells that were allowed to accumulate H_2 for 24 hours in the dark. The following strains were assayed: the hydrogenase double mutant (-*hydA1-1* -*hydA2-1*), a 137c wild-type strain (WT), the A31 parental strain, and the A31[*aadA*] and A31[cp*hydA*] transformants.

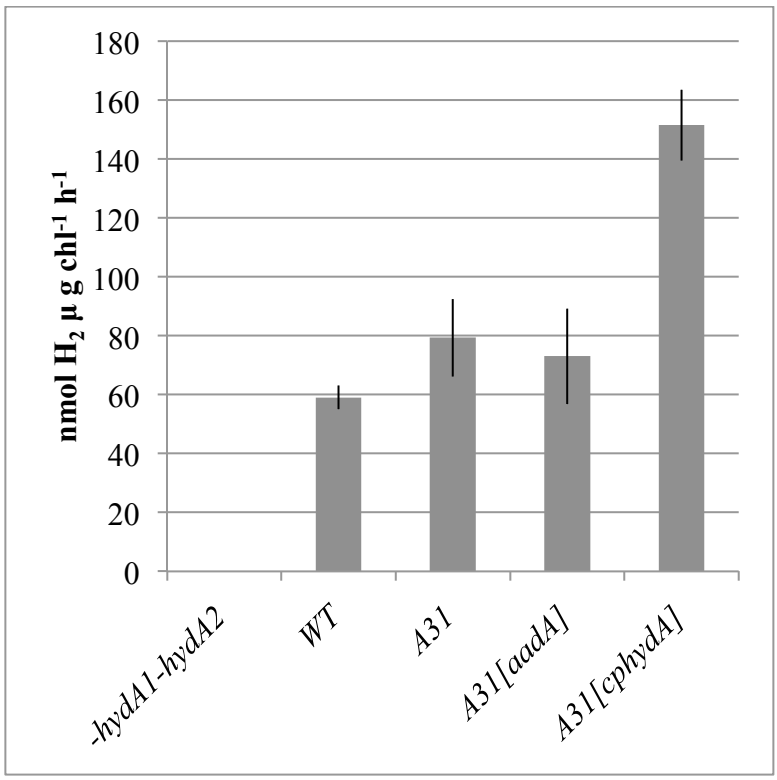

Figure 3-20: MV-mediated H_2 production in permeabilized cells. Hydrogen production was measured in anaerobically-grown cells that were permeabilized by detergent and provided reduced methyl viologen as electron donor to hydrogenase (see Materials and Methods for details). The following strains were assayed: the hydrogenase double mutant (-*hydA1-1* -*hydA2-1*), a 137c wild-type strain (WT), the A31 parental strain, and the A31[*aadA*] and A31[cp*hydA*] transformants.

References

[1] Stephens E, Ross IL, King Z, Mussgnug JH, Kruse O, Posten C, Borowitzka MA, Hankamer B. An economic and technical evaluation of microalgal biofuels. Nat Biotechnol 2010;28(2):126–128.

[2] Melis A, Zhang L, Forestier M, Ghirardi ML, Seibert M. Sustained photobiological hydrogen gas production upon reversible inactivation of oxygen evolution in the green alga *Chlamydomonas reinhardtii*. Plant Physiol 2000;122(1):127–136.

[3] Vignais PM, Billoud B. Occurrence, Classification, and Biological Function of Hydrogenases: An Overview. Chem Rev 2007;107(10):4206–4272.

[4] Moura J, Moura I, Huynh BH, Krüger HJ, Teixeira M, DuVarney RC, DerVartanian DV, Xavier AV, Peck HD, LeGall J. Unambiguous identification of the nickel EPR signal in 61 Ni-enriched *Desulfovibrio gigas* hydrogenase. Biochem Biophys Res Commun 1982;108(4):1388–1393.

[5] Huynh BH, Czechowski MH, Krüger HJ, DerVartanian DV, Peck HD, LeGall J. *Desulfovibrio vulgaris* hydrogenase: a nonheme iron enzyme lacking nickel that exhibits anomalous EPR and Mössbauer spectra. Proc Natl Acad Sci U S A 1984;81(12):3728–3732.

[6] Fauque G, Peck HD, Moura JJ, Huynh BH, Berlier Y, DerVartanian DV, Teixeira M, Przybyla AE, Lespinat PA, Moura I. The three classes of hydrogenases from sulfate-reducing bacteria of the genus *Desulfovibrio*. FEMS Microbiol Rev 1988;4(4):299–344.

[7] Adams MW. The structure and mechanism of iron-hydrogenases. Biochim Biophys Acta 1990;1020(2):115–145.

[8] Gaffron, H, Rubin J. Fermentative and Photochemical Production of Hydrogen in Algae. J Gen Physiol 1942;26(2):219–240.

[9] Nicolet Y, Piras C, Legrand P, Hatchikian CE, Fontecilla-Camps JC. *Desulfovibrio desulfuricans* iron hydrogenase: the structure shows unusual coordination to an active site Fe binuclear center. Structure 1999;7(1):13–23.

[10] Zhang L, Happe T, Melis A. Biochemical and morphological characterization of sulfur-deprived and H_2-producing *Chlamydomonas reinhardtii* (green alga). Planta 2002;214(4):552–561.

[11] Ihara M, Nishihara H, Yoon K-S, Lenz O, Friedrich B, Nakamoto H, Kojima K, Honma D, Kamachi T, Okura I. Light-driven Hydrogen Production by a Hybrid Complex of a [NiFe]-Hydrogenase and the Cyanobacterial Photosystem I. Photochem Photobiol 2006;82(3):676.

[12] Nicolet Y, De Lacey AL, Vernède X, Fernández VM, Hatchikian EC, Fontecilla-Camps JC. Crystallographic and FTIR Spectroscopic Evidence of Changes in Fe Coordination Upon Reduction of the Active Site of the Fe-Only Hydrogenase from *Desulfovibrio desulfuricans*. J Am Chem Soc 2001;123(8):1596–1601.

[13] Yacoby I, Pochekailov S, Toporik H, Ghirardi ML, King PW, Zhang S. Photosynthetic electron partitioning between [FeFe]-hydrogenase and ferredoxin:NADP+-oxidoreductase (FNR) enzymes in vitro. Proc Natl Acad Sci U S A 2011;108(23):9396–9401.

[14] Berggren G, Adamska A, Lambertz C, Simmons TR, Esselborn J, Atta M, Gambarelli S, Mouesca JM, Reijerse E, Lubitz W, Happe T, Artero V, Fontecave M. Biomimetic assembly and activation of [FeFe]-hydrogenases. Nature 2013:1–5.

[15] Woessner JP, Masson A, Harris EH, Bennoun P, Gillham NW, Boynton JE. Molecular and genetic analysis of the chloroplast ATPase of *Chlamydomonas*. Plant Mol Biol 1984;3(3):177–190.

[16] Lubner CE, Knörzer P, Silva PJN, Vincent KA, Happe T, Bryant DA, Golbeck JH. Wiring an [FeFe]-Hydrogenase with Photosystem I for Light-Induced Hydrogen Production. Biochemistry 2010;49(48):10264–10266.

[17] Lubitz W, Reijerse E, van Gastel M. [NiFe] and [FeFe] Hydrogenases Studied by Advanced Magnetic Resonance Techniques. Chem Rev 2007;107(10):4331–4365.

[18] Lubner CE, Applegate AM, Knörzer P, Ganago A, Bryant DA, Happe T, Golbeck JH. Solar hydrogen-producing bionanodevice outperforms natural photosynthesis. Proc Natl Acad Sci U S A 2011;108(52):20988–20991.

[19] Mulder DW, Ratzloff MW, Shepard EM, Byer AS, Noone SM, Peters JW, Broderick JB, King PW. EPR and FTIR Analysis of the Mechanism of H_2 Activation by [FeFe]-Hydrogenase HydA1 from *Chlamydomonas reinhardtii*. J Am Chem Soc 2013;135(18):130424124821007.

[20] Ramundo S, Rahire M, Schaad O, Rochaix JD. Repression of Essential Chloroplast Genes Reveals New Signaling Pathways and Regulatory Feedback Loops in *Chlamydomonas*. Plant Cell 2013;25(1):167–186.

[21] Stripp ST, Goldet G, Brandmayr C, Sanganas O, Vincent KA, Haumann M, Armstrong FA, Happe T. How oxygen attacks [FeFe]-hydrogenases from photosynthetic organisms. Proc Natl Acad Sci U S A 2009;106(41):17331–17336.

[22] Fischer N, Stampacchia O, Redding K, Rochaix JD. Selectable marker recycling in the chloroplast. Mol Gen Genet 1996;251(3):373–380.

[23] Meuser JE, D'Adamo S, Jinkerson RE, Mus F, Yang W, Ghirardi ML, Seibert M, Grossman AR, Posewitz MC. Genetic disruption of both *Chlamydomonas reinhardtii* [FeFe]-hydrogenases: Insight into the role of *HYDA2* in H_2 production. Biochem Biophys Res Commun 2012;417(2):704–709.

[24] Gaffron H. The Oxyhydrogen Reaction in Green Algae and the Reduction of Carbon Dioxide in the Dark. Science 1940;91(2370):529–530.

[25] Harris EH, Stern DB, Witman G. The *Chlamydomonas* Sourcebook. San Diego: Academic Press, 1989.

[26] Gaffron H. Reduction of Carbon Dioxide Coupled with the Oxyhydrogen Reaction in Algae. J Gen Physiol 1942;26(2):241–267.

[27] Boyer ME, Stapleton JA, Kuchenreuther JM, Wang CW, Swartz JR. Cell-free synthesis and maturation of [FeFe] hydrogenases. Biotechnol Bioeng 2008;99(1):59–67.

[28] Boynton JE, Gillham NW, Harris EH, Hosler JP, Johnson AM, Jones AR, Randolph-Anderson BL, Robertson D, Klein TM, Shark KB. Chloroplast transformation in *Chlamydomonas* with high velocity microprojectiles. Science 1988;240(4858):1534–1538.

[29] Liebgott PP, Leroux F, Burlat B, Dementin S, Baffert C, Lautier T, Fourmond V, Ceccaldi P, Cavazza C, Meynial-Salles I, Soucaille P, Fontecilla-Camps JC, Guigliarelli B, Bertrand P, Rousset M, Léger C. Relating diffusion along the substrate tunnel and oxygen sensitivity in hydrogenase. Nat Chem Biol 2009;6(1):63–70.

[30] Posewitz MC, Dubini A, Meuser JE, Seibert M, Ghirardi ML. Hydrogenases, hydrogen production, and anoxia. The Chlamydomonas Sourcebook: Organellar and Metabolic Processes. Vol. 2. Elsevier, 2009.

[31] Forestier M, King P, Zhang L, Posewitz M, Schwarzer S, Happe T, Ghirardi ML, Seibert M. Expression of two [Fe]-hydrogenases in *Chlamydomonas reinhardtii* under anaerobic conditions. Eur J Biochem 2003;270(13):2750–2758.

[32] Happe T, Mosler B, Naber JD. Induction, localization and metal content of hydrogenase in the green alga *Chlamydomonas reinhardtii*. Eur J Biochem 1994;222(3):769–774.

[33] Beers R, Sizer I. A spectrophotometric method for measuring the breakdown of hydrogen peroxide by catalase. J Biol Chem 1952;195(1):133–140.

[34] Buchman GW, Schuster DM, Rashtchian A. Selective RNA amplification: a novel method using dUMP-containing primers and uracil DNA glycosylase. PCR Methods Appl 1993;3(1):28–31.

[35] Franzén LG, Rochaix JD, Heijne von G. Chloroplast transit peptides from the green alga *Chlamydomonas reinhardtii* share features with both mitochondrial and higher plant chloroplast presequences. FEBS Lett 1990;260(2):165–168.

[36] Porra RJ, Thompson WA, Kriedemann PE. Determination of accurate extinction coefficients and simultaneous equations for assaying chlorophylls a and b extracted with four different solvents: verification of the concentration of chlorophyll standards by atomic absorption spectroscopy. Biochim Biophys Acta 1989;975(3):384–394.

[37] Keegstra K. Transport and routing of proteins into chloroplasts. Cell 1989;56(2):247.

38] Shao N, Beck CF, Lemaire S, Krieger-Liszkay A. Photosynthetic electron flow affects H_2O_2 signaling by inactivation of catalase in *Chlamydomonas reinhardtii*. Planta 2008;228(6):1055–1066.

[39] Nakano Y, Asada K. Hydrogen peroxide is scavenged by ascorbate-specific peroxidase in spinach chloroplasts. Plant and Cell Physiol 1981;22(5):867–880.

[40] Mulder DW, Boyd ES, Sarma R, Lange RK, Endrizzi JA, Broderick JB, Peters JW. Stepwise [FeFe]-hydrogenase H-cluster assembly revealed in the structure of $HydA^{\Delta EFG}$. Nature 2010;465(7295):248–251.

[41] Happe T, Naber JD. Isolation, characterization and N-terminal amino acid sequence of hydrogenase from the green alga *Chlamydomonas reinhardtii*. Eur J Biochem 1993;214(2):475–481.

[42] Lill R. Function and biogenesis of iron–sulphur proteins. Nature 2009;460(7257):831–838.

[43] Behn W, Herrmann RG. Circular molecules in the β-satellite DNA of *Chlamydomonas reinhardii*. Mol Gen Genet 1977;157(1):25–30.

[44] Pilon M, Abdel-Ghany SE, Van Hoewyk D, Ye H, Pilon-Smits EAH. Biogenesis of iron-sulfur cluster proteins in plastids. Genetic Engineering. Springer US, 2006. 101–117.

[45] Esselborn J, Lambertz C, Adamska-Venkatesh A, Simmons T, Berggren G, Noth J, Siebel J, Hemschemeier A, Artero V, Reijerse E, Fontecave M, Lubitz W, Happe T. Spontaneous activation of [FeFe]-hydrogenases by an inorganic [2Fe] active site mimic. Nat Chem Biol 2013;9(10)607-609.

[46] Posewitz MC. Discovery of Two Novel Radical S-Adenosylmethionine Proteins Required for the Assembly of an Active [Fe] Hydrogenase. J Biol Chem 2004;279(24):25711–25720.

[47] Redding K, MacMillan F, Leibl W, Brettel K, Hanley J, Rutherford AW, Breton J, Rochaix J-D. A systematic survey of conserved histidines in the core subunits of Photosystem I by site-directed mutagenesis reveals the likely axial ligands of P700. EMBO J 1998;17(1):50–60.

[48] Kuchenreuther JM, Britt RD, Swartz JR. New Insights into [FeFe]-Hydrogenase Activation and Maturase Function. PLoS ONE 2012;7(9):e45850.

[49] Shepard EM, McGlynn SE, Bueling AL, Grady-Smith CS, George SJ, Winslow MA, Cramer SP, Peters JW, Broderick JB. Synthesis of the 2Fe subcluster of the [FeFe]-hydrogenase H cluster on the HydF scaffold. Proc Natl Acad Sci U S A 2010;107(23):10448–10453.

[50] Stuart TS, Gaffron H. The mechanism of hydrogen photoproduction by several algae. Planta 1972;106(2):101–112.

[51] Ball SG, Dirick L, Decq A, Martiat JC, Matagne R. Physiology of starch storage in the monocellular alga *Chlamydomonas reinhardtii*. Plant Sci 1990;66(1):1–9.

[52] Abeles FB. Cell-free Hydrogenase from *Chlamydomonas*. Plant Physiol 1964;39(2):169–176.

[53] Fouchard S, Hemschemeier A, Caruana A, Pruvost J, Legrand J, Happe T, Peltier G, Cournac L. Autotrophic and Mixotrophic Hydrogen Photoproduction in Sulfur-Deprived *Chlamydomonas* Cells. Appl Environ Microbiol 2005;71(10):6199–6205.

[54] Saenger W. The structure of the blue starch-iodine complex. Naturwissenschaften 1984;71(1):31–36.

[55] Chochois V, Dauvillee D, Beyly A, Tolleter D, Cuine S, Timpano H, Ball S, Cournac L, Peltier G. Hydrogen Production in *Chlamydomonas*: Photosystem II -Dependent and -Independent Pathways Differ in Their Requirement for Starch Metabolism. Plant Physiol 2009;151(2):631–640.

[56] Kato J, Yamahara T, Tanaka K, Takio S, Satoh T. Characterization of catalase from green algae *Chlamydomonas reinhardtii*. J Plant Physiol 1997;151(3):262–268.

[57] Gibbs M, Gfeller RP, Chen C. Fermentative metabolism of *Chlamydomonas reinhardii* III. Photoassimilation of acetate. Plant Physiol 1986;82(1):160–166.

[58] Michelet L, Roach T, Fischer BB, Bedhomme M, Lemaire S, Krieger-Liszkay A. Down-regulation of catalase activity allows transient accumulation of a hydrogen peroxide signal in *Chlamydomonas reinhardtii*. Plant Cell Environ 2013;36(6):1204–1213.

[59] Godde D, Trebst A. NADH as electron donor for the photosynthetic membrane of *Chlamydomonas reinhardii*. Arch Microbiol 2013;127(3):245–252.

[60] Kruse O, Rupprecht J, Bader K-P, Thomas-Hall S, Schenk PM, Finazzi G, Hankamer B. Improved photobiological H_2 production in engineered green algal cells. J Biol Chem 2005;280(40):34170–34177.

[61] Gfeller RP, Gibbs M. Fermentative Metabolism of *Chlamydomonas reinhardtii*: I. Analysis of Fermentative Products from Starch in Dark and Light. Plant Physiol 1984;75(1):212–218.

[62] Ohta S, Miyamoto K, Miura Y. Hydrogen evolution as a consumption mode of reducing equivalents in green algal fermentation. Plant Physiol 1987;83(4):1022–1026.

[63] Komine Y, Kwong L, Anguera MC, Schuster G, Stern DB. Polyadenylation of three classes of chloroplast RNA in *Chlamydomonas reinhadtii*. RNA 2000;6(4):598–607.

[64] Noth J, Krawietz D, Hemschemeier A, Happe T. Pyruvate:Ferredoxin Oxidoreductase Is Coupled to Light-independent Hydrogen Production in *Chlamydomonas reinhardtii*. J Biol Chem 2013;288(6):4368–4377.

[65] Wykoff DD, Davies JP, Melis A, Grossman AR. The regulation of photosynthetic electron transport during nutrient deprivation in *Chlamydomonas reinhardtii*. Plant Physiol 1998;117(1):129–139.

[66] Sweeney WV, Rabinowitz, JC. Proteins containing 4Fe-4S clusters: an overview. Annu Rev Biochem 1980;49(1):139–161.

[67] Happe T, Kaminski A. Differential regulation of the Fe-hydrogenase during anaerobic adaptation in the green alga *Chlamydomonas reinhardtii*. Eur J Biochem 2002;269(3):1022–1032.

[68] Hemschemeier A, Fouchard S, Cournac L, Peltier G, Happe T. Hydrogen production by *Chlamydomonas reinhardtii*: an elaborate interplay of electron sources and sinks. Planta 2007;227(2):397–407.

[69] Eivazova ER, Markov SA. Conformational regulation of the hydrogenase gene expression in green alga *Chlamydomonas reinhardtii*. Int J Hydrogen Energy 2012;37(23):17788–17793.

[70] Hicks GR, Hironaka CM, Dauvillee D, Funke RP, D'Hulst C, Waffenschmidt S, Ball SG. When Simpler Is Better. Unicellular Green Algae for Discovering New Genes and Functions in Carbohydrate Metabolism. Plant Physiol 2001;127(4):1334–1338.

[71] Whitney LAS, Loreti E, Alpi A, Perata P. Alcohol dehydrogenase and hydrogenase transcript fluctuations during a day-night cycle in *Chlamydomonas reinhardtii*: the role of anoxia. New Phytol 2010;190(2):488–498.

[72] Driesener RC, Challand MR, McGlynn SE, Shepard EM, Boyd ES, Broderick JB, Peters JW, Roach PL. [FeFe]-Hydrogenase Cyanide Ligands Derived From S-Adenosylmethionine-Dependent Cleavage of Tyrosine. Angew Chem Int Ed 2010;49(9):1687–1690.

[73] Crack JC, Green J, Cheesman MR, Le Brun NE, Thomson AJ. Superoxide-mediated amplification of the oxygen-induced switch from [4Fe-4S] to [2Fe-2S] clusters in the transcriptional regulator FNR. Proc Natl Acad Sci U S A 2007;104(7):2092–2097.

[74] Zeng J, Zhang M, Sun X. Molecular Hydrogen Is Involved in Phytohormone Signaling and Stress Responses in Plants. PLoS ONE 2013;8(8):e71038.

[75] Kuchka MR, Goldschmidt-Clermont M, van Dillewijn J, Rochaix JD. Mutation at the *Chlamydomonas* nuclear *NAC2* locus specifically affects stability of the chloroplast *psbD* transcript encoding polypeptide D2 of PS II. Cell 1989;58(5):869–876.

[76] Nickelsen J, van Dillewijn J, Rahire M, Rochaix JD. Determinants for stability of the chloroplast *psbD* RNA are located within its short leader region in *Chlamydomonas reinhardtii*. EMBO J. 1994;13(13):3182–3191.

[77] Stirnberg M, Happe T. Identification of a cis-acting element controlling anaerobic expression of the *hydA*-gene from *Chlamydomonas reinhardtii*. Biohydrogen III, J. Miyake, Y. Igarashi and M. Rögner (Eds) 2004:117–127.

[78] Pape M, Lambertz C, Happe T, Hemschemeier A. Differential Expression of the *Chlamydomonas* [FeFe]-Hydrogenase-Encoding HYDA1 Gene Is Regulated by the COPPER RESPONSE REGULATOR1. Plant Physiol 2012;159(4):1700–1712.

[79] Mulder DW, Ortillo DO, Gardenghi DJ, Naumov AV, Ruebush SS, Szilagyi RK, Huynh B, Broderick JB, Peters JW. Activation of $HydA^{\Delta EFG}$ Requires a Preformed [4Fe-4S] Cluster. Biochemistry 2009;48(26):6240–6248.

[80] Moroney JV, Husic HD, Tolbert NE, Kitayama M, Manuel LJ, Togasaki RK. Isolation and characterization of a mutant of *Chlamydomonas reinhardtii* deficient in the CO_2 concentrating mechanism. Plant Physiol 1989;89(3):897–903.

[81] Thyssen C, Hermes M, Sültemeyer D. Isolation and characterisation of *Chlamydomonas reinhardtii* mutants with an impaired CO_2-concentrating mechanism. Planta 2003;217(1):102–112.

[82] Kuchenreuther JM, Grady-Smith CS, Bingham AS, George SJ, Cramer SP, Swartz JR. High-Yield Expression of Heterologous [FeFe] Hydrogenases in *Escherichia coli*. PLoS ONE 2010;5(11):e15491.

[83] Mubarakshina MM, Ivanov BN, Naydov IA, Hillier W, Badger MR, Krieger-Liszkay A. Production and diffusion of chloroplastic H_2O_2 and its implication to signalling. J Exp Bot 2010;61(13):3577–3587.

Chapter 4

Conclusions

In this dissertation, the characteristics of two electron transport proteins have been investigated. In Chapter 2, it was demonstrated that mutation of a leucine residue in PSI whose peptide nitrogen acts as a hydrogen bond donor to the PhQ cofactor resulted in an unexpected acceleration of PhQ•- to F_X oxidation kinetics in the mutant set. Increasing the size of the residue side chain as with the tyrosine residue, or introducing beta-branching with threonine, appeared to perturb the hydrogen bonding to the PhQ, destabilize the phyllosemiquinone, and thus increase the forward driving force for electron transfer. This acceleration of oxidation kinetics between the two cofactors is the first presented for this organism, and suggests the ability to engineer *Chlamydomonas* for increased electron transfer rates with additional novel destabilizing mutations.

Chapter 3 demonstrates the first example of a nuclear-expressed, chloroplast-localized metalloprotein successfully synthesized and functioning *in situ*. A chloroplast codon-optimized hydrogenase (cp*hydA*) was transformed into the organelle and produced transcript and cpHydA apoprotein under both aerobic and anaerobic conditions. More importantly, it evolved twice the amount of hydrogen as the parent and control strains under anaerobic conditions, supporting the hypothesis that it was producing a functional protein. The initially difficulties in maintaining the system point to the importance of native regulation. However, this proof-of-concept encourages work on the designed PSI-hydrogenase fusion described in Appendix 2 for continuous photo-production of hydrogen.

APPENDIX 1

Permission to reproduce selected figures in Chapter 2 from the American Chemical Society

Copyright Clearance Center RightsLink®

Home Create Account Help

ACS Publications High quality. High impact.

Title: Interquinone Electron Transfer in Photosystem I As Evidenced by Altering the Hydrogen Bond Strength to the Phylloquinone(s)

Author: Stefano Santabarbara, Kiera Reifschneider, Audrius Jasaitis, Feifei Gu, Giancarlo Agostini, Donatella Carbonera, Fabrice Rappaport, and Kevin E. Redding

Publication: The Journal of Physical Chemistry B

Publisher: American Chemical Society

Date: Jul 1, 2010

User ID

Password

Enable Auto Login

LOGIN

Forgot Password/User ID?

If you're a copyright.com user, you can login to RightsLink using your copyright.com credentials. Already **a RightsLink user** or want to learn more?

PERMISSION/LICENSE IS GRANTED FOR YOUR ORDER AT NO CHARGE

This type of permission/license, instead of the standard Terms & Conditions, is sent to you because no fee is being charged for your order. Please note the following:

- Permission is granted for your request in both print and electronic formats, and translations.
- If figures and/or tables were requested, they may be adapted or used in part.
- Please print this page for your records and send a copy of it to your publisher/graduate school.
- Appropriate credit for the requested material should be given as follows: "Reprinted (adapted) with permission from (COMPLETE REFERENCE CITATION). Copyright (YEAR) American Chemical Society." Insert appropriate information in place of the capitalized words.
- One-time permission is granted only for the use specified in your request. No additional uses are granted (such as derivative works or other editions). For any other uses, please submit a new request.

BACK CLOSE WINDOW

APPENDIX 2

Designing a PSI-hydrogenase fusion for direct and continuous photo-production of hydrogen *in vivo*

Introduction

As outlined in the overall Introduction, there is a significant need for sustainable and scale-able alternative fuel options. Despite concerns about energy density, storage, and distribution of hydrogen fuel, it is being considered as a viable option for specific applications. As also mentioned in the foregoing text, despite an apparently simple structure, the *Chlamydomonas reinhardtii* hydrogenases have a high specific activity[1], making the organism well suited for the photo-production of biohydrogen. Precedence has already been set for the use of *C. reinhardtii* as a biohydrogen producer[2,3]. However, with the sulfur-deprivation methods currently in use[4], the reported *in vivo* hydrogen yields from this organism are far shy of the theoretical maximum. Temporal separation of photosynthetic oxygen evolution and carbon accumulation from metabolite catabolism and H_2 production addresses the vexing problem of oxygen sensitivity of the [FeFe]-hydrogenase, but the adaptation is time-intensive[5], and the absence of sulfur is detrimental to production of cellular proteins[6] and eventually lethal for the cells. Understandably, this is a large detractor for any production enterprise. As photosynthesis operates with relatively high efficiency (about 40% when calculated from photosynthetically active radiation (PAR)), it is natural to pursue methods to harness this electron flow for human applications. In this applied section of the research, a preliminary system design has been completed that would achieve *continuous* light-driven hydrogen production by way of a hybrid complex of the endogenous [FeFe]-hydrogenase and PsaC of Photosystem I in *C. reinhardtii* (Figure A2-1).

The design is for a fusion protein that directly links the FeS-cluster containing PsaC with the hydrogenase to allow direct electron transfer between the two. *In vivo,*

these two complexes are not redox partners, but the transfer appears thermodynamically possible. The terminal FeS clusters F_A and F_B of PSI have redox potentials between -440 and -480 mV[7], close to values of the H^+/H_2 couple at -420 mV[8]. In essence, the two proteins would be arranged in such a way as to align the FeS clusters in both, and extend a 'molecular wire' throughout the complex, facilitating electron transfer and expediting the hydrogen production process.

The conceptual design of the system has been completed, as has the molecular biology methodology for constructing the fusion. Work on the selective system, expression of the native uptake hydrogenase under control of a repressible promoter, and directed evolution of successful fusion-containing strains (Figure A2-2) is being continued by other researchers.

Design of the PsaC-HydA fusion

The ideal fusion protein would place the hydrogen-generating catalytic site (H-cluster) of the hydrogenase as close as possible to the terminal [4Fe-4S] cluster (F_B) found in the PsaC cluster of PSI. The H-cluster does not need to be so close to F_B that it allows ultra-fast electron transfer (i.e. >1 ns^{-1}), however it must be competitive with the back-reaction from F_A/F_B ($\tau \approx 100$ ms). A rate of 10^3 s^{-1} would thus be sufficient to give ~99% yield, corresponding to a distance of ~20 Å under optimal conditions, according to the Moser-Dutton 'ruler'[9]. An ideal rate would be 1-2 orders of magnitude faster, so as to avoid being the limiting factor for overall electron transfer through the PETC (which is usually at the level of cytochrome b_6f).

Using the predicted structure model of HydA2[10] (82% sequence identity with HydA1 with deviations not located in the catalytic centre) and the structure of cyanobacterial PsaC[11], it has been determined that the most logical insertion point for HydA is within an outward-facing β-hairpin in PsaC, which caps the F_B cluster (Figure A2-3). The N- and C-termini of the hydrogenase are close to each other, making this fusion a possibility. In the β-hairpin of PsaC, none of the residues are ligands to the FeS cluster, lessening the risk of function disruption when inserting HydA. In this orientation, the fusion protein would place the H-cluster of HydA within 17-18 Å of the F_B cluster (edge-to-edge).

A similar proof-of-concept fusion was constructed by Ihara[8] wherein a fusion of the [NiFe]-hydrogenase from *Ralstonia eutropha* with PsaE from *Thermosynechococcus elongatus* produced a viable, albeit sluggish, hydrogen-producing *in vitro* assembly. Ihara's success, as well as that of Yacoby[12] and Lubner[13,14] and colleagues is encouraging, but the design described here, by virtue of using endogenous enzymes and directed evolution, may result in a more robust and commercially viable *in vivo* system. A fully biological system allows for a cost-effective scale-up and continual self-repair of the system not available in an *in vitro* electrode-hydrogenase system. Using the enzymes endogenous to the organism ensures compatibility between the components. Native electron donors are known to work, and no new maturases or chaperones are required. The work detailed in Chapter 3 demonstrated that the native hydrogenase could be expressed in the chloroplast. Finally, a defined but flexible selection scheme affords the organism the opportunity to direct evolution to optimize growth and production.

The selective system and directed evolution

The system depicted in Figure A2-4 was designed to allow directed evolution to select for fusion-containing variants that thrive under ambient conditions (and also in the presence of O_2). Photosynthetic electron flow passes through PSI, and from PsaC, through the fused hydrogenase. An added repressible uptake hydrogenase uses H_2 produced by the fusion hydrogenase to reduce ferredoxin. By making electron transfer via the fusion the only pathway that results in Fd reduction, only this pathway will result in the continuation of essential cell activities like growth and CO_2 fixation. A selective pressure is thus applied toward the generation of organisms that optimize the fusion system and all associated components. It is expected that the system will work poorly at first, and it is also likely that the organisms must be provided a "leg up" by initially providing a milder environment such as low O_2 and/or additional H_2 to feed into the uptake hydrogenase (top H_2ase in Figure A2-4). Over time, and increasingly stressful conditions, the system is set up such that organisms will be rewarded for increased electron throughput by faster growth, and the most optimized variants will come to dominate the culture.

Expressing the uptake hydrogenase under control of a repressible promoter

To install an uptake hydrogenase under control of a repressible promoter, the *hydA1* gene can be placed under control of the METE promoter, which is repressed by the presence of cobalamin[15]. This can be introduced into a *hydA1/hydA2* knockout, wherein addition of cobalamin would repress the expression of the soluble uptake hydrogenase while allowing the fusion hydrogenase to function. The ability to switch off

the uptake hydrogenase allows the measurement of H_2 production to see if growth and improvements are due to better hydrogen production, better uptake, or both (Figure A2-5). Note that in the repressed system, the proton pump still makes ATP and so cells will maintain energy reserves, but they will not grow in the absence of an organic carbon source. Optimizing this system is the overarching goal in the continuation of this project.

Materials and Methods

Fusion protein design

DNA sequence data for *C. reinhardtii psaC* and *HYDA2* were obtained as Gene ID numbers 2717046 and 5720168 from the NCBI PubMed database (National Center for Biotechnology Information, U.S. National Library of Medicine). Protein crystal structure data for PsaC was obtained from the cyanobacterial structure[11] and that for HydA2 was obtained from the authors of Chang, et. al.[10]. Visualization of the proteins and construction of a hypothetical fusion protein was accomplished in Swiss-PDB viewer software (Swiss Institute of Bioinformatics).

Designing the ligation independent cloning (LIC) site and primers

A protocol for ligation-independent cloning, and guidelines for the design of successful primers were derived from the literature [16-18]. Degenerate primers listed in Table A2-1 below were obtained from Invitrogen. See 'Results' for design rationale.

Synthesized fusion gene

After submitting the sequence depicted in Figure A2-6, the sequence was codon-optimized (Genscript) to reflect the relatively AT-rich bias of the *C. reinhardtii* chloroplast, as compared to the GT-rich nuclear genome. The fusion gene was synthesized by Genscript (Piscataway, NJ) and provided as a library of sixteen individual clones in pUC57 vectors (Table A2-2). Note that there are actually only fifteen unique amino acids coded by the degenerate codon 'XXT'; serine is represented twice.

Cloning mutants with different codons at the PsaC-HydA junction

Each of the sixteen different fusion gene library components were cloned separately into the chloroplast transformation vector pBSEP5.8 (courtesy of Jean-David Rochaix, Université de Genève) with NdeI and BglII (enzymes from New England Biolabs). Transformation into NEB 5α competent cells was followed by selection on LB with ampicillin (100 mg L^{-1}) and spectinomycin (100 mg L^{-1}). Putative clones were verified by test-digestion with NdeI and BglII as well as verification of the sequence of the degenerate region using primers designed to amplify the *psaC* gene (*psaC*-3': GATCTCACCAAGATACT and *psaC*-5': GATATGGAGATGACATA (ASU DNA Laboratory)).

Bioballistic transformation

For test transformation of *psaC*Δ recipient strains, transformation was performed by an adapted method of Boynton[19]. For each of the transformations listed in Table A2-3, 1 μg of plasmid pBSEP5.8 or K52R53-SA (both generously provided by J.D.

Rochaix, and described in the literature [20,21]) was adsorbed onto 1-μm diameter tungsten nanoparticles (50 mg mL^{-1}, J.D. Rochaix) in a mixture with $CaCl_2$ (1 M) and spermidine (20 mM). Recipient strains were prepared by first counting cells with a hemocytometer (Hausser Scientific), and concentrating by centrifugation to plate 10^7 cells per Tris- acetate- phosphate (TAP) or Tris- bicarbonate- phosphate plate[22]. Each shot with a homemade helium-driven gene-gun delivered 10 μL of the DNA mixture (200 ng DNA) per plate. Transformants of pBSEP5.8 were screened under high light for restoration of photosynthetic ability, and K52R53-SA transformants were screened under low light for spectinomycin resistance. The *psaC* region of both transformant sets was sequenced using *psaC* primers as above to confirm strain identity (ASU DNA Laboratory).

Light sensitivity and reconstruction assay

In order to develop selective light conditions to screen fusion transformants, the parental *psaC*Δ strain was mixed with transformant *psaC*Δ[*K52R53-SA*], a mutant with low PSI accumulation, in order to see if light levels alone could select for the strains with low PSI. Strains were cultured in the dark in TAP media to mid-log phase growth. Cell concentration was determined by hemocytometer (Hausser Scientific) and cells of the *psaC*Δ strain alone, the *psaC*Δ[*K52R53-SA*] strain diluted into the *psaC*Δ strain at 1/1000 and the *psaC*Δ[*K52R53-SA*] strain alone were plated at 10^3, 10^4, and 10^5 cells/plate and grown on TAP plates at light fluxes of 0, 50, and 100 μmol photos m^{-2} s^{-1}. Growth was documented after one week.

Optimization of PsaC immunoblotting

New α-PsaC antibodies were obtained from Agrisera for testing. TK membranes were loaded by equal protein (samples were diluted into TK membranes from a *psaC*Δ strain) and prepared PSI particles were diluted into SDS buffer and run on a 4-12% Tris-Glycine gel (Novex, Invitrogen), then transferred to a PVDF membrane (Millipore). The blot was probed with the primary α-PsaC antibody from Agrisera at 1:1000 for 1.5 h and the secondary goat anti-rabbit HRP conjugate was used at 1:10,000 (Bio-Rad) for 1 h then visualized with ECL (SuperSignal West Femto Chemiluminescent Substrate, Thermo).

Results and Discussion

Fusion gene design

Using DNA and protein sequence data as described in Materials and Methods, the fusion protein was designed with the sequence in Figure A2-6. In the first section of PsaC (red in A2-6), the native *C. reinhardtii* sequence is WDGCK for residues 30-34. Asp (D) was made degenerate (bold X in A2-6) and replaced with the amino acids in Table A2-2, while deleting the Cys (C) and Lys (K). In the HydA2 model[10], the HydA2 protein ends in YVP, but the sequence shows that it continues with GGAEA. In the ligation independent cloning method, the GG was retained and the AEA replaced with the LIC-introduced flexible linker, at the C-terminal end.

Designing the ligation independent cloning (LIC) site and primers

The linker region in Figure A2-7A was modified to engineer a six-cutter site into the space. A restriction site that required minimal adaptation (silent mutations only) for enzyme recognition was preferred. Upon removal of the ASA linker, replacement with the restriction site GGCGCC was accomplished with only two codon substitutions: GGT to GGC for Gly, and GCA and GCC for Ala (Figure A2-7B). DNA T4 polymerase exhibits 3' to 5' exonuclease activity, and in the presence of a single dNTP, will chew back from a cut site until stopped by that nucleotide in the sequence. In the presence of dATP, the sequence had to be modified to extend the 'sticky end' overlap after this exonuclease activity (Figure A2-7C). There are three six-cutter enzymes with the shown recognition sequence: KasI, SfoI, and NarI. The SfoI enzyme is ideal. The cleavage position allows us to end the designed primer sequence at the Gly before the linker, creating flexibility in the linker region. Primers have been designed such that when the fusion gene is digested at an engineered SfoI site (Figure A2-7D) and chewed back with DNA T4 polymerase in the presence of dATP (Figure A2-7E), the primers will anneal to these overhangs. When ligated, they should produce a plasmid containing the new flexible linker. The preset nucleotide in the wobble position (i.e. the 'T' of 'XXT') provides an additional 'lock' between the two primers to ensure annealing. The pBSEP5.8 (*psaC* vector) sequence has no recognition sites for SfoI (GGCGCC), making the introduced site unique in the plasmid.

Subcloning the synthesized fusion gene into a psaC vector

The gene sequence in Figure A2-8 was submitted to Genscript for synthesis and delivered in a pUC57 vector. The sequence was cloned into the SfoI site in the MCS to inactivate it, making the engineered site unique in this vector. As described in the Materials and Methods, the fusion sequence was subcloned into the chloroplast transformation vector pBSEP5.8. Other researchers are now introducing the second region of degeneracy via ligation independent cloning in preparation for transformation.

Test transformations of recipient strains

Plasmids containing the fusion genes encoding different variants of the PsaC-HydA2-PsaC chimeric protein were designed to be shot into a *psaCΔ* algal background. Test transformations were performed to check both transformability and growth phenotypes of variable PSI-accumulating strains (Table A2-3). Initial test transformation of the 1001-11A *psaCΔ* strain was performed, but repeated when a His_6-tagged parent strain was generated by the method of Gulis[23]. Any future downstream efforts to purify and assay a successful fusion *in vitro* would be greatly simplified by IMAC purification. The *psbAΔ psaCΔ* strain was test-transformed with the thought that the absence of PSII would be helpful if there was a desire to limit O_2 levels in the cell.

The *psaCΔ* strain was readily transformed with plasmid pBSEP5.8 and produced dark green colonies with strong growth on minimal media (TBP) under high light conditions (data not shown).

Light sensitivity and reconstruction assay

In order to select for fusion transformants shot into a *psaCΔ* strain, a light sensitivity assay was constructed. Under high light conditions, the partially photosynthetically-restored *psaC*Δ[K52R53-*SA*] appears morphologically distinct from the *psaCΔ* parent strain with larger and darker colonies. At the 10^4 and 10^5 cells/plate concentration however, some 'background' growth from the deletion is observed. At these plating concentrations, the 1/1000 mixture, intended to represent expected transformation efficiency, does show several isolatable transformants, however the background growth is still present and efficient screening of a library should not require single-colony picking in order to separate from background growth. Cells plated at a lower cell concentration (1.0×10^3 cells/plate) under high light conditions do not show background growth in the *psaCΔ* strain, and yielded 3-4 colonies per plate in the 1/1000 mixture (data not shown). In order to decrease the number of plates required to saturate the screen, a second reconstruction assay using media with fractional amounts of acetate and higher cell concentrations should be tested.

PsaC immunoblot optimization

When the completed fusion gene is transformed into a *psaCΔ* background, the only PsaC protein present will be that contributed by the fusion. Immunoblotting is a good method for measuring protein accumulation. A new *C. reinhardtii* α-PsaC antibody was provided by Agrisera for testing, and conditions for immunoblotting were optimized. These are presented in 'Materials and Methods' of this section, and the blot appears in

Figure A2-9 showing detection down to the level of 1.25 μg WT TK membranes diluted into membranes from a *psaCΔ* strain.

Conclusions

Taken with the proof of concept research in Chapter 3 demonstrating the feasibility of expressing a hydrogenase in the *Chlamydomonas* chloroplast, the design work and construction of molecular biology tools presented here will support the construction of a fusion protein of PSI and the native hydrogenase. The difficulties encountered with selective pressure in Chapter 3 should be less of an issue here, as the selection criterion (photosynthetic growth) is directly linked to a successful assembly of the fusion. The background strain contains no PsaC, so reversion to a WT phenotype is not likely. In addition, this experimental approach retains the benefit of flexibility. The 'fusion protein' is actually a library of sequence possibilities. By providing the organism options as opposed to one designed outcome, the chance for success increases as the organism can adapt what will work best in a given circumstance.

Table A2-1: Sequence of primers designed to introduce region of degeneracy by ligation-independent cloning.

Primer name	Sequence
n=2-s	CCTGGTGGCNNTNNT
n=2-as	NNANNACGGTCGGTTT
n=3-s	CCTGGTGGCNNTNNTNNT
n=3-as	NNANNANNACGGTCGGTTT
n=4-s	CCTGGTGGCNNTNNTNNTNNT
n=4-as	NNANNANNANNACGGTCGGTTT

Table A2-2: Identity of the degenerate codon 'XXT' in plasmids created from a synthesized fusion gene library.

Codon	Amino acid	Codon	Amino acid
AAT	Asn/N	GAT	Asp/D
ACT	Thr/T	GCT	Ala/A
AGT	Ser/S	GGT	Gly/G
ATT	Ile/I	GTT	Val/V
CAT	His/H	TAT	Tyr/Y
CCT	Pro/P	TCT	Ser/S
CGT	Arg/R	TGT	Cys/C
CTT	Leu/L	TTT	Phe/F

Table A2-3: Test transformations for completing *psaCΔ* strains.

Strain name	Traits	Test transformed with:
1001-11A	*psaCΔ*	pBSEP5.8 (*psaC*+)
1001-11A	*psaCΔ*	K52R53-SA (30% WT PSI accumulation)
1001-11A::H6	*psaCΔ,* H6-tagged *psaA*	pBSEP5.8 (*psaC*+)
1001-11A::H6	*psaCΔ,* H6-tagged *psaA*	K52R53-SA (30% WT PSI accumulation)
Fud7*psaC*Δ	*psbAΔ psaCΔ*	pBSEP5.8 (*psaC*+)

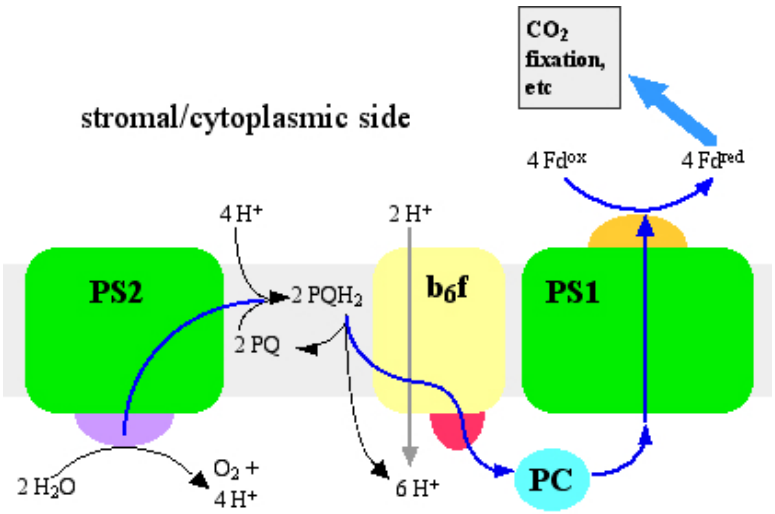

Native System

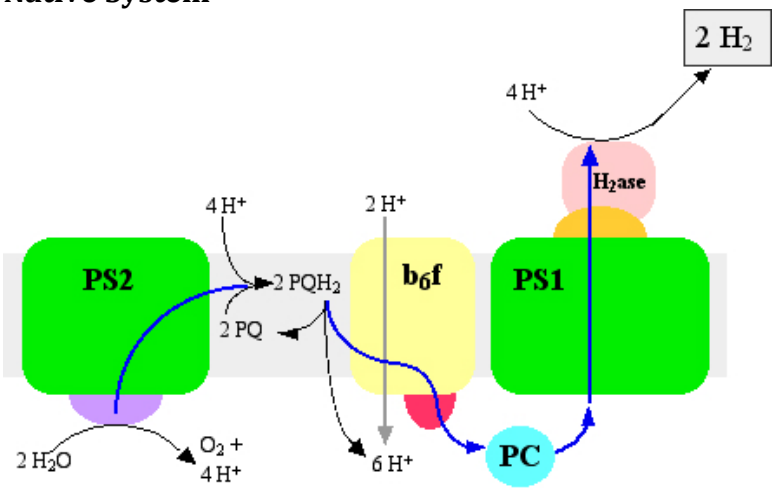

Engineered System

Figure A2-1: **Schematic of a hybrid complex of the endogenous [FeFe]-hydrogenase and PsaC of PS1 in *C. reinhardtii.*** The fusion places the electron transport proteins in close proximity in order to facilitate direct electron transport and the photo-production of biohydrogen.

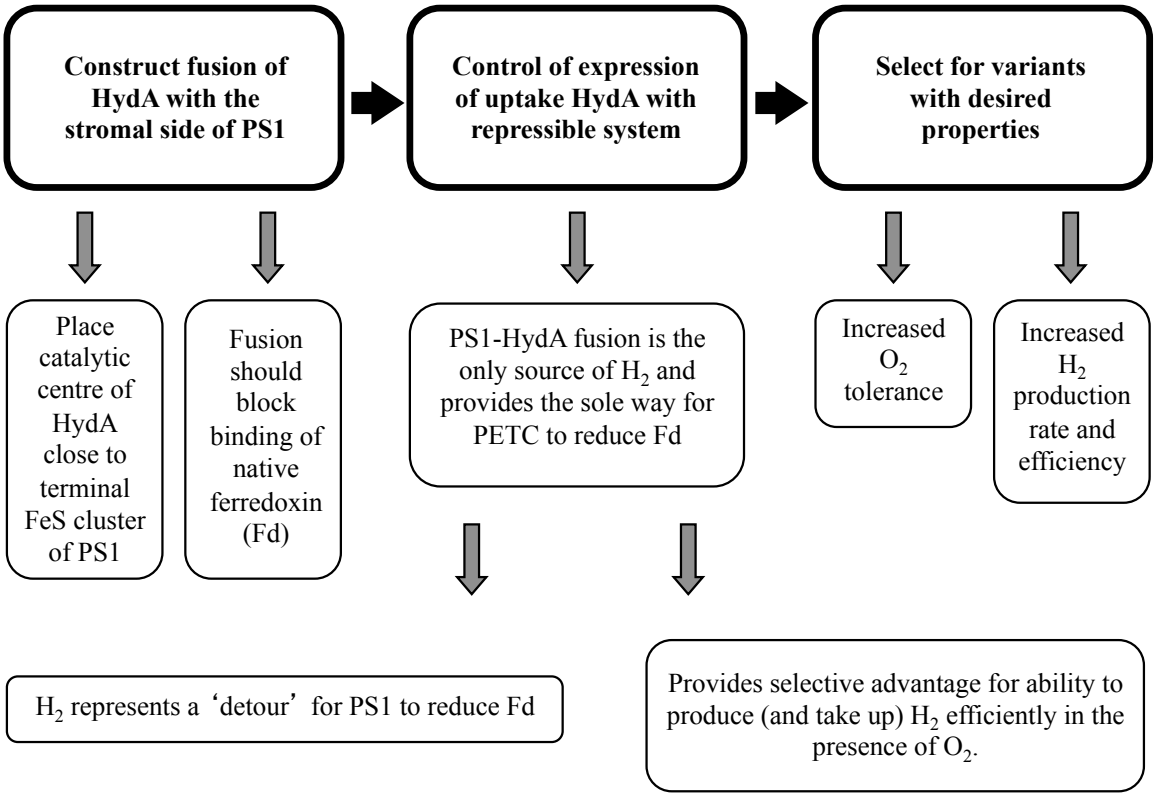

Figure A2-2: Experimental strategy to obtain an organism demonstrating consistent production of H_2. The fusion places the H-cluster of the hydrogenase close enough to the terminal FeS cluster of PS1 to allow forward electron transfer. The fusion should block the binding of the native ferredoxin. If the uptake function of hydrogenase in the system is provided by a repressible system only (Figure A2-4), the PS1-HydA fusion is the only source of H_2 and thus the only way for the organism to reduce ferredoxin and so donate to FNR and produce NADPH for essential metabolic functions. In this way, the production of hydrogen represents a 'detour' along the way to reduce ferredoxin and provides a selective advantage to strains able to produce and take up hydrogen efficiently in the presence of oxygen. In the last stage of selection, strains will be exposed to increasing concentrations of O_2 and tested for their ability to both adapt to the atmosphere and produce increased H_2 at increased rates.

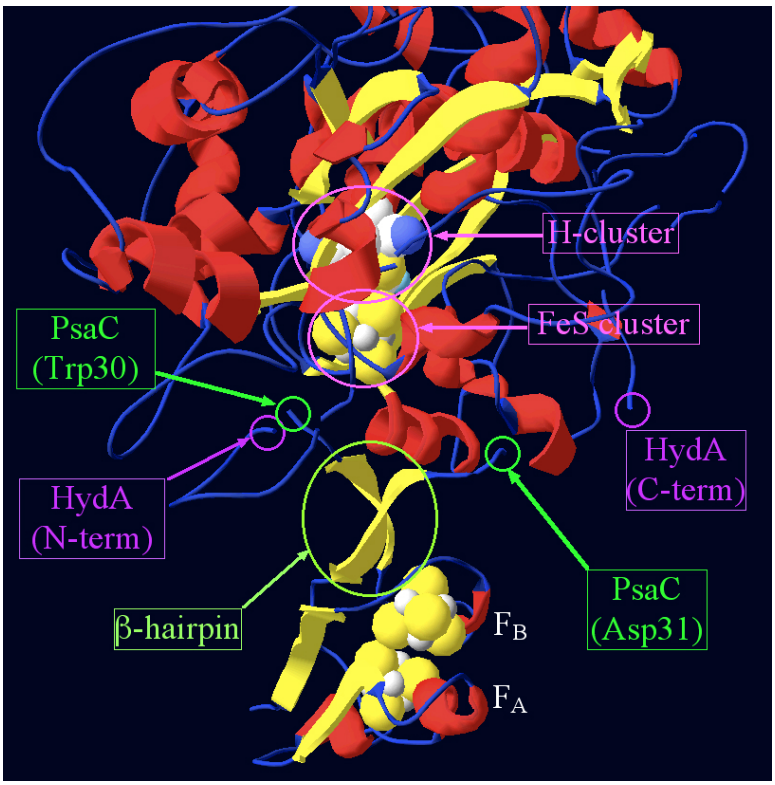

Figure A2-3: Modeled PsaC-HydA fusion. Created in Swiss-PDB Viewer, the structure is based on the coordinates of the HydA2 homology model[10] and the cyanobacterial PsaC[11]. Here, a β-hairpin (Leu25-Ser41) caps the F_B cluster, and a cut (shown) after Gly33 in PsaC should accommodate insertion of the hydrogenase. This orientation should also block the binding of the native ferredoxin.

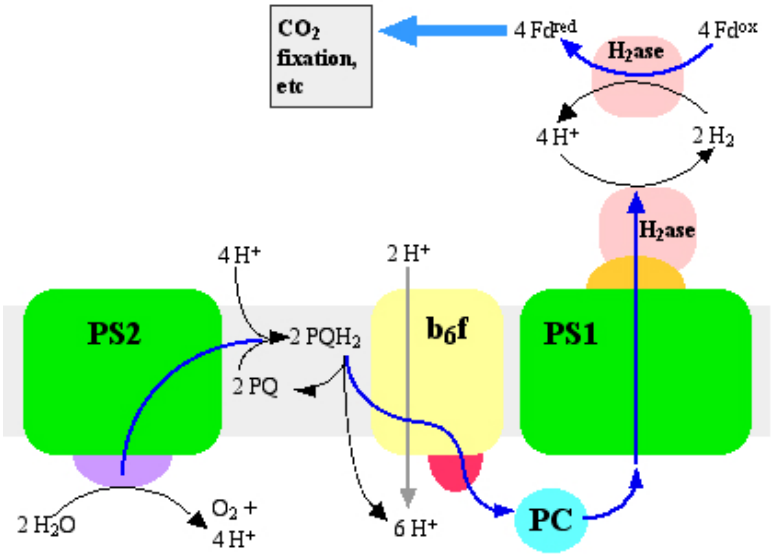

Figure A2-4: Use of a repressible uptake hydrogenase in the fusion system. Here, electrons from the PETC are routed through the fusion system. The fusion of the hydrogenase to PSI should block binding of the native ferredoxin. In the presence of a native but regulated uptake hydrogenase, electrons from hydrogen oxidation eventually reduce ferredoxin. If all of the H_2 is recycled by the system, the fusion should mimic the native situation in *C. reinhardtii*. This provides a selective advantage for variants that optimize function of the fusion system.

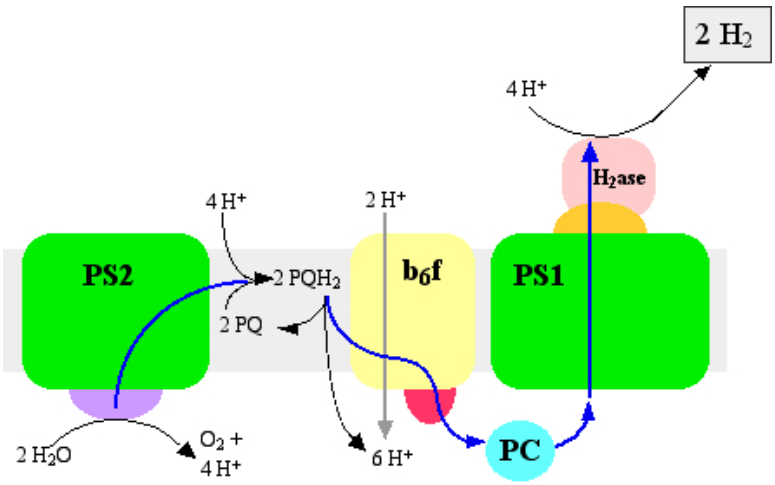

Figure A2-5: Repressing the uptake hydrogenase allows measurement of evolved H_2. Temporary repression of the uptake hydrogenase would allow for measurement of hydrogen production and the comparison of co-evolved strains. Note that for every two water molecules split by the oxygen-evolving complex, ten protons are pumped across the thylakoid membrane, maintaining the proton motive force and production of ATP.

MAHIVKIYDTCIGCTQCVRACPLDVLEMVPW**D**G//CK//ASQMASAPRTEDCVGC
KRCETACPTDFLSVRVYLGSESTRSMGLSY

A

ATATDAVPHWKLALEELDKPKDGGRKVLIAQVAPAVRVAIAESFGLAPGAVSPG
KLATGLRALGFDQVFDTLFAADLTIMEEGTELLHRLKEHLEAHPHSDEPLPMFTS
CCPGWVAMMEKSYPELIPFVSSCKSPQMMMGAMVKTYLSEKQGIPAKDIVMVS
VMPCVRKQGEADREWFCVSEPGVRDVDHVITTAELGNIFKERGINLPELPDSDW
DQPLGLGSGAGVLFGTTGGVMEAALRTAYEIVTKEPLPRLNLSEVRGLDGIKEAS
VTLVPAPGSKFAELVAERLAHKVEEAAAAEAAAAVEGAVKPPIAYDGGQGFSTD
DGKGGLKLRVAVANGLGNAKKLIGKMVSGEAKYDFVEIMACPAGCVGGGGQP
RSTDKQITQKRQAALYDLDERNTLRRSHENEAVNQLYKEFLGEPLSHRAHELLH
THYVP

B

MAHIVKIYDTCIGCTQCVRACPLDVLEMVPW**X**GATATDAVPHWKLALEELDKP
KDGGRKVLIAQVAPAVRVAIAESFGLAPGAVSPGKLATGLRALGFDQVFDTLFA
ADLTIMEEGTELLHRLKEHLEAHPHSDEPLPMFTSCCPGWVAMMEKSYPELIPFV
SSCKSPQMMMGAMVKTYLSEKQGIPAKDIVMVSVMPCVRKQGEADREWFCVS
EPGVRDVDHVITTAELGNIFKERGINLPELPDSDWDQPLGLGSGAGVLFGTTGGV
MEAALRTAYEIVTKEPLPRLNLSEVRGLDGIKEASVTLVPAPGSKFAELVAERLA
HKVEEAAAAEAAAAVEGAVKPPIAYDGGQGFSTDDGKGGLKLRVAVANGLGN
AKKLIGKMVSGEAKYDFVEIMACPAGCVGGGGQPRSTDKQITQKRQAALYDLD
ERNTLRRSHENEAVNQLYKEFLGEPLSHRAHELLHTHYVPGGXXXASQMASAP
RTEDCVGCKRCETACPTDFLSVRVYLGSESTRSMGLSY

C

Figure A2-6: Protein sequence for PsaC-HydA fusion. In **A**, red text indicates the PsaC polypeptide. The bold and black Asp (D) is converted into a degenerate codon for sequence flexibility (see Table A2-2 for the codon identities) in the fusion. After the glycine, the PsaC hairpin is cut for insertion of the hydrogenase, removing the Cys and Lys in the process. The second half of PsaC is used in its entirety for the C-terminal end of the fusion. In **B**, the HydA2 sequence as extracted from the Chang model[10] is presented. All (black) residues are included in the fusion. In **C**, the final designed fusion is shown with red text again indicating the PsaC polypeptide, the bold X representing the degenerate codon described above, and the black text highlighting the HydA2 contribution. The two gray Gly, while not present in the Chang model, are present in the HydA2 protein sequence. The following blue text shows the flexible linker to be added by ligation independent cloning.

```
 - HYDA2-----------| linker     |---- PsaC -
 Y   V   P   G   G   A   S   A   A   S   Q   M
TAT GTA CCA GGT GGT GCA TCT GCT GCA AGT CAA ATG
ATA CAT GGT CCA CCA CGT AGA CGA CGT TCA GTT TAC

TATGTACCAGGTGGTGCATCTGCTGCAAGTCAAATG
ATACATGGTCCACCACGTAGACGACGTTCAGTTTAC
```

A

```
TATGTACCAGGTGGCGCCAGTCAAATG
ATACATGGTCCACCGCGGTCAGTTTAC
```

B

```
TATGTACCTGGTGGCGCCAGCCAAATG
ATACATGGACCACCGCGGTCGGTTTAC
```

C

```
TATGTACCTGGTGGC        GCCAGCCAAATG
ATACATGGACCACCG        CGGTCGGTTTAC
```

D

```
TATGTA                 GCCAGCCAAATG
ATACATGGACCACCG                  AC
```

E

```
 Y   V   P   G   G          A   S   Q   M
TAT GTA CCT GGT GGC-(XXT)n-GCC AGC CAA ATG
ATA CAT GGA CCA CCG-(XXA)n-CGG TCG GTT TAC
```

F

Figure A2-7: Ligation-independent cloning site design and method of sequence insertion. (A) Between the C-terminal end of the hydrogenase, and point of fusion with PsaC, the sequence encoding ASA was deleted. (B) Silent substitutions resulted in the creation of a six-cutter restriction site at the insertion point. (C) Silent nucleotide changes extend the sticky-end overlap which will result from T4 polymerase action in the presence of dATP. (D) Digestion with SfoI results in a blunt cut. (E) Exonuclease/polymerase activity of T4 DNA polymerase in the presence of dATP creates sticky ends. (F) Annealing with designed LIC primers (blue and green) results in insertion of a new linker of random sequence.

CATATGGCTCATATCGTTAAAATTTACGATACTTGTATTGGTTGTACTCAATG
TGTACGTGCTTGTCCATTAGATGTTTTAGAAATGGTTCCATGGNNTGGTGCAA
CAGCTACTGATGCTGTTCCACACTGGAAATTAGCATTAGAAGAATTAGATAA
ACCTAAAGATGGTGGTCGTAAAGTTTTAATTGCTCAAGTAGCACCAGCTGTTC
GTGTAGCAATTGCTGAAAGTTTTGGTTTAGCACCAGGTGCTGTATCACCTGGT
AAATTAGCTACAGGTTTACGTGCATTAGGTTTCGATCAAGTTTTCGATACTTT
ATTCGCTGCAGATTTAACAATTATGGAAGAAGGTACTGAATTATTACATCGTT
TAAAAGAACACTTAGAAGCTCATCCACACTCTGATGAACCATTACCTATGTTT
ACAAGTTGTTGTCCTGGTTGGGTTGCTATGATGGAAAAATCTTATCCAGAATT
AATTCCTTTCGTATCATCTTGTAAAAGTCCACAAATGATGATGGGTGCTATGG
TTAAAACTTATTTATCAGAAAAACAAGGTATTCCAGCTAAAGATATTGTTATG
GTATCTGTTATGCCTTGTGTTCGTAAACAAGGTGAAGCTGATCGTGAATGGTT
TTGTGTATCAGAACCAGGTGTACGTGATGTTGATCATGTAATTACAACTGCTG
AATTAGGTAATATTTTCAAAGAACGTGGTATTAATTTACCAGAATTACCTGAT
AGTGATTGGGATCAACCATTAGGTTTAGGTTCAGGTGCTGGTGTTTTATTTGG
TACTACTGGTGGTGTAATGGAAGCTGCATTACGTACAGCTTATGAAATTGTTA
CTAAAGAACCATTACCTCGTTTAAATTTATCAGAAGTACGTGGTTTAGATGGT
ATTAAAGAAGCTTCAGTTACATTAGTACCAGCACCTGGTTCTAAATTTGCAGA
ATTAGTTGCTGAACGTTTAGCACACAAAGTAGAAGAAGCTGCAGCTGCAGAA
GCTGCAGCTGCAGTTGAAGGTGCTGTAAAACCACCTATTGCTTATGATGGTG
GTCAAGGTTTTTCAACTGATGATGGTAAAGGTGGTTTAAAATTACGTGTAGCA
GTTGCTAATGGTTTAGGTAATGCTAAAAAATTAATTGGTAAAATGGTTTCAGG
TGAAGCAAAATATGATTTCGTAGAAATTATGGCATGTCCAGCTGGTTGTGTA
GGTGGTGGTGGTCAACCTCGTTCTACAGATAAACAAATTACTCAAAAACGTC
AAGCTGCATTATATGATTTAGATGAACGTAATACATTACGTCGTAGTCATGAA
AATGAAGCTGTTAATCAATTATATAAAGAATTCTTAGGTGAACCATTATCACA
TCGTGCTCACGAATTATTACATACACACTATGTACCTGGTGGCGCCAGCCAAA
TGGCGTCAGCTCCACGCACTGAAGACTGTGTAGGTTGCAAACGTTGTGAAAC
AGCTTGTCCTACTGACTTCTTAAGTGTTCGTGTTTATCTAGGTTCAGAAAGCA
CAAGAAGTATGGGCTTATCTTACTAATTTTTTAATTCAGATCT

Figure A2-8: DNA sequence of synthesized fusion gene. Restriction sites noted: in colours: NdeI (red), SfoI (blue), and BglII (green). The yellow highlighted site was designed with two degenerate nucleotides (25% A, 25% G, 25% C, 25% T) to produce a library with the degenerate codon identities shown in Table A2-2.

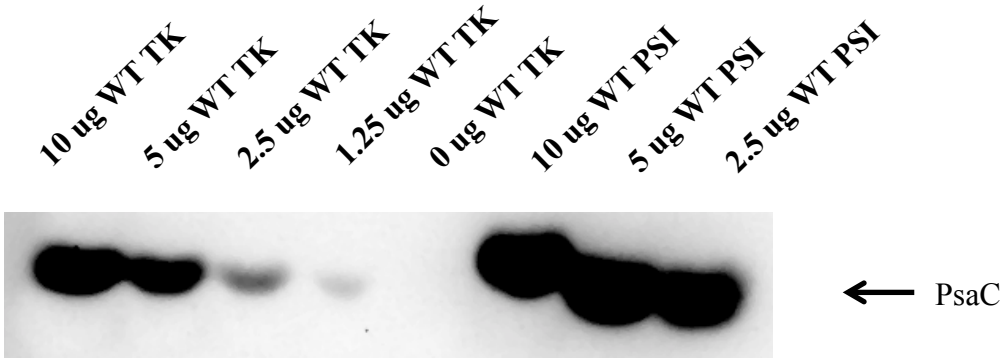

Figure A2-9: Anti-PsaC immunoblot. Thylakoid membranes and PSI particles were prepared as in Chapter 2 Materials and Methods. Thylakoid membranes were loaded on equal protein by dilution into a *psaC*Δ TK preparation. The PSI particles were diluted into sample buffer. The preparations were separated by SDS-PAGE then subjected to immunobloting with anti-PsaC antibodies.

References

[1] Adams MW. The structure and mechanism of iron-hydrogenases. Biochim Biophys Acta 1990;1020(2):115–145.

[2] Kruse O, Rupprecht J, Bader K-P, Thomas-Hall S, Schenk PM, Finazzi G, Hankamer B. Improved photobiological H_2 production in engineered green algal cells. J Biol Chem 2005;280(40):34170–34177.

[3] Melis A, Zhang L, Forestier M, Ghirardi ML, Seibert M. Sustained photobiological hydrogen gas production upon reversible inactivation of oxygen evolution in the green alga *Chlamydomonas reinhardtii*. Plant Physiol 2000;122(1):127–136.

[4] Melis A, Happe T. Hydrogen Production. Green Algae as a Source of Energy. Plant Physiol 2001;127(3):740–748.

[5] Kosourov S, Tsygankov A, Seibert M, Ghirardi ML. Sustained hydrogen photoproduction by *Chlamydomonas reinhardtii*: Effects of culture parameters. Biotechnol Bioeng 2002;78(7):731–740.

[6] Zhang L, Happe T, Melis A. Biochemical and morphological characterization of sulfur-deprived and H_2-producing *Chlamydomonas reinhardtii* (green alga). Planta 2002;214(4):552–561.

[7] Sétif P. Ferredoxin and flavodoxin reduction by Photosystem I. Biochim Biophys Acta 2001;1507(1-3):161–179.

[8] Ihara M, Nishihara H, Yoon K-S, Lenz O, Friedrich B, Nakamoto H, Kojima K, Honma D, Kamachi T, Okura I. Light-driven Hydrogen Production by a Hybrid Complex of a [NiFe]-Hydrogenase and the Cyanobacterial Photosystem I. Photochem Photobiol 2006;82(3):676.

[9] Moser CC, Keske JM, Warncke K, Farid RS, Dutton PL. Nature of biological electron transfer. Nature 1992;355(6363):796–802.

[10] Chang CH, King PW, Ghirardi ML, Kim K. Atomic Resolution Modeling of the Ferredoxin:[FeFe] Hydrogenase Complex from *Chlamydomonas reinhardtii*. Biophys J 2007;93(9):3034–3045.

[11] Jordan P, Fromme P, Witt HT, Klukas O, Saenger W, Krauss N. Three-dimensional structure of cyanobacterial Photosystem I at 2.5 angstrom resolution. Nature 2001;411(6840):909–917.

[12] Yacoby I, Pochekailov S, Toporik H, Ghirardi ML, King PW, Zhang S. Photosynthetic electron partitioning between [FeFe]-hydrogenase and ferredoxin:NADP+-oxidoreductase (FNR) enzymes in vitro. Proc Natl Acad Sci U S A 2011;108(23):9396–9401.

[13] Lubner CE, Knörzer P, Silva PJN, Vincent KA, Happe T, Bryant DA, Golbeck JH. Wiring an [FeFe]-Hydrogenase with Photosystem I for Light-Induced Hydrogen Production. Biochemistry 2010;49(48):10264–10266.

[14] Lubner CE, Applegate AM, Knörzer P, Ganago A, Bryant DA, Happe T, Golbeck JH. Solar hydrogen-producing bionanodevice outperforms natural photosynthesis. Proc Natl Acad Sci U S A 2011;108(52):20988–20991.

[15] Croft MT, Lawrence AD, Raux-Deery E, Warren MJ, Smith AG. Algae acquire vitamin B_{12} through a symbiotic relationship with bacteria. Nature 2005;438(7064):90–93.

[16] Aslanidis C, de Jong PJ. Ligation-independent cloning of PCR products (LIC-PCR). Nucleic Acids Res 1990;18(20):6069–6074.

[17] Aslanidis C, de Jong PJ, Schmitz G. Minimal length requirement of the single-stranded tails for ligation-independent cloning (LIC) of PCR products. PCR Methods Appl 1994;4(3):172–177.

[18] Li C, Evans RM. Ligation independent cloning irrespective of restriction site compatibility. Nucleic Acids Res 1997;25(20):4165–4166.

[19] Boynton JE, Gillham NW, Harris EH, Hosler JP, Johnson AM, Jones AR, Randolph-Anderson BL, Robertson D, Klein TM, Shark KB. Chloroplast transformation in *Chlamydomonas* with high velocity microprojectiles. Science 1988;240(4858):1534–1538.

[20] Fischer N, Stampacchia O, Redding K, Rochaix JD. Selectable marker recycling in the chloroplast. Mol Gen Genet 1996;251(3):373–380.

[21] Fischer N, Sétif P, Rochaix JD. Targeted mutations in the *psaC* gene of *Chlamydomonas reinhardtii*: preferential reduction of F_B at low temperature is not accompanied by altered electron flow from Photosystem I to ferredoxin. Biochemistry 1997;36(1):93–102.

[22] Harris EH, Stern DB, Witman G. The *Chlamydomonas* Sourcebook. San Diego: Academic Press, 1989.

[23] Gulis G, Narasimhulu KV, Fox LN, Redding KE. Purification of His_6-tagged Photosystem I from *Chlamydomonas reinhardtii*. Photosynth Res 2008;96(1):51–60.

References

1. Abeles FB. 1964. Cell-free Hydrogenase from *Chlamydomonas*. *Plant Physiology* 39(2):169–176.

2. Adams MW. 1990. The structure and mechanism of iron-hydrogenases. *Biochimica et Biophysica Acta* 1020(2):115–145.

3. Aslanidis C and de Jong PJ. 1990. Ligation-independent cloning of PCR products (LIC-PCR). *Nucleic Acids Research* 18(20):6069–6074.

4. Aslanidis C, de Jong PJ, and Schmitz G. 1994. Minimal length requirement of the single-stranded tails for ligation-independent cloning (LIC) of PCR products. *Genome Research* 4(3):172–177.

5. Ball SG, Dirick L, Decq A, Martiat JC, and Matagne R. 1990. Physiology of starch storage in the monocellular alga *Chlamydomonas reinhardtii*. *Plant Science* 66(1):1–9. Elsevier.

6. Beckmann J, Lehr F, Finazzi G, Hankamer B, Posten C, Wobbe L, and Kruse O. 2009. Improvement of light to biomass conversion by de-regulation of light-harvesting protein translation in *Chlamydomonas reinhardtii*. *Journal of Biotechnology* 142(1):70–77.

7. Beers R and Sizer I. 1952. A spectrophotometric method for measuring the breakdown of hydrogen peroxide by catalase. *Journal of Biological Chemistry* 195(1):133–140.

8. Behn W and Herrmann RG. 1977. Circular molecules in the β-satellite DNA of *Chlamydomonas reinhardii*. *Molecular and General Genetics* 157(1):25–30. Springer.

9. Ben-Shem A, Frolow F, and Nelson N. 2003. Crystal structure of plant Photosystem I. *Nature* 426(6967):630–635.

10. Berggren G, Adamska A, Lambertz C, Simmons TR, Esselborn J, Atta M, Gambarelli S, et al. 2013. Biomimetic assembly and activation of [FeFe]-hydrogenases. *Nature* 499(7456):66–69.

11. Béal D, Rappaport F, and Joliot P. 1999. A new high-sensitivity 10-ns time-resolution spectrophotometric technique adapted to in vivo analysis of the photosynthetic apparatus. *Review of Scientific Instruments* 70(1):202–207.

12. Biggins J. 1990. Evaluation of selected benzoquinones, naphthoquinones, and anthraquinones as replacements for phylloquinone in the A1 acceptor site of the Photosystem I reaction center. *Biochemistry* 29(31):7259–7264.

13. Boyer ME, Stapleton JA, Kuchenreuther JM, Wang CW, and Swartz JR. 2008. Cell-free synthesis and maturation of [FeFe] hydrogenases. *Biotechnology and Bioengineering* 99(1):59–67.

14. Boynton JE, Gillham NW, Harris EH, Hosler JP, Johnson AM, Jones AR, Randolph-Anderson BL, Robertson D, Klein TM, and Shark KB. 1988. Chloroplast transformation in *Chlamydomonas* with high velocity microprojectiles. *Science* 240(4858):1534–1538.

15. Brettel K and Leibl W. 2001. Electron transfer in Photosystem I. *Biochimica et Biophysica Acta* 1507(1-3):100–114.

16. Buchman GW, Schuster DM, and Rashtchian A. 1993. Selective RNA amplification: a novel method using dUMP-containing primers and uracil DNA glycosylase. *Genome Research* 3(1):28–31.

17. Byrdin M, Santabarbara S, Gu F, Fairclough WV, Heathcote P, Redding K, and Rappaport F. 2006. Assignment of a kinetic component to electron transfer between iron–sulfur clusters F_X and $F_{A/B}$ of Photosystem I. *Biochimica et Biophysica Acta* 1757(11):1529–1538.

18. Chang CH, King PW, Ghirardi ML, and Kim K. 2007. Atomic Resolution Modeling of the Ferredoxin:[FeFe] Hydrogenase Complex from *Chlamydomonas reinhardtii*. *Biophysical Journal* 93(9):3034–3045.

19. Chochois V, Dauvillee D, Beyly A, Tolleter D, Cuine S, Timpano H, Ball S, Cournac L, and Peltier G. 2009. Hydrogen Production in *Chlamydomonas*: Photosystem II-Dependent and -Independent Pathways Differ in Their Requirement for Starch Metabolism. *Plant Physiology* 151(2):631–640.

20. Crack JC, Green J, Cheesman MR, Le Brun NE, and Thomson AJ. 2007. Superoxide-mediated amplification of the oxygen-induced switch from [4Fe-4S] to [2Fe-2S] clusters in the transcriptional regulator FNR. *Proceedings of the National Academy of Sciences U.S.A.* 104(7):2092–2097.

21. Croft MT, Lawrence AD, Raux-Deery E, Warren MJ, and Smith AG. 2005. Algae acquire vitamin B_{12} through a symbiotic relationship with bacteria. *Nature* 438(7064):90–93.

22. Driesener RC, Challand MR, McGlynn SE, Shepard EM, Boyd ES, Broderick JB, Peters JW, and Roach PL. 2010. [FeFe]-Hydrogenase Cyanide Ligands Derived From S-Adenosylmethionine-Dependent Cleavage of Tyrosine. *Angewandte Chemie, International Edition* 49(9):1687–1690.

23. Eivazova ER and Markov SA. 2012. Conformational regulation of the hydrogenase gene expression in green alga Chlamydomonas reinhardtii. *International Journal of Hydrogen Energy* 37(23):17788–17793.

24. Esselborn J, Lambertz C, Adamska-Venkatesh A, Simmons T, Berggren G, Noth J, Siebel J, et al. 2013. Spontaneous activation of [FeFe]-hydrogenases by an inorganic [2Fe] active site mimic. *Nature Chemical Biology* 9(10):607-609.

25. Fauque G, Peck HD, Moura JJ, Huynh BH, Berlier Y, DerVartanian DV, Teixeira M, Przybyla AE, Lespinat PA, and Moura I. 1988. The three classes of hydrogenases from sulfate-reducing bacteria of the genus *Desulfovibrio*. *FEMS Microbiology Reviews* 4(4):299–344.

26. Fischer N, Sétif P, and Rochaix JD. 1997. Targeted mutations in the *psaC* gene of *Chlamydomonas reinhardtii*: preferential reduction of F_B at low temperature is not accompanied by altered electron flow from Photosystem I to ferredoxin. *Biochemistry* 36(1):93–102.

27. Fischer N, Stampacchia O, Redding K, and Rochaix JD. 1996. Selectable marker recycling in the chloroplast. *Molecular and General Genetics* 251(3):373–380.

28. Forestier M, King P, Zhang L, Posewitz M, Schwarzer S, Happe T, Ghirardi ML, and Seibert M. 2003. Expression of two [Fe]-hydrogenases in *Chlamydomonas reinhardtii* under anaerobic conditions. *European Journal of Biochemistry* 270(13):2750–2758.

29. Fouchard S, Hemschemeier A, Caruana A, Pruvost J, Legrand J, Happe T, Peltier G, and Cournac L. 2005. Autotrophic and Mixotrophic Hydrogen Photoproduction in Sulfur-Deprived *Chlamydomonas* Cells. *Applied and Environmental Microbiology* 71(10):6199–6205.

30. Franzén LG, Rochaix JD, and Heijne von G. 1990. Chloroplast transit peptides from the green alga *Chlamydomonas reinhardtii* share features with both mitochondrial and higher plant chloroplast presequences. *FEBS Letters* 260(2):165–168.

31. Gaffron H. 1940. The Oxyhydrogen Reaction in Green Algae and the Reduction of Carbon Dioxide in the Dark. *Science* 91(2370):529–530.

32. Gaffron H. 1942. Reduction of Carbon Dioxide Coupled with the Oxyhydrogen Reaction in Algae. *The Journal of General Physiology* 26(2):241–267.

33. Gfeller RP and Gibbs M. 1984. Fermentative Metabolism of *Chlamydomonas reinhardtii*: I. Analysis of Fermentative Products from Starch in Dark and Light. *Plant Physiology* 75(1):212–218.

34. Ghirardi ML, Togasaki RK, and Seibert M. 1997. Oxygen sensitivity of algal H_2 production. *Biotechnology for Fuels and Chemicals.* Humana Press. pp.141–151.

35. Ghirardi ML, Zhang L, Lee JW, Flynn T, Seibert M, Greenbaum E, and Melis A. 2000. Microalgae: a green source of renewable H_2. *Trends in Biotechnology* 18(12):506–511.

36. Gibbs M, Gfeller RP, and Chen C. 1986. Fermentative metabolism of *Chlamydomonas reinhardii* III. Photoassimilation of acetate. *Plant Physiology* 82(1):160–166. Am Soc Plant Biol.

37. Godde D and Trebst A. 2013. NADH as electron donor for the photosynthetic membrane of *Chlamydomonas reinhardii*. *Archives of Microbiology* 127(3):245–252.

38. Guergova-Kuras M, Boudreaux B, Joliot A, Joliot P, and Redding K. 2001. Evidence for two active branches for electron transfer in Photosystem I. *Proceedings of the National Academy of Sciences U.S.A.* 98(8):4437–4442.

39. Gulis G, Narasimhulu KV, Fox LN, and Redding KE. 2008. Purification of His_6-tagged Photosystem I from *Chlamydomonas reinhardtii*. *Photosynthesis Research* 96(1):51–60.

40. Happe T, Mosler B, and Naber JD. 1994. Induction, localization and metal content of hydrogenase in the green alga *Chlamydomonas reinhardtii*. *European Journal of Biochemistry* 222(3):769–774.

41. Happe T and Naber JD. 1993. Isolation, characterization and N-terminal amino acid sequence of hydrogenase from the green alga *Chlamydomonas reinhardtii*. *European Journal of Biochemistry* 214(2):475–481.

42. Happe T and Kaminski A. 2002. Differential regulation of the Fe-hydrogenase during anaerobic adaptation in the green alga *Chlamydomonas reinhardtii*. *European Journal of Biochemistry* 269(3):1022–1032.

43. Harris EH. 2001. *Chlamydomonas* as a model organism. *Annual Review of Plant Biology* 52(1):363–406.

44. Harris EH, Stern DB, and Witman G. 1989. *The Chlamydomonas Sourcebook*. San Diego: Academic Press.

45. Hemschemeier A, Fouchard S, Cournac L, Peltier G, and Happe T. 2007. Hydrogen production by *Chlamydomonas reinhardtii*: an elaborate interplay of electron sources and sinks. *Planta* 227(2):397–407.

46. Henderson JN. 2003. Disassembly and Degradation of Photosystem I in an *in vitro* System Are Multievent, Metal-dependent Processes. *Journal of Biological Chemistry* 278(41):39978–39986.

47. Hicks GR, Hironaka CM, Dauvillee D, Funke RP, D'Hulst C, Waffenschmidt S, and Ball SG. 2001. When Simpler Is Better. Unicellular Green Algae for Discovering New Genes and Functions in Carbohydrate Metabolism. *Plant Physiology* 127(4):1334–1338.

48. Huynh BH, Czechowski MH, Krüger HJ, DerVartanian DV, Peck HD, and LeGall J. 1984. *Desulfovibrio vulgaris* hydrogenase: a nonheme iron enzyme lacking nickel that exhibits anomalous EPR and Mössbauer spectra. *Proceedings of the National Academy of Sciences U.S.A.* 81(12):3728–3732.

49. Ihara M, Nishihara H, Yoon K-S, Lenz O, Friedrich B, Nakamoto H, Kojima K, Honma D, Kamachi T, and Okura I. 2006. Light-driven Hydrogen Production by a Hybrid Complex of a [NiFe]-Hydrogenase and the Cyanobacterial Photosystem I. *Photochemistry and Photobiology* 82(3):676.

50. Itoh S, Iwaki M, and Ikegami I. 2001. Modification of Photosystem I reaction center by the extraction and exchange of chlorophylls and quinones. *Biochimica et Biophysica Acta* 1507(1-3):115–138.

51. Jones CS and Mayfield SP. 2012. Algae biofuels: versatility for the future of bioenergy. *Current Opinion in Biotechnology* 23(3):346–351.

52. Jordan P, Fromme P, Witt HT, Klukas O, Saenger W, and Krauss N. 2001. Three-dimensional structure of cyanobacterial Photosystem I at 2.5 angstrom resolution. *Nature* 411(6840):909–917.

53. Kato J, Yamahara T, Tanaka K, Takio S, and Satoh T. 1997. Characterization of catalase from green algae *Chlamydomonas reinhardtii*. *Journal of Plant Physiology* 151(3):262–268.

54. Keegstra K. 1989. Transport and routing of proteins into chloroplasts. *Cell* 56(2):247.

55. Komine Y, Kwong L, Anguera MC, Schuster G, and Stern DB. 2000. Polyadenylation of three classes of chloroplast RNA in *Chlamydomonas reinhadtii*. *RNA* 6(4):598–607.

56. Kosourov S, Tsygankov A, Seibert M, and Ghirardi ML. 2002. Sustained hydrogen photoproduction by *Chlamydomonas reinhardtii*: Effects of culture parameters. *Biotechnology and Bioengineering* 78(7):731–740.

57. Krabben L, Schlodder E, Jordan R, Carbonera D, Giacometti G, Lee H, Webber AN, and Lubitz W. 2000. Influence of the Axial Ligands on the Spectral Properties of P700 of Photosystem I: A Study of Site-Directed Mutants. *Biochemistry* 39(42):13012–13025.

58. Kruse O and Ben Hankamer. 2010. Microalgal hydrogen production. *Current Opinion in Biotechnology* 21(3):238–243.

59. Kruse O, Rupprecht J, Bader K-P, Thomas-Hall S, Schenk PM, Finazzi G, and Hankamer B. 2005. Improved photobiological H_2 production in engineered green algal cells. *Journal of Biological Chemistry* 280(40):34170–34177.

60. Kuchenreuther JM, Britt RD, and Swartz JR. 2012. New Insights into [FeFe] Hydrogenase Activation and Maturase Function. *PLoS ONE* 7(9):45850.

61. Kuchenreuther JM, Grady-Smith CS, Bingham AS, George SJ, Cramer SP, and Swartz JR. 2010. High-Yield Expression of Heterologous [FeFe] Hydrogenases in Escherichia coli. *PLoS ONE* 5(11):15491.

62. Kuchka MR, Goldschmidt-Clermont M, van Dillewijn J, and Rochaix JD. 1989. Mutation at the *Chlamydomonas* nuclear *NAC2* locus specifically affects stability of the chloroplast *psbD* transcript encoding polypeptide D2 of PS II. *Cell* 58(5):869–876.

63. Lefebvre-Legendre L, Rappaport F, Finazzi G, Ceol M, Grivet C, Hopfgartner G, and Rochaix J-D. 2007. Loss of phylloquinone in *Chlamydomonas* affects plastoquinone pool size and Photosystem II synthesis. *Journal of Biological Chemistry* 282(18):13250–13263.

64. Li C and Evans RM. 1997. Ligation independent cloning irrespective of restriction site compatibility. *Nucleic Acids Research* 25(20):4165–4166.

65. Li Y, Lucas M-G, Konovalova T, Abbott B, MacMillan F, Petrenko A, Sivakumar V, et al. 2004. Mutation of the Putative Hydrogen-Bond Donor to P700 of Photosystem I. *Biochemistry* 43(39):12634–12647.

66. Li Y, van der Est A, Lucas M-G, Ramesh VM, Gu F, Petrenko A, Lin S, Webber AN, Rappaport F, and Redding K. 2006. Directing electron transfer within Photosystem I by breaking H-bonds in the cofactor branches. *Proceedings of the National Academy of Sciences U.S.A.* 103(7):2144–2149.

67. Liebgott P-P, Leroux F, Burlat B, Dementin S, Baffert C, Lautier T, Fourmond V, et al. 2009. Relating diffusion along the substrate tunnel and oxygen sensitivity in hydrogenase. *Nature Chemical Biology* 6(1):63–70.

68. Lill R. 2009. Function and biogenesis of iron–sulphur proteins. *Nature* 460(7257):831–838.

69. Lubitz W, Reijerse E, and van Gastel M. 2007. [NiFe] and [FeFe] Hydrogenases Studied by Advanced Magnetic Resonance Techniques. *Chemical Reviews* 107(10):4331–4365.

70. Lubner CE, Applegate AM, Knörzer P, Ganago A, Bryant DA, Happe T, and Golbeck JH. 2011. Solar hydrogen-producing bionanodevice outperforms natural photosynthesis. *Proceedings of the National Academy of Sciences U.S.A.* 108(52):20988–20991.

71. Lubner CE, Knörzer P, Silva PJN, Vincent KA, Happe T, Bryant DA, and Golbeck JH. 2010. Wiring an [FeFe]-Hydrogenase with Photosystem I for Light-Induced Hydrogen Production. *Biochemistry* 49(48):10264–10266.

72. Maul JE. 2002. The *Chlamydomonas reinhardtii* Plastid Chromosome: Islands of Genes in a Sea of Repeats. *Plant Cell* 14(11):2659–2679.

73. McConnell MD, Cowgill JB, Baker PL, Rappaport F, and Redding KE. 2011. Double Reduction of Plastoquinone to Plastoquinol in Photosystem 1. *Biochemistry* 50(51):11034–11046.

74. Melis A and Happe T. 2001. Hydrogen Production. Green Algae as a Source of Energy. *Plant Physiology* 127(3):740–748.

75. Melis A, Zhang L, Forestier M, Ghirardi ML, and Seibert M. 2000. Sustained photobiological hydrogen gas production upon reversible inactivation of oxygen evolution in the green alga *Chlamydomonas reinhardtii*. *Plant Physiology* 122(1):127–136.

76. Merchant SS, Prochnik SE, Vallon O, Harris EH, Karpowicz SJ, Witman GB, Terry A, et al. 2007. The *Chlamydomonas* Genome Reveals the Evolution of Key Animal and Plant Functions. *Science* 318(5848):245–250.

77. Meuser JE, D'Adamo S, Jinkerson RE, Mus F, Yang W, Ghirardi ML, Seibert M, Grossman AR, and Posewitz MC. 2012. Genetic disruption of both *Chlamydomonas reinhardtii* [FeFe]-hydrogenases: Insight into the role of *HYDA2* in H_2 production. *Biochemical and Biophysical Research Communications* 417(2):704–709. Elsevier Inc.

78. Michelet L, Roach T, Fischer BB, Bedhomme M, Lemaire S, and Krieger-Liszkay A. 2013. Down-regulation of catalase activity allows transient accumulation of a hydrogen peroxide signal in *Chlamydomonas reinhardtii*. *Plant, Cell and Environment* 36(6):1204–1213.

79. Moroney JV, Husic HD, Tolbert NE, Kitayama M, Manuel LJ, and Togasaki RK. 1989. Isolation and characterization of a mutant of Chlamydomonas reinhardtii deficient in the CO_2 concentrating mechanism. *Plant Physiology* 89(3):897–903.

80. Moser CC, Keske JM, Warncke K, Farid RS, and Dutton PL. 1992. Nature of biological electron transfer. *Nature* 355(6363):796–802.

81. Moser C and Dutton PL. 2006. Application of Marcus Theory to Photosystem I Electron Transfer. In *Advances in Photosynthesis and Respiration*, ed. J Golbeck, 24: 583–594. Springer Netherlands.

82. Moura J, Moura I, Huynh BH, Krüger HJ, Teixeira M, DuVarney RC, DerVartanian DV, Xavier AV, Peck HD, and LeGall J. 1982. Unambiguous identification of the nickel EPR signal in 61 Ni-enriched *Desulfovibrio gigas* hydrogenase. *Biochemical and Biophysical Research Communications* 108(4):1388–1393.

83. Mubarakshina MM, Ivanov BN, Naydov IA, Hillier W, Badger MR, and Krieger-Liszkay A. 2010. Production and diffusion of chloroplastic H_2O_2 and its implication to signalling. *Journal of Experimental Botany* 61(13):3577–3587.

84. Mula S, McConnell MD, Ching A, Zhao N, Gordon HL, Hastings G, Redding KE, and van der Est A. 2012. Introduction of a Hydrogen Bond between Phylloquinone PhQ Aand a Threonine Side-Chain OH Group in Photosystem I. *Journal of Physical Chemistry B* 116(48):14008–14016.

85. Mulder DW, Boyd ES, Sarma R, Lange RK, Endrizzi JA, Broderick JB, and Peters JW. 2010. Stepwise [FeFe]-hydrogenase H-cluster assembly revealed in the structure of $HydA^{\Delta EFG}$. *Nature* 465(7295):248–251.

86. Mulder DW, Ortillo DO, Gardenghi DJ, Naumov AV, Ruebush SS, Szilagyi RK, Huynh B, Broderick JB, and Peters JW. 2009. Activation of $HydA^{\Delta EFG}$ Requires a Preformed [4Fe-4S] Cluster. *Biochemistry* 48(26):6240–6248.

87. Mulder DW, Ratzloff MW, Shepard EM, Byer AS, Noone SM, Peters JW, Broderick JB, and King PW. 2013. EPR and FTIR Analysis of the Mechanism of H_2 Activation by [FeFe]-Hydrogenase HydA1 from *Chlamydomonas reinhardtii*. *Journal of the American Chemical Society* 135(18):130424124821007.

88. Mulder DW, Shepard EM, Meuser JE, Joshi N, King PW, Posewitz MC, Broderick JB, and Peters JW. 2011. Insights into [FeFe]-Hydrogenase Structure, Mechanism, and Maturation. *Structure* 19(8):1038–1052. Elsevier Ltd.

89. Munge B, Das SK, Ilagan R, Pendon Z, Yang J, Frank HA, and Rusling JF. 2003. Electron Transfer Reactions of Redox Cofactors in Spinach Photosystem I Reaction Center Protein in Lipid Films on Electrodes. *Journal of the American Chemical Society* 125(41):12457–12463.

90. Murray J and King D. 2012. Climate policy: Oil's tipping point has passed. *Nature* 481(7382):433–435.

91. Nakano Y and Asada K. 1981. Hydrogen peroxide is scavenged by ascorbate-specific peroxidase in spinach chloroplasts. *Plant and Cell Physiology* 22(5):867–880.

92. Nickelsen J, van Dillewijn J, Rahire M, and Rochaix JD. 1994. Determinants for stability of the chloroplast *psbD* RNA are located within its short leader region in *Chlamydomonas reinhardtii*. *EMBO Journal.* 13(13):3182–3191.

93. Nicolet Y, De Lacey AL, Vernède X, Fernández VM, Hatchikian EC, and Fontecilla-Camps JC. 2001. Crystallographic and FTIR Spectroscopic Evidence of Changes in Fe Coordination Upon Reduction of the Active Site of the Fe-Only Hydrogenase from *Desulfovibrio desulfuricans*. *Journal of the American Chemical Society* 123(8):1596–1601.

94. Nicolet Y, Piras C, Legrand P, Hatchikian CE, and Fontecilla-Camps JC. 1999. *Desulfovibrio desulfuricans* iron hydrogenase: the structure shows unusual coordination to an active site Fe binuclear center. *Structure* 7(1):13–23.

95. Noth J, Krawietz D, Hemschemeier A, and Happe T. 2013. Pyruvate:Ferredoxin Oxidoreductase Is Coupled to Light-independent Hydrogen Production in Chlamydomonas reinhardtii. *Journal of Biological Chemistry* 288(6):4368–4377.

96. Oey M, Ross IL, Stephens E, Steinbeck J, Wolf J, Radzun KA, Kügler J, Ringsmuth AK, Kruse O, and Hankamer B. 2013. RNAi Knock-Down of LHCBM1, 2 and 3 Increases Photosynthetic H_2 Production Efficiency of the Green Alga *Chlamydomonas reinhardtii*. *PLoS ONE* 8(4):61375.

97. Ohad I, Adir N, Koike H, Kyle DJ, and Inoue Y. 1990. Mechanism of photoinhibition *in vivo*. A reversible light-induced conformational change of reaction center II is related to an irreversible modification of the D1 protein. *Journal of Biological Chemistry* 265(4):1972–1979.

98. Ohta S, Miyamoto K, and Miura Y. 1987. Hydrogen evolution as a consumption mode of reducing equivalents in green algal fermentation. *Plant Physiology* 83(4):1022–1026.

99. Ozawa SI, Kosugi M, Kashino Y, Sugimura T, and Takahashi Y. 2012. 5'-Monohydroxyphylloquinone is the Dominant Naphthoquinone of PSI in the Green Alga *Chlamydomonas reinhardtii*. *Plant and Cell Physiology* 53(1):237–243.

100. Pape M, Lambertz C, Happe T, and Hemschemeier A. 2012. Differential Expression of the Chlamydomonas [FeFe]-Hydrogenase-Encoding HYDA1 Gene Is Regulated by the COPPER RESPONSE REGULATOR1. *Plant Physiology* 159(4):1700–1712.

101. Peden EA, Boehm M, Mulder DW, Davis R, Old WM, King PW, Ghirardi ML, and Dubini A. 2013. Identification of global ferredoxin interaction networks in *Chlamydomonas reinhardtii*. *Journal of Biological Chemistry*: jbc-M113

102. Picard V, Ersdal-Badju E, Lu A, and Bock SC. 1994. A rapid and efficient one-tube PCR-based mutagenesis technique using Pfu DNA polymerase. *Nucleic Acids Research* 22(13):2587–2591.

103. Pilon M, Abdel-Ghany SE, Van Hoewyk D, Ye H, and Pilon-Smits EAH. 2006. Biogenesis of iron-sulfur cluster proteins in plastids. *Genetic Engineering*, pp. 101–117. Springer.

104. Porra RJ, Thompson WA, and Kriedemann PE. 1989. Determination of accurate extinction coefficients and simultaneous equations for assaying chlorophylls a and b extracted with four different solvents: verification of the concentration of chlorophyll standards by atomic absorption spectroscopy. *Biochimica et Biophysica Acta* 975(3):384–394.

105. Posewitz MC. 2004. Discovery of Two Novel Radical S-Adenosylmethionine Proteins Required for the Assembly of an Active [Fe] Hydrogenase. *Journal of Biological Chemistry* 279(24):25711–25720.

106. Posewitz MC, Dubini A, Meuser JE, Seibert M, and Ghirardi ML. 2009. Hydrogenases, hydrogen production, and anoxia. *The Chlamydomonas Sourcebook: Organellar and Metabolic Processes* 2:217–246.

107. Ramundo S, Rahire M, Schaad O, and Rochaix JD. 2013. Repression of Essential Chloroplast Genes Reveals New Signaling Pathways and Regulatory Feedback Loops in *Chlamydomonas*. *Plant Cell* 25(1):167–186.

108. Rappaport F, Diner BA, and Redding K. 2006. Optical measurements of secondary electron transfer in Photosystem I. In *Photosystem I*, pp. 223–244. Springer.

109. Redding K, MacMillan F, Leibl W, Brettel K, Hanley J, Rutherford AW, Breton J, and Rochaix J-D. 1998. A systematic survey of conserved histidines in the core subunits of Photosystem I by site-directed mutagenesis reveals the likely axial ligands of P700. *EMBO Journal* 17(1):50–60.

110. Rostrup-Nielsen J, Sehested J, and Nørskov J. 2002. Hydrogen and synthesis gas by steam- and CO_2 reforming. In *Advances in Catalysis Volume 47*, pp. 65–139. Elsevier.

111. Rubin J. 1942. Fermentative and Photochemical Production of Hydrogen in Algae. *The Journal of General Physiology*. 26(2) 216-240.

112. Saenger W. 1984. The structure of the blue starch-iodine complex. *Naturwissenschaften* 71(1):31–36.

113. Santabarbara S, Heathcote P, and Evans MCW. 2005. Modelling of the electron transfer reactions in Photosystem I by electron tunnelling theory: The phylloquinones bound to the PsaA and the PsaB reaction centre subunits of PS I are almost isoenergetic to the iron–sulfur cluster F_X. *Biochimica et Biophysica Acta* 1708(3):283–310.

114. Santabarbara S, Jasaitis A, Byrdin M, Gu F, Rappaport F, and Redding K. 2008. Additive effect of mutations affecting the rate of phylloquinone reoxidation and directionality of electron transfer within photosystem I. *Photochemistry and Photobiology* 84(6):1381–1387.

115. Santabarbara S, Reifschneider K, Jasaitis A, Gu F, Agostini G, Carbonera D, Rappaport F, and Redding KE. 2010. Interquinone Electron Transfer in Photosystem I As Evidenced by Altering the Hydrogen Bond Strength to the Phylloquinone(s). *Journal of Physical Chemistry B* 114(28):9300–9312.

116. Sétif P. 2001. Ferredoxin and flavodoxin reduction by photosystem I. *Biochimica et Biophysica Acta* 1507(1-3):161–179.

117. Shao N, Beck CF, Lemaire S, and Krieger-Liszkay A. 2008. Photosynthetic electron flow affects H_2O_2 signaling by inactivation of catalase in *Chlamydomonas reinhardtii*. *Planta* 228(6):1055–1066.

118. Shepard EM, McGlynn SE, Bueling AL, Grady-Smith CS, George SJ, Winslow MA, Cramer SP, Peters JW, and Broderick JB. 2010. Synthesis of the 2Fe subcluster of the [FeFe]-hydrogenase H cluster on the HydF scaffold. *Proceedings of the National Academy of Sciences U.S.A.* 107(23):10448–10453.

119. Shimogawara K, Fujiwara S, Grossman A, and Usuda H. 1998. High-efficiency transformation of *Chlamydomonas reinhardtii* by electroporation. *Genetics* 148(4):1821–1828.

120. Srinivasan N and Golbeck JH. 2009. Protein–cofactor interactions in bioenergetic complexes: The role of the A_{1A} and A_{1B} phylloquinones in Photosystem I. *Biochimica et Biophysica Acta* 1787(9):1057–1088.

121. Srinivasan N, Karyagina I, Bittl R, van der Est A, and Golbeck JH. 2009. Role of the Hydrogen Bond from Leu722 to the A_{1A} Phylloquinone in Photosystem I. *Biochemistry* 48(15):3315–3324.

122. Stephens E, Ross IL, King Z, Mussgnug JH, Kruse O, Posten C, Borowitzka MA, and Hankamer B. 2010. An economic and technical evaluation of microalgal biofuels. *Nature Biotechnology* 28(2):126–128.

123. Stirnberg M and Happe T. 2004. Identification of a cis-acting element controlling anaerobic expression of the hydA-gene from *Chlamydomonas reinhardtii*. *Biohydrogen III, J. Miyake, Y. Igarashi and M. Rögner (eds)* pp.117–127. Elsevier.

124. Stripp ST, Goldet G, Brandmayr C, Sanganas O, Vincent KA, Haumann M, Armstrong FA, and Happe T. 2009. How oxygen attacks [FeFe] hydrogenases from photosynthetic organisms. *Proceedings of the National Academy of Sciences U.S.A.* 106(41):17331–17336.

125. Stuart TS and Gaffron H. 1972. The mechanism of hydrogen photoproduction by several algae. *Planta* 106(2):101–112.

126. Sweeney WV and Rabinowitz JC. 1980. Proteins containing 4Fe-4S clusters: an overview. *Annual Review of Biochemistry* 49:139–161.

127. Thyssen C, Hermes M, and Sültemeyer D. 2003. Isolation and characterisation of *Chlamydomonas reinhardtii* mutants with an impaired CO_2-concentrating mechanism. *Planta* 217(1):102–112.

128. U.S. Department of Energy. Comparison of Fuel Cell Technologies. Energy Efficiency & Renewable Energy. February 2011. Retrieved from http://www1.eere.energy.gov/hydrogenandfuelcells/fuelcells/pdfs/fc_comparison_chart.pdf

129. US Energy Information Administration. International Energy Outlook 2013. DOE/EIA-0484(2013) 2013:1–312. Retrieved from http://www.eia.gov/forecasts/ieo/*DOE/EIA-0484(2013)*:1–312.

130. Vignais PM and Billoud B. 2007. Occurrence, Classification, and Biological Function of Hydrogenases: An Overview. *Chemical Reviews* 107(10):4206–4272.

131. Whitney LAS, Loreti E, Alpi A, and Perata P. 2010. Alcohol dehydrogenase and hydrogenase transcript fluctuations during a day-night cycle in *Chlamydomonas reinhardtii*: the role of anoxia. *New Phytologist* 190(2):488–498.

132. Woessner JP, Masson A, Harris EH, Bennoun P, Gillham NW, and Boynton JE. 1984. Molecular and genetic analysis of the chloroplast ATPase of *Chlamydomonas*. *Plant Molecular Biology* 3(3):177–190.

133. Wykoff DD, Davies JP, Melis A, and Grossman AR. 1998. The regulation of photosynthetic electron transport during nutrient deprivation in *Chlamydomonas reinhardtii*. *Plant Physiology* 117(1):129–139.

134. Yacoby I, Pochekailov S, Toporik H, Ghirardi ML, King PW, and Zhang S. 2011. Photosynthetic electron partitioning between [FeFe]-hydrogenase and ferredoxin:NADP+-oxidoreductase (FNR) enzymes in vitro. *Proceedings of the National Academy of Sciences U.S.A.* 108(23):9396–9401.

135. Zeng J, Zhang M, and Sun X. 2013. Molecular Hydrogen Is Involved in Phytohormone Signaling and Stress Responses in Plants. *PLoS ONE* 8(8):71038.

136. Zhang L, Happe T, and Melis A. 2002. Biochemical and morphological characterization of sulfur-deprived and H_2-producing *Chlamydomonas reinhardtii* (green alga). *Planta* 214(4):552–561.